Faculty of Science and Engineering
Department of Petroleum Engineering

Investigation of fatigue failure in composite versus steel coiled tube for application in mine site drilling

Siamak Mishani

This thesis is presented for the Degree of
Doctor of Philosophy
of
Curtin University

August 2017

Declaration

To the best of my knowledge and belief this thesis contains no material previously published by any other person except where due acknowledgment has been made. This thesis contains no material which has been accepted for the award of any other degree or diploma in any university.

Name: Siamak Mishani

Signature: 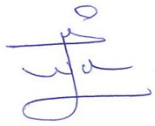 Date: 23/08/2017

Abstract

A coiled tubing drilling rig is an alternative rig to the conventional rotary rig in which high strength continuous steel tube is used instead of short length steel pipes or rods. Fibre reinforced composite tube could be an alternative to steel tube with potentially greater reliability and higher fatigue life to that of steel under high internal hydrostatic pressure. However, the behaviour of composite materials under dynamic load conditions is a complex subject. A good understanding of the interlaminar delamination within a framework of meso-cracking progression in the matrix structure can help to predict the fatigue failure in the composite material and assist in the improved design of composite tubing.

This research investigates the fatigue life of steel and composite coiled tubes through appropriate failure criteria. Using a non-linear finite element model, I compared the theoretical fatigue life of both materials with laboratory scale tests.

I developed a finite element numerical model to predict the fatigue life of the conventional steel coiled tube (HS-90) at specific internal pressure and also cumulative fatigue life of the model at variable internal pressures (known as the "running meters method"). I validated the numerical modelling results using lab-scale experimental equipment I helped develop for testing tubing.

Laboratory test results showed the numerical analysis of the bending behaviour of the steel coiled tube string illustrated the tendency of the string to be pushed against the well bore during running and pulling out a bore hole. This would be the cause of excessive external steel wear. By comparison, I found that composite tubing did not experience this problem (due to the nature of its construction being a major benefit in using composite tubing).

I predicted the fatigue life of HS-90 steel coiled tubes from experimental results using the Weibull distribution method and validated them with finite element numerical modelling results. I also detected internal defects in the carbon and glass fibre composite tubes, using CT-Scanning methods observing micro-cracks, delamination, and void distributions.

Test results on steel showed that the minimum cyclic bending life occurs when the weld seam in HS-90 conventional coiled tube is placed against the bending block side.

While HT-125 steel coiled tube has more than twice the fatigue life of HS-90 steel coiled tube, the test results also illustrated that the weld seam areas of HT-125 steel coiled tube have almost the same cyclic fatigue life and consequently the same micro-structural behaviour as the rest of the coiled tube body. Moreover, the HT-125 showed better fatigue life performance than HS-90 at higher internal hydrostatic pressures and therefore HT-125 is a great advancement over HS-90.

The finite element analysis of interlaminar delamination failure in the composite laminate showed that the normal resistance to crack propagation is much less than the shear resistance and the required “applied load” for crack propagation in the carbon fibre laminate is almost three times more than that for glass fibre laminate.

When compared with a composite tube the research found that despite the composite fibre arrangement, the fatigue life of a composite can be affected by damage in the vicinity of the resin structure. However, the use of a suitable thermoplastic liner or elastic resin can recover this deficit in the behaviour of the matrix material.

The cyclic life of the composite tube was almost 5 times longer than the conventional (HS-90) steel coiled tube and 3 times longer than the best (HT-125) steel on the market. This was the most important new knowledge of this research, and points to the preferred use of composite tubing in the future, rather than steel, based on their comparative fatigue lives. The additional ability to embed electronic sensors within the composite resin structure strengthens the composite case.

Acknowledgements

First and foremost, I would like to express my deepest sense of gratitude to my research advisor, Professor Brian Evans for his invaluable encouragement, suggestions, and continuous support to aid me to successfully develop and complete this research work.

I would also like to thank Dr. Masood Mostofi for providing valuable comments to develop my research. My sincere thanks goes to Dr. Christopher Lagat for his patience, motivation, and immense knowledge. I highly appreciate my committee members, including Professor Reza Rezaee and Dr. Mohammad Sarmadivaleh for their support and guidance throughout the research stages.

I am using this opportunity to express my sincere gratitude to Professor Vamegh Rasouli for accepting me into his group, his aspiring guidance and friendly advice; and Dr. Reem Raufail who provided precious remarks and suggestions.

The completion of this research would not have been possible without the support of Deep Exploration Technologies Cooperative Research Centre (DET CRC), and Curtin University's Department of Petroleum Engineering. I gratefully acknowledge the help of many friends including Mr. Peter Jaensch from Boartlongyear Co, for his valuable contribution in the construction of the tube's end-connectors and Dr. Lionel Esteban from CSIRO for his kind support and professional interpretation of images, and many others who shared knowledge and experiences with me.

Most importantly, none of this work could have happened without my family support. My wife, daughter and son; who experienced some ups and downs and offered their unconditional love and encouragement.

Contents

List of Figures

List of Tables

Nomenclature

δ	Load point displacement
σ_{11}	Normal stress parallel to the fibre direction
σ_{22}	Normal stress transverse to the fibre-parallel direction
σ_{33}	Normal stress transverse to the fibre-perpendicular direction
a	Delamination crack length
b	Delamination sample width
d_u	Crack displacement in the x direction
d_v	Crack displacement in the y direction
E	Young's modulus of elasticity
G_I	Strain energy release rate in Mode-I testing for pure normal stress
G_{II}	Strain energy release rate in Mode-II testing for pure shear stress
G_{III}	Strain energy release rate in for pure sliding stress
G_T	Total strain energy release rate
$2h$	Sample thickness
N	Fatigue life
P	Load
R_X	Node reaction force in the x direction
R_Y	Node reaction force in the y direction
σ_1^T	Tensile strength in longitudinal direction
σ_1^C	Compressive strength in longitudinal direction
σ_2^T	Tensile strength in transverse direction
σ_2^C	Compressive strength in transverse direction
τ_{12}^F	Shear strength in the 1-2 plane
ε_1^T	Ultimate tensile strain in the longitudinal direction
ε_1^C	Ultimate compressive strain in the longitudinal direction
ε_2^T	Ultimate tensile strain in the transverse direction
ε_2^C	Ultimate compressive strain in the transverse direction

σ_1 , σ_2	Maximum normal stresses in the lamina
τ_{12}	Maximum shear stress in the lamina
ε_1, ε_2 , ε_3	Principal normal strain components
γ_{12}	Shear strain in-plane
γ_{12} , γ_{12}	Shear strain through thickness
σ_1 , σ_2 , σ_3	Principal normal stress components
τ_1 , τ_2 , τ_3	Principal shear stress components
E_1 , E_2 , E_3	Young's moduli in each material axis
G_{12}	Shear modulus in-plane
G_{13} , G_{23}	Shear moduli through thickness
ν_{12}	Poisson's ratio in-plane
ν_{13} , ν_{23}	Poisson's ratios through thickness
σ_1^F	Strength in longitudinal direction
σ_2^F	Strength in transverse direction
τ_{12}^F	Shear strength in the 1-2 plane
γ_{12}^F	Ultimate shear strain in the lamina plane
$S_{y,nom}$	Nominal yield strength
$\frac{\Delta\varepsilon}{2}$	Total strain amplitude
ε_a	Total strain amplitude
$\frac{\Delta\varepsilon_e}{2}$	Elastic strain amplitude
$\frac{\Delta\varepsilon_p}{2}$	Plastic strain amplitude
σ_a	Stress range
K'	Cyclic strength coefficient
n'	Cyclic strain hardening exponent
$2N_f$	Number of load reversals to failure
σ'_f	Fatigue strength coefficient
ε'_f	Fatigue ductility coefficient
B	Fatigue strength exponent
c	Fatigue ductility exponent
ε_l	Longitudinal strain rate
D_p	Outside diameter of pipe

D_R	Outside diameter of Reel
D_n	Fatigue damage (equals 0 for n = 0 and equals 1 for n = N)
E_0	Initial Young's modulus
E_f	Failure Young's modulus
E_n	Young's modulus of the material subjected to the nth cyclic load
D_{max}	Maximum coiled tube outer diameter
D_{min}	Minimum coiled tube outer diameter
ε_l	Longitudinal strain
σ_1^T	Tensile strength in longitudinal direction
σ_2^T	Tensile strength in transverse direction
τ_{12}^T	Shear strength in-plane direction
σ_1 , σ_3	Maximum normal stresses in the lamina
σ_{12} , σ_{13}	Maximum stresses components in the lamina
S_{12} , S_{13}	Allowable shear strength components in the lamina
X_T , Y_T	Allowable tensile strength in the lamina
X_C , Y_C	Allowable compressive strength in the lamina
j	Total number of failures
N	Failure order number
t	Life time
η	Scale parameter , or characteristic life
β	Shape parameter , or Weibull slop
γ	Location parameter , or failure free life

Chapter 1 Introduction

1.1 Background

A need to increase the development of resources for the mineral industry on the Australian continent has resulted in deeper exploration drilling activities over recent years. The Deep Exploration Technology Cooperative Research Centre (DET CRC) project was initiated in 2010 under the Australian Government's CRC program (Hillis, 2015). The aim of the DET CRC program was to develop new sets of drilling exploration technologies, methods and equipment based on cheaper and safer operations for the mining industry. Subsequent studies suggested that the use of a coiled (spoolable) tubing drilling rig could offer a new and improved drilling method and be a suitable alternative to the conventional rotary drilling rig in finding deeper minerals. The main and most expensive consumable component of any coiled tubing rig is the continuous-length of steel coiled tube drill string, which must be bent and straightened many times during its life span. Consequently, a steel coiled tube's performance is influenced by two main factors: (a) low-cyclic fatigue, and (b) degradation of material grade during the bending cycle.

Due to requiring the tubing to undergo repeated bending events over a constrained radius of curvature, the coiled tube undergoes a low-cycle fatigue phenomena, which usually leads to catastrophic fatigue failure (Sisak & Crawford, 1994). Plastic bending of the tube string along with high internal hydraulic pressure causes a residual stress on the body of the tube. As a result there is a material property degradation from accumulated residual stresses during cyclic loading and also potential anisotropic behaviour of the low alloy steel material. Consequently, a proper tube material and appropriate manufacturing process have been developed.

This thesis tests and expands on a comparison exercise between steel and an alternative material - composite. Composite filament wound fibre reinforced tube with the possible addition of a thermoplastic liner (as a pressure barrier) with high strength and stiffness to weight ratios also presents an alternative fatigue life characteristic

compared to steel (Harris, 1986). A composite coiled tube may have advantages over steel. However, the heterogeneous and anisotropic behaviour of a composite material may make the design and working life prediction of a composite tube more complex than that of a steel tube (Nielsen, 2005).

The aim and objective of this research is to investigate the fatigue failure of a composite tube versus a steel coiled tube for application in mine exploration drilling. In this thesis, the fatigue failure process will be investigated through the most appropriate failure criteria. A mathematical finite element model will be used to develop the fatigue and failure analysis. This will be compared with experiments, performed to validate the finite element model results. Statistical analysis of the experimental data will also be performed and discussed.

1.2 Coiled tubing drilling rig

Coiled tubing technology has been practiced in regular oil field borehole cementing and scale removal applications for the last 30 years (Afghoul *et al.*, 1994). Recently, coiled tubing operations have become a proven technology in drilling. In order to facilitate the transportation and drilling rig manoeuvring, the coiled tubing unit design is that of a rig with a smaller foot-print and light in weight (Mazerov, 2008). This capability speeds the drilling operation while decreasing the cost of drilling activities. A typical arrangement of the main components of a coiled tubing rig schematically shown in Figure 1-1 include:

- Work reel which is used to spool the continuous tube string,
- Gooseneck to direct the coiled tube string into and out of the injector head in a smooth path with a specific radius of curvature,
- Injector head, mounted on the top of the wellhead, used to push coiled tube string in and pull it out of the hole,
- Power pack and related control panel for operating the coiled tubing system; for comprehensive control and monitoring the whole mechanism, and
- Fluid pumping system, used to supply operating pressure and circulation fluid.

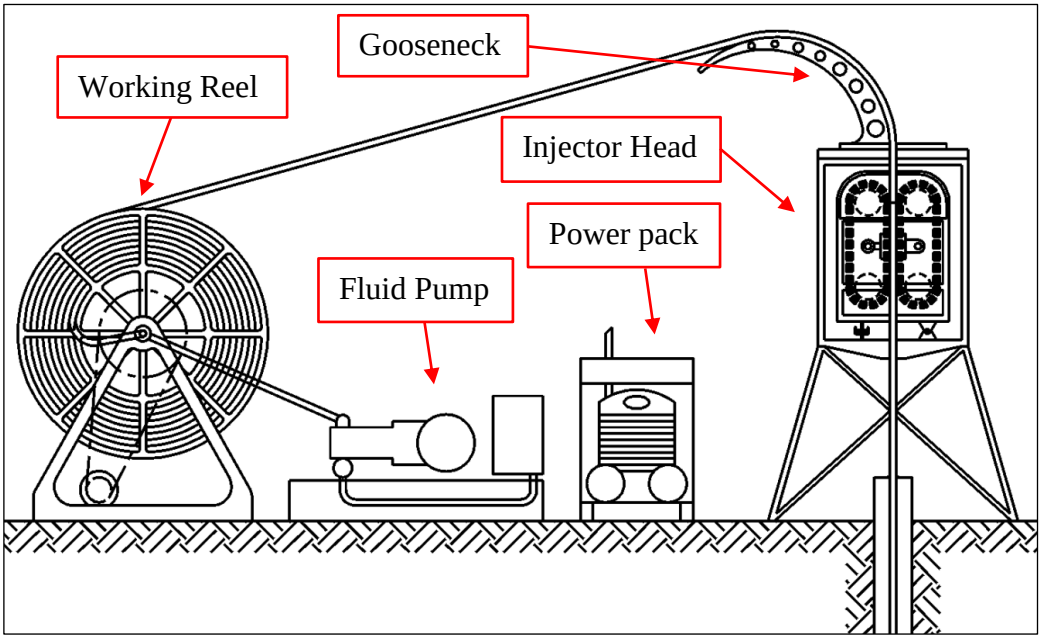

Figure 1-1: Sketch of coiled tubing unit (Zhong *et al.*, 2009).

The advantages of utilizing a coiled tubing rig as opposed to a conventional rotary rig for drilling operations are:

- No need to make pipe connections, so faster running in and pulling out pipe from the well,
- Circulating while tripping in and out of the well,
- Easy rig moves manned by less rig crew, and
- Real time down-hole data gathering through an electric wire (for steel coiled tube) and fibre optic lines (for composite coiled tube).

Some of disadvantages of coiled tubing drilling can be listed as:

- Limited pulling load and lower weight-on-bit compared to conventional rotary rig due to less tube strength and low weight per length of tube, respectively,
- Low pumping flow rate for limited coiled tube diameter, and
- Short coiled tube life due to cyclic fatigue and need to replace coiled tube so high operational cost.

Due to the repeated cyclic bending loading on and off the working reel and gooseneck, the coiled tubing string experiences a high degree of stress to its structural body. Apart from normal steel corrosion and mechanical damage, the tri-axial forces applied on a coiled tubing string result in (Zifeng *et al.*, 2012):

- Axial load (tension or compressional forces),

- Internal and external pressure (hoop stresses),
- Bending load (on the gooseneck and working reel).

These stresses cause the coiled tube to plastically deform after every bending and subsequent straightening event which introduce significant residual strain in the coiled tube body (Avakov *et al.*, 1993). The accumulated residual strain in the coiled tube string leads to localized damage and ultimately tube failure.

Figure 1-2 schematically shows the bending events of the tube during running in and out of a well. A coiled tube string experiences three events of plastic deformation when it runs into a well, due to straightening (event 1), bending (event 2) and straightening (event 3) where pulling off the working reel, bending onto the gooseneck and pulling into the injector head are events causing fatigue. In retrieving the coiled tube from the well, three more events occur; bending (event 4), straightening (event 5) and bending (event 6) for running onto the gooseneck, leaving the gooseneck and spooling onto the working reel, respectively (Sas-Jaworsky & Williams, 1993). In total, the coiled tubing string experiences six events of plastic deformation which together are called a "round trip".

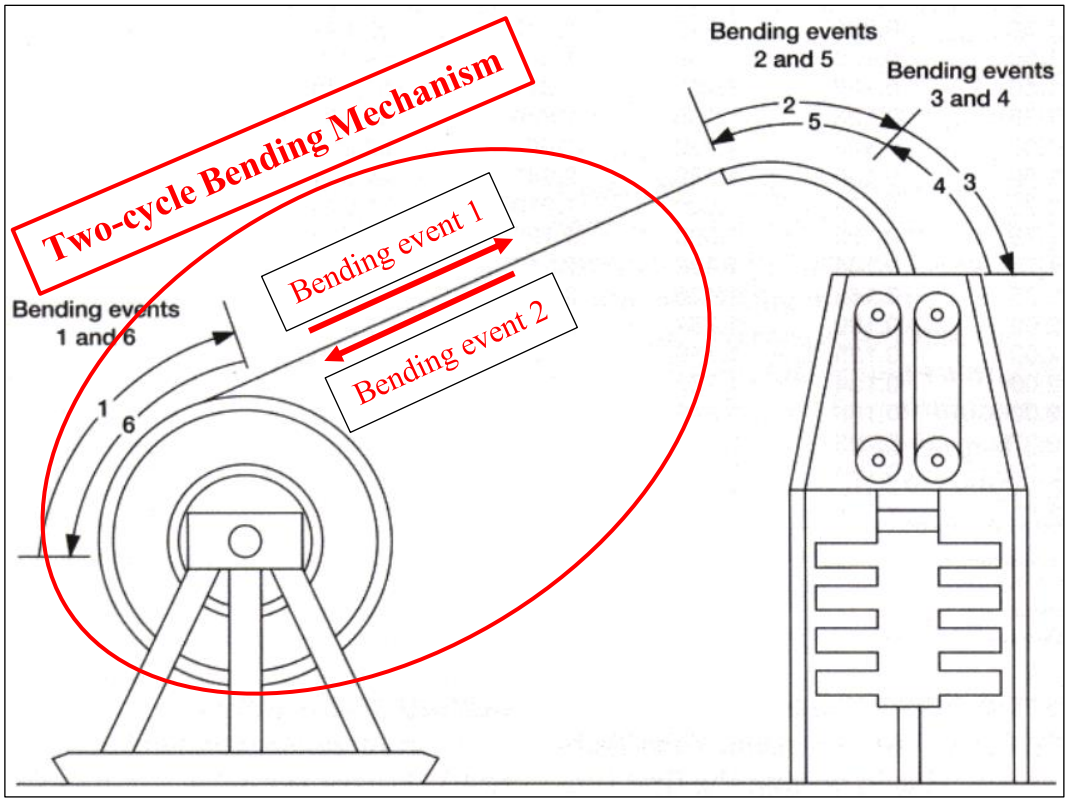

Figure 1-2: Bending events during a trip cycle with and without gooseneck (Sas-Jaworsky & Williams, 1993).

Figure 1-2 shows that four out of six events of the round trip occur at the gooseneck side of the tripping path. Therefore, by eliminating the gooseneck and assuming the same radius of curvature for a working reel and gooseneck, the cyclic life of a coiled tube could theoretically increase by three times. This new bending mechanism is illustrated in Figure 1-2 coloured red as a "two-cycle bending mechanism". In order to minimize tool face deviation during coiled tubing drilling, a three-roller straightener (as shown in Figure 1-4) may be used to make a reverse bend to the coiled tube to remove the majority of the residual bend (Newman, 2015), but not the residual stress. Consequently, a coiled tubing string can be fed with an almost straight shape into the well. Figure 1-3 shows the prototype coiled tube rig which has been manufactured for the DET CRC program, whereby the straightener component has been placed between the working reel and the injector head.

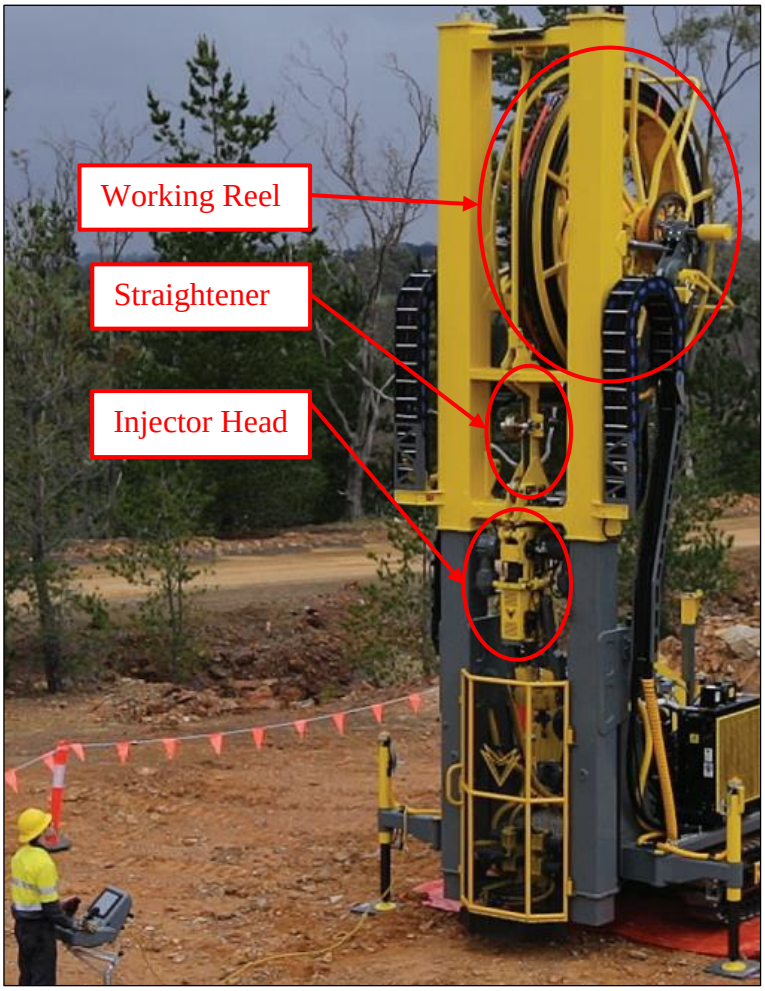

Figure 1-3: RoXplorer coiled tubing rig, Courtesy of DET CRC.

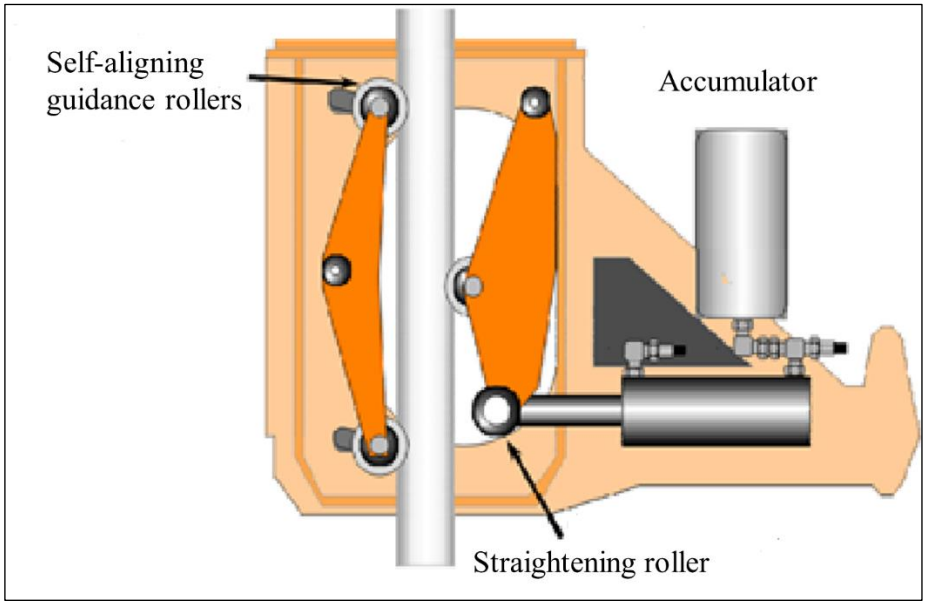

Figure 1-4: Straightener mechanism (Newman *et al.*, 2014).

1.3 Objectives and Scope

The overall objective of this research is to develop a failure analysis method and to evaluate the fatigue life of composite versus steel coiled tubes. My literature review illustrates that few studies have been conducted to predict the fatigue life of composite and steel coiled tubes based on non-linear finite element analysis. Hence in this research, fatigue life analysis of composite and steel tubes have been undertaken using non-linear finite element analysis. The analytical method was then to be validated by experimental studies. The specific objectives of this research therefore includes:

- Modelling fatigue life of commercial HS-90 conventional steel coiled tube via experimental study and analysis of experimental results through statistical methods. Using the extracted data as a baseline for comparison with any higher grade of steel and new designed composite coiled tubes.
- Creating non-linear finite element models and applying fatigue parameters to simulate cyclic bending of steel tube under bending and straightening events in a test machine, in order to obtain theoretical fatigue life values of steel coiled tube.
- Testing cyclic bending fatigue behaviour of ultra-high strength coiled tube (BlueCoil) via the fatigue test machine, and studying the strength of the heat affected areas around its weld line with respect to the rest of the tube body

during cyclic bending experiments. The fatigue life of BlueCoil would be compared with conventional coiled tube.

- Studying the damage evolution parameters of composite interlaminar delamination through finite element modelling under Mode-I unidirectional fracture toughness test conditions.
- Developing a quasi-flexible hybrid composite tube with a thermoplastic liner, as an internal pressure barrier, for imposing high pressure fluid into the tube under cyclic bending load conditions. Obtaining the cyclic bending life of a composite tube through experimental work via a fatigue test machine.
- Creating non-linear finite element models to simulate bending of composite coiled tube while pushing on a curved block (simulating a reel). Interpreting the ply-by-ply stresses and strains and progressive failure analysis using Hashin's failure criterion. Studying behaviour of the layers and interlayers of composite tubes under compression and tension loads.

1.4 Thesis structure

This thesis is divided into two parts, as shown in Figure 1-5. In the first part (Chapters 3 and 4), steel coiled tube fatigue behaviours are studied. The second part (Chapters 5 and 6), focuses on composite coiled tube fatigue behaviours.

- Chapter 1 provides an overview of coiled tubing drilling, objectives and limitations of this research, and presents a brief description of the structure of the thesis.
- Chapter 2 reviews coiled tubing history, steel and composite coiled tube material properties, fatigue failure mechanisms in homogeneous and orthotropic materials, and finite element analysis parameters.
- Chapter 3 discusses an overview of the failure mechanism of an elastoplastic steel material, a finite element modelling of steel coiled tube during bending by utilising a purpose-built bending machine; the cyclic fatigue life of conventional steel coiled tubes presented in the experimental study. Finally, the conclusion compares statistically processed test results with the fatigue life prediction from the finite element modelling.

- Chapter 4 addresses the Hi-Tech steel coiled tube experimental work results. I study the effect of ballooning and fatigue failure in HT-125 (BlueCoil) steel coiled tube in terms of the weld line position.
- Chapter 5 covers fracture analysis and delamination theory of composite structures. I utilise virtual crack closure techniques in finite element modelling to interpret crack propagation behaviour in a composite laminate with different matrix structure, with conclusion comparing the effect of using different matrix materials. The conclusion discusses the stress and strain behaviours in different layers of composite tube and compares these with the stress and strain behaviour of composite tube with a thermoplastic liner.
- Chapter 6 presents orthotropic material behaviours of composite failure criteria with multilayer finite element modelling of composite coiled tube with the internal pressure barrier liner.
- Chapter 7 discusses the analysis of the simulation and experimental results and compares composite versus steel coiled tube fatigue life performances. It then makes a number of recommendations for further work.
- Following the References, Appendix 'A' presents an appropriate method of producing unidirectional composite laminate using the vacuum bagging technique.

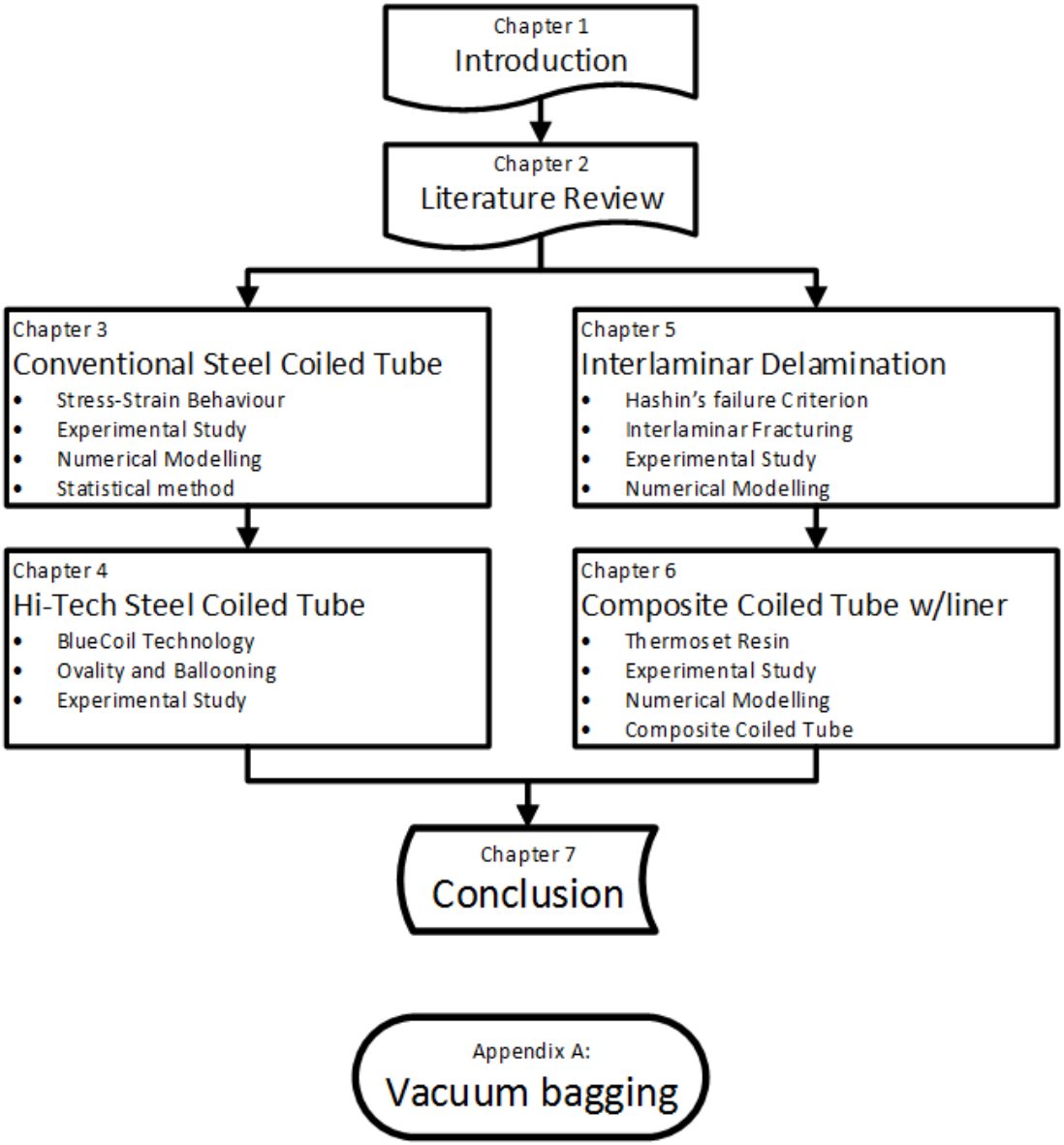

Figure 1-5: Research structure diagram.

References

Afghoul, A. C., Amaravadi, S., Boumali, A., Calmeto, J. C. N., Lima, J., Lovell, J., . . . Staal, T. (1994). Coiled tubing: the next generation. *Oilfield Review*, *6*(4), 9-23.

Avakov, V., Foster, J., & Smith, E. (1993). *Coiled tubing life prediction*. Paper presented at the Offshore Technology Conference, houston ,Texas.

Harris, B. (1986). *Engineering composite materials*. London, UK: Institute of metals London.

Hillis, R. (2015). *Coiled tubing drilling and real-time sensing—Enabling 'prospecting drilling'in the 21st Century.* Paper presented at the ASEG Extended Abstracts 2015: 24th International Geophysical Conference and Exhibition.

Mazerov, K. (2008). Bigger coil sizes, hybrid rigs, rotary steerable advances push coiled tubing drilling to next level. *Drilling Contractor*, 54-60.

Newman. (2015). *Residual curvature and moments in CT due to bending.* Paper presented at the SPE/ICoTA Coiled Tubing & Well Intervention Conference & Exhibition, The woodlands, Texas.

Newman, Kelleher, & Smalley. (2014). *CT extended reach: Can we reach farther?* Paper presented at the SPE/ICoTA Coiled Tubing and Well Intervention Conference and Exhibition, The Woodlans, Texas.

Nielsen, L. F. (2005). *Composite materials: properties as influenced by phase geometry*. Lyngby, Denmark: Springer.

Sas-Jaworsky, A., & Williams, J. G. (1993). *Development of composite coiled tubing for oilfield services*. Paper presented at the SPE Annual Technical Conference and Exhibition, Houston, Texas.

Sisak, W., & Crawford, D. (1994). *The fatigue life of coiled tubing.* Paper presented at the SPE/IADC Drilling Conference, Dallas ,Texas.

Zhong, A., Ehtesham, A., & Howard, R. (2009). *Successful development of coiled-tubing connectors using virtual testing.* Paper presented at the SIMULIA Costumer conference.

Zifeng, L., Xuejiao, L., & Peng, W. (2012). Prebending coiled tubing and its fatigue life prediction. *Journal of Energy Resources Technology, 134*(3), 034502.

Chapter 2 Literature Review

2.1 Background

Research to improve the cost efficiency in minerals drilling is currently being undertaken in Australia. Coiled tubing drilling technology is one of the options being considered as it has the potential to reduce cost and save time in exploration drilling operations. Another advantage of using coiled tubing technology includes a reduced foot-print (Afghoul *et al.*, 1994), hence less environmental impact and reduced safety risk to personnel. Coiled (spoolable) tubing is a well-established technology that has been common practice in the oil and gas industry for drilling and work-over applications since the 1960s (Newman, 1991). Coiled tubing operations are currently based on using conventional steel coiled tubes. Conventional coiled tubes are manufactured from High Strength Low Alloy (HSLA) steel. Recently, a new technology has produced new high-tech steel material that results in better operating performances. Based on a long history of application, coiled tubing services are generally perceived to be the safest and the most reliable with more successful deployments compared with other drilling approaches. Coiled tube must withstand many different loading scenarios, including bending strain, axial loading stress, hoop stress resulting from internal and external pressure, and a combination of these stresses (Starbuck & Eberle, 2000).

Another alternative coiled tube material is that of composite manufacture (Williams & Sas-Jaworsky, 2000). Composite tube material consists of glass and carbon fibres with resin wound on a thermoplastic liner (as an internal hydrostatic pressure barrier). The fibres are embedded into a thermoset epoxy resin and then cured to a certain temperature in an oven. A composite coiled tubing string could give more advantages over conventional and even high-tech steel coiled tubes in terms of higher failure resistance and improvement in cyclic fatigue life (Starbuck & Eberle, 2000). However, because of the complexity of the behaviour of composite materials under dynamic

stress conditions, there is a serious need for data to be generated according to basic principles and reported accordingly (Boller, 1964).

Steel coiled tubing suffers from a number of performance limitations, notably low-cycle fatigue as a result of the bending motion during coiling (Starbuck & Eberle, 2000). This is revealed as plastic deformation caused by repeated elastoplastic bending on the curved surfaces. Moreover, the internal pressure of the coiled tube accelerates fatigue failure by increasing the ballooning effect (Sisak & Crawford, 1994). By comparison, Composite Coiled Tube (CCT) offers the potential to exceed the performance of steel coiled tubing in many cases, particularly with respect to the cyclic life performance, where the bending strains may be absorbed during spooling and unspooling the tube around a large diameter curved surface (working reel).

This chapter is divided into two main parts. The first section discusses composite materials and the mechanics of orthotropic materials, explaining how lamina material stiffness is obtained, and the history of manufacturing and operation of composite coiled tube. The second part is about failure analysis including the development and theory behind the failure of elastoplastic steel materials, the relationship between stress and strain when combined elastic and plastic strain rates occur, and the history of manufacturing and operation of conventional and high-tech coiled tubes.

2.2 Composite coiled tube

2.2.1 Failure analysis of composite material

The application of fibre-reinforced composite materials has grown due to their high stiffness, high strength and good fatigue life (Sisak & Crawford, 1994). Composite materials have an inhomogeneous and anisotropic structural behaviour and hence, the fatigue life prediction of a composite material is more complicated than that of homogeneous steel. This results in different damage sequences in a composite material consisting of matrix cracking, de-laminations, interface failure, fibre fracture, etc (Degrieck & Van Paepegem, 2001).

The cyclic fatigue behaviour of steel is far different from that of fibre-reinforced composites. As shown in Figure 2-1, in a steel material, the fatigue regularly starts and continues without any significant reduction in stiffness. This phenomena goes on until in the last bending cycles, micro-cracks appear in the composite structure. The growth

of the micro-crack easily convert to a large crack and sudden failure of the steel structure happens.

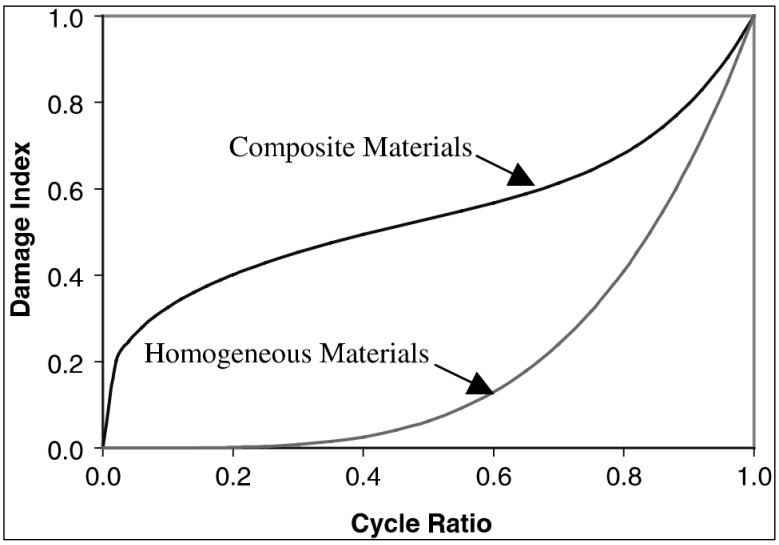

Figure 2-1: Fatigue damage accumulation (Mao & Mahadevan, 2002).

Figure 2-2 shows that failure processes in a fibre-reinforced composite is divided into three regimes: the damage process starts very early with small matrix cracks and then grows steadily between the layers (interface) as a delamination, and finally breakage in fibre completes the failure process. The damage behaviour indicates that computing the stresses within the interface between fibre layers is very important for understanding the failure mechanisms.

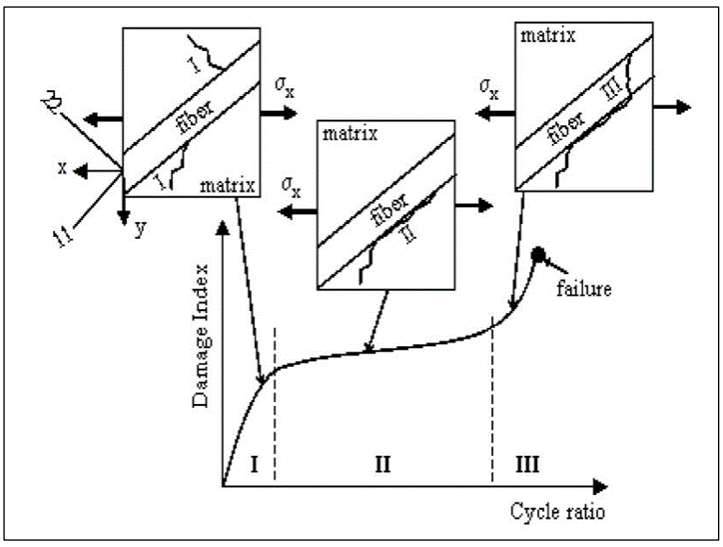

Figure 2-2: Three stages in fatigue processes in composites (Reifsnider *et al.*, 1983).

2.2.2 Finite element modelling

There are different methods of failure analysis in the context of the failure mechanics. Two main cases when modelling the damage in composite materials are delamination and fibre/Matrix damage (ANSYS®, 2013).

Delamination describes the behaviour of crack propagation along a weak path through the interface between the fibre layers. The numerical modelling of delamination in a laminate composite material will be described in Chapter 5. There are two methods of modelling delamination (Hamitouche *et al.*, 2008):

- Virtual Crack Closure Technique (VCCT),
- Cohesive Zone Model (CZM) method.

Fibre/Matrix damage criteria involves evaluation of stresses inside the fibre/matrix layers to determine failure behaviour of the composite material. The numerical modelling of a multi-layer hybrid composite tube will be described in Chapter 6. Some of the general composite failure criteria includes (Kattan & Voyiadjis, 2005):

- Maximum stress failure theory,
- Maximum strain failure theory,
- Tsai-Wu failure theory,
- Tsai-Hill failure theory,
- Hashin's failure criterion.

The strength relates to the failure stress level, the longitudinal direction is the fibre direction and the transverse direction is the direction perpendicular to the fibre.

2.2.3 Maximum stress failure theory

In the maximum stress failure theory, the composite tube laminate fails when the normal or shear stress component becomes equal or more than the corresponding strength. The disadvantage of the maximum stress failure theory is that there is no interaction relationship between the stress components. The failure theory equation is shown as follows (Kattan & Voyiadjis, 2005):

$$\sigma_1^C < \sigma_1 < \sigma_1^T \tag{2.1}$$

$$\sigma_2^C < \sigma_2 < \sigma_2^T \tag{2.2}$$

$$|\tau_{12}| < \tau_{12}^F \tag{2.3}$$

where:

σ_1^T	Tensile strength in longitudinal direction
σ_1^C	Compressive strength in longitudinal direction
σ_2^T	Tensile strength in transverse direction
σ_2^C	Compressive strength in transverse direction
τ_{12}^F	Shear strength in the 1-2 plane
σ_1 , σ_2	Maximum normal stresses in the lamina
τ_{12}	Maximum shear stress in the lamina

2.2.4 Maximum strain failure theory

In the maximum strain failure theory, the composite tube laminate fails when the normal or shear strain component becomes equal to or more than, the corresponding ultimate strain. The disadvantage of the maximum stress failure theory is that there is no interaction between the strain components. This failure theory equation is shown as follows (Kattan & Voyiadjis, 2005):

$$\varepsilon_1^C < \varepsilon_1 < \varepsilon_1^T \quad (2.4)$$

$$\varepsilon_2^C < \varepsilon_2 < \varepsilon_2^T \quad (2.5)$$

$$|\gamma_{12}| < \gamma_{12}^F \quad (2.6)$$

where:

ε_1^T	Ultimate tensile strain in the longitudinal direction
ε_1^C	Ultimate compressive strain in the longitudinal direction
ε_2^T	Ultimate tensile strain in the transverse direction
ε_2^C	Ultimate compressive strain in the transverse direction
γ_{12}^F	Ultimate shear strain in the lamina plane
ε_1,ε_2, γ_{12}	Principal axis strain components

2.2.5 Tsai-Hill failure theory

The Tsai-Hill failure theory is based on interaction failure theory and is derived from the von Mises distortion energy criterion in homogenous and anisotropic unidirectional lamina. Based on this theory, failure occurs when the value of distortion

energy is equal to or more than the strength of the composite lamina. The Tsai-Hill Failure Theory cannot recognize the compression and tensile stresses in composite lamina. Therefore, this underestimates the maximum failure stress on the composite structure. The advantage of the Tsai-Hill failure theory is that there is interaction between the stress components. This failure theory equation is shown as follows (Tsai & Wu, 1971):

$$\left(\frac{\sigma_1}{\sigma_1^T}\right)^2 - \frac{\sigma_1\sigma_2}{(\sigma_1^T)^2} + \left(\frac{\sigma_2}{\sigma_2^T}\right)^2 + \left(\frac{\tau_{12}}{\tau_{12}^T}\right)^2 \leq 1 \quad (2.7)$$

where:

σ_1 , σ_2	Maximum normal stresses in-plane
τ_{12}	Maximum shear stress in-plane
σ_1^T	Tensile strength in longitudinal direction
σ_2^T	Tensile strength in transverse direction
τ_{12}^T	Shear strength in-plane direction

2.2.6 Tsai-Wu failure theory

The Tsai-Hill failure theory is based on interaction failure theory. It is derived from the total strain energy failure theory. The advantage of the Tsai-Wu failure theory is that there is an interaction between the stress components, and it cannot distinguish between the compression and tensile stresses in a composite lamina. The main disadvantage of using this failure theory is the complexity of calculations. This failure theory equation is shown as follows (Tsai & Wu, 1971):

$$F_{11}\sigma_1^2 + F_{22}\sigma_2^2 + F_6\tau_6^2 + F_1\sigma_1 + F_2\sigma_2 + 2F_{12}\sigma_1\sigma_2 \leq 1 \quad (2.8)$$

Longitudinal force parameters:

$$F_1 = \frac{1}{\sigma_1^T} - \frac{1}{\sigma_1^C} \quad (2.9)$$

$$F_{11} = \frac{1}{\sigma_1^T\sigma_1^C} \quad (2.10)$$

Transverse force parameters:

$$F_2 = \frac{1}{\sigma_2^T} - \frac{1}{\sigma_2^C} \quad (2.11)$$

$$F_{22} = \frac{1}{\sigma_2^T \sigma_2^C} \tag{2.12}$$

And shear force parameter:

$$F_{66} = \frac{1}{(\tau_6^F)^2} \tag{2.13}$$

where:

σ_1 , σ_2	Maximum normal stresses in the lamina
τ_6	Maximum shear stress in the lamina
σ_1^T	Tensile strength in longitudinal direction
σ_1^C	Compressive strength in longitudinal direction
σ_2^T	Tensile strength in transverse direction
σ_2^C	Compressive strength in transverse direction
F_i , F_{ij}	Material strength parameters where i, j=1 to 6

2.2.7 Hashin's failure criterion

Hashin's failure criterion is a three dimensional element method which includes fibre and matrix failure in a unidirectional composite laminate. This criterion distinguishes between tension and compressional load within the layers and explains how a composite layer fails under applied load. Hashin's failure criterion predicts the failure of the composite layers through the following equations (Hashin & Rotem, 1973):

Fibre tensile failure:

$$\left(\frac{\sigma_1}{X_T}\right)^2 + \left(\frac{\sigma_{12}}{S_{12}}\right)^2 + \left(\frac{\sigma_{13}}{S_{13}}\right)^2 \geq 1 \tag{2.14}$$

Fibre compressive failure:

$$\left(\frac{\sigma_1}{X_C}\right)^2 + \left(\frac{\sigma_{12}}{S_{12}}\right)^2 + \left(\frac{\sigma_{13}}{S_{13}}\right)^2 \leq 1 \tag{2.15}$$

Matrix tensile failure:

$$\left(\frac{\sigma_3}{Y_T}\right)^2 + \left(\frac{\sigma_{12}}{S_{12}}\right)^2 + \left(\frac{\sigma_{13}}{S_{13}}\right)^2 \geq 1 \tag{2.16}$$

Matrix compressive failure:

$$\left(\frac{\sigma_3}{Y_C}\right)^2 + \left(\frac{\sigma_{12}}{S_{12}}\right)^2 + \left(\frac{\sigma_{13}}{S_{13}}\right)^2 \leq 1 \qquad (2.17)$$

where:

σ_1 , σ_3	Maximum normal stresses in the lamina
σ_{12} , σ_{13}	Maximum stresses components in the lamina
S_{12} , S_{13}	Allowable shear strength components in the lamina
X_T , Y_T	Allowable tensile strength in the lamina
X_C , Y_C	Allowable compressive strength in the lamina

2.2.8 Composite coiled tube characteristics

An alternative to high strength steel for manufacturing a coiled tube string is composite material. The composite material is made of a fibre (carbon, glass or both of them) string or tape embedded in a matrix (resin) which is regularly wound around a liner as a pressure barrier and covered by a wear resistant layer. Coiled (spoolable) composite tube technology was first used as surface pipe in the 1990s. Later, Halliburton and Statoil companies developed an advanced well intervention system using composite coiled tube with 1.5 inch outer diameter and 0.25 inch wall thickness in North Sea oil and gas fields, in early 2000 (Coats *et al.*, 2002).

Today, a variety of composite coiled tube is being considered mainly in continuous pipe laying for highly corrosive environments (Feechan *et al.*, 2003). For most well intervention operations, composite coiled tube is used to apply corrosive well chemicals down hole as well as for extended reach work-over operations. Other benefits of composite compared to steel coiled tube include less weight, less friction loss, negligible residual stress and strain and the ability to transfer data via electric conductor or optical fibre embedded in the tube wall.

2.3 Steel coiled tube

2.3.1 Fatigue life modelling of steel coiled tube

Fatigue failure in a metallic structure is the progressive and localized damage process caused by cyclic loading and unloading. During repeatedly applied loads

above a certain threshold, plastic deformation may be followed by micro-cracking which occurs at the high stress concentrated zone such as at a bending point. The process of a developing fatigue, can be described as having three stages (Lee *et al.*, 2005):

- Crack initiation,
- Crack propagation,
- Catastrophic failure.

There are two recognized forms of cyclic loading fatigue: High-Cycle Fatigue (HCF) for elastic load cycling, and Low-Cycle Fatigue (LCF) for plastic load cycling. The amount of cyclic bending before failure is an accepted method for evaluating fatigue life in steel structures. The number of cycles to establish a structure's fatigue life can be specified through either stress-life or strain-life methods. Stress-based fatigue damage is used for elastic cycling and strain-based fatigue damage is used for plastic load cycling. There is a typical relationship between the number of bending events in a certain internal pressure and fatigue life of steel coiled tubing. As shown in Figure 2-3, it has been proven that the higher the internal pressure, the less the cyclic life. The higher the radius of curvature of the tube bending, the greater the cyclic life of steel coiled tube.

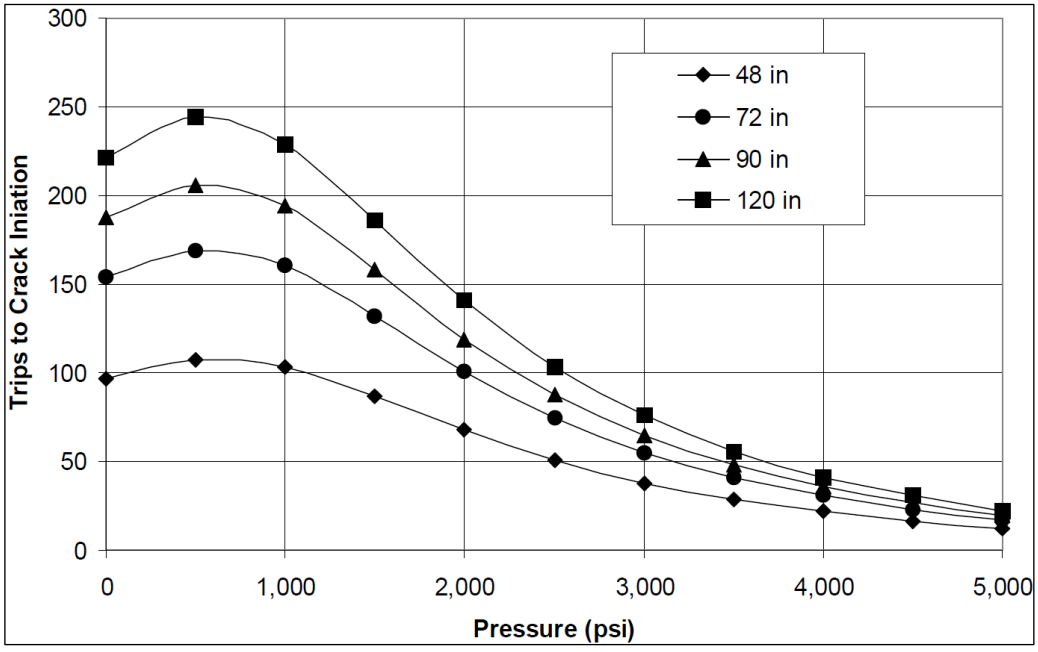

Figure 2-3: Typical fatigue life versus internal pressure and bending radii (CTES, 2005).

The first comprehensive study on low-cyclic fatigue behaviour was conducted by Coffin in 1950s (Coffin & Tavernelli, 1959). He considered the Bauschinger effect (Bauschinger, 1886) to describe fatigue in ductile metals. Then, Manson suggested the four-point correlation and universal slopes methods (Manson, 1965). This method was used to depict the strain-life curve on a log-log scale for the plastic and elastic strains separately (Figure 2-4). In Manson's method, the strain-life fatigue curve properties are estimated from uniaxial tensile experiments (Park & Song, 1995). The Coffin-Manson equation is presented below:

$$\frac{\Delta\varepsilon}{2} = \frac{\Delta\varepsilon_e}{2} + \frac{\Delta\varepsilon_p}{2} = \frac{\sigma'_f}{E}(2N_f)^b + \varepsilon'_f(2N_f)^c \tag{2.18}$$

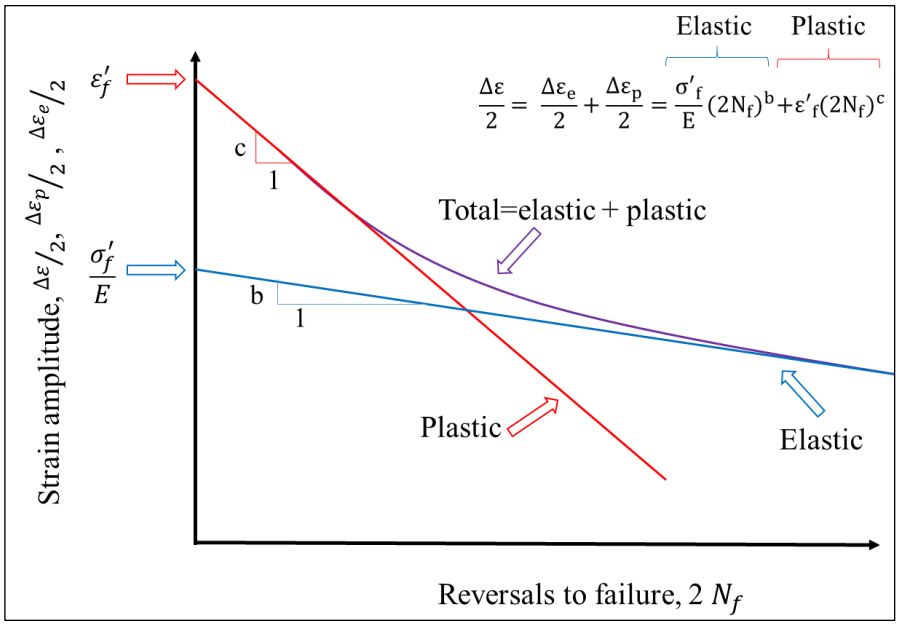

Figure 2-4: Strain amplitude versus number of reversal to failure (Ong, 1993).

where:

$\frac{\Delta\varepsilon}{2}$	Total strain amplitude
$\frac{\Delta\varepsilon_e}{2}$	Elastic strain amplitude
$\frac{\Delta\varepsilon_p}{2}$	Plastic strain amplitude
$2N_f$	Number of load reversals to failure
σ'_f	Fatigue strength coefficient

ε'_f Fatigue ductility coefficient

b Fatigue strength exponent

c Fatigue ductility exponent

The Ramberg-Osgood method (Ramberg & Osgood, 1943) is a stress-strain relation to describe stress versus strain hysteresis loop and considers the strain hardening and softening of the metallic material. The Ramberg-Osgood equation is presented below:

$$\frac{\Delta\varepsilon}{2} = \frac{\Delta\varepsilon_e}{2} + \frac{\Delta\varepsilon_p}{2} = \frac{\sigma_a}{2E} + \left(\frac{\sigma_a}{2K'}\right)^{1/n'} \quad (2.19)$$

where:

σ_a Stress range

K' Cyclic strength coefficient

n' Cyclic strain hardening exponent

The Ramberg-Osgood and the Manson-Coffin equations are not physical laws however they have been derived from a large amount of collected monotonic tensile experimental data (Meggiolaro & Castro, 2004).

Paris-Erdogan law (Power law) and the plane strain fracture toughness (K_{IC}) are used to characterise fatigue crack propagation rates in metallic structures during cycling load condition. The fatigue crack growth damage is proportional to the plastic displacement in the crack tips (Chell, 1984). In this research, fatigue failure analysis was evaluated using Ramberg-Osgood and the Manson-Coffin methods which characterise strain hardening behaviours of steel materials.

2.3.2 Steel coiled tube history

The earliest continuous length of coiled tubing technology was applied to pipelines laid from the coast of England to the coast of France (PLUTO project) in June, 1944. The 3 inches outer diameter tubes with 0.212 inch wall thickness and 12 meters length were butt-welded to produce approximately 1,200 meters of coiled tubing string. These 1,200 meters pieces of coiled tubing strings were butt-welded together, spooled onto a floating drum and unspooled across the English Channel. The first oil and gas application for coiled tubing operations was performed by Bowen Tools in 1965 (Fultz & Pittard, 1990). A 1.315 inch outer diameter and 0.125 inch wall thickness butt-

welding coiled tubing string with 40 Kpsi yield strength was spooled onto a 9 feet diameter working reel and run through in injector head with 30,000 lb pulling capacity (Sas-Jaworsky & Williams, 1993).

The steel coiled tube manufacturing process improved until 1980 when Southwestern Pipe produced new flat strips from High Strength Low Alloy (HSLA) Steel with 70 Kpsi yield strength. Then Quality Tubing invented a bias welding procedure with less heat-affected welding areas to replace the butt welding method. Over the past four decades, manufacturers have produced coiled tubes with a higher yield strength and more corrosion resistance (Feechan *et al.*, 2003) but the weakness of the heat treated welding zone remains a controversial topic.

References

Afghoul, A. C., Amaravadi, S., Boumali, A., Calmeto, J. C. N., Lima, J., Lovell, J., . . . Staal, T. (1994). Coiled tubing: the next generation. *Oilfield Review, 6*(4), 9-23.

ANSYS®, A. R. (2013). *ANSYS mechanical user's Gguide*. Canonsburg, PA: ANSYS, Inc.

Bauschinger, J. (1886). On the change of the position of the elastic limit of iron and steel under cyclic variations of stress. *Mitt. Mech.-Tech. Lab., Munich, 13*(1).

Boller, K. H. (1964). Effect of pre-cycle stresses on fatigue life of plastic laminates reinforced with unwoven fibers. *Defense Technical Information center*(AD0606769).

Chell, G. (1984). Fatigue Crack growth laws for brittle and ductile materials including the effects of statics modes and elstic-plastic deformation. *Fatigue & Fracture of Engineering Materials & Structures, 7*(4), 237-250.

Coats, A., Farabee, M., Song, H., & Berning, S. (2002). *Drilling with composites: An overview of an integrated composite coiled tubing drilling system and components.* Paper presented at the Offshore Technology Conference, Houston, Texas.

Coffin, L., & Tavernelli, J. (1959). The cyclic straining and fatigue of metals. *Trans Metall Soc AIME, 215*, 794-807.

CTES, L. (2005). Coiled tubing manual. *CTES CT Manual, 21*(7), 2005.

Degrieck, J., & Van Paepegem, W. (2001). Fatigue damage modeling of fibre-reinforced composite materials: review. *Applied Mechanics Reviews, 54*(4), 279-300.

Feechan, M., Makselon, C., & Nolet, S. (2003). *Field experience with composite coiled tubing.* Paper presented at the SPE/ICoTA Coiled Tubing Conference and Exhibition, Houston, Texas.

Fultz, J., & Pittard, F. (1990). *Openhole drilling using coiled tubing and a positive displacement mud motor.* Paper presented at the SPE Annual Technical Conference and Exhibition.

Hamitouche, L., Tarfaoui, M., & Vautrin, A. (2008). An interface debonding law subject to viscous regularization for avoiding instability: application to the delamination problems. *Engineering Fracture Mechanics, 75*(10), 3084-3100.

Hashin, Z., & Rotem, A. (1973). A fatigue failure criterion for fiber reinforced materials. *Journal of composite materials, 7*(4), 448-464.

Kattan, P., & Voyiadjis, G. Z. (2005). *Mechanics of composite materials with Matlab*. Baton Rouge, LA: Springer.

Lee, Y.-L., Jwo, P., Hathaway, R. B., & Barkey, M. E. (2005). *Fatigue testing and analysis: theory and practice* (Vol. 13). Burlington, MA: ELSEVIER Butterworth-Heinemann.

Manson, S. (1965). Fatigue: a complex subject—some simple approximations. *Experimental mechanics, 5*(7), 193-226.

Mao, H., & Mahadevan, S. (2002). Fatigue damage modelling of composite materials. *Composite structures, 58*(4), 405-410.

Meggiolaro, M., & Castro, J. (2004). Statistical evaluation of strain-life fatigue crack initiation predictions. *International journal of fatigue, 26*(5), 463-476.

Newman. (1991). Determining the working life of a coiled tubing string. *Offshore, incorporating the Oilman, 51*, 31-32.

Ong, J. (1993). An improved technique for the prediction of axial fatique life from tensile data. *International journal of fatigue, 15*(3), 213-219.

Park, J.-H., & Song, J.-H. (1995). Detailed evaluation of methods for estimation of fatigue properties. *International journal of fatigue, 17*(5), 365-373.

Ramberg, W., & Osgood, W. R. (1943). Description of stress-strain curves by three parameters.

Reifsnider, K., Henneke, E., Stinchcomb, W., & Duke, J. (1983). Damage mechanics and NDE of composite laminates. *Mechanics of composite materials: Recent advances*, 399-420.

Sas-Jaworsky, A., & Williams, J. G. (1993). *Development of composite coiled tubing for oilfield services*. Paper presented at the SPE Annual Technical Conference and Exhibition, Houston, Texas.

Sisak, W., & Crawford, D. (1994). *The fatigue life of coiled tubing.* Paper presented at the SPE/IADC Drilling Conference, Dallas ,Texas.

Starbuck, J. M., & Eberle, C. (2000). Analytical solution for the design of spoolable composite tubing. *Mechanics of Materials, 3*.

Tsai, S. W., & Wu, E. M. (1971). A general theory of strength for anisotropic materials. *Journal of composite materials, 5*(1), 58-80.

Williams, & Sas-Jaworsky, A. (2000). *Composite spoolable pipe development, advancements, and limitations.* Paper presented at the Offshore Technology Conference, Houston, Texas.

Chapter 3 Fatigue life analysis in steel coiled tubes using Weibull statistical distribution method

3.1 Background

During normal well site operations, coiled tube passes over the reel and guide arch, deforming plastically as it runs, in and out of the well. In addition, the internal pressure due to fluid in the tube imposes hoop stresses (Avakov *et al.*, 1993). The accumulated plastic deformation results in low-cycle fatigue of the coiled tube body. Due to imperfections of the steel structure, the amount of bending cycles, during the same operating conditions in fatigue failure experiments, vary significantly. Hence the optimized fatigue life criterion for a coiled tubing string is highly subjective. This study determines the optimum fatigue life for steel coiled tube specimens with 90 Kpsi minimum yield strength using a statistical model.

A purposely-built testing machine was used to test cyclic life for twelve tubes, 6 feet in length and 2 inches outer diameter, under constant internal pressure and a fixed radius of curvature of 55 inches. The tubes underwent bending cyclic loading to destruction for evaluation of their fatigue life. Six of the tube specimens were tested at 1,000 psi and six at 3,500 psi internal pressure.

Due to the limited number of tube specimens, fatigue tests were conducted with the pre-determined weld-line positioned against the bending surface of the test machine. The statistical analysis of experimental data was analysed using the two-parameter Weibull distribution method to compute the confidence level for the different internal tube pressures. The confidence levels assist in finding a more accurate safety margin for fatigue life estimation and consequently optimized drilling costs.

This work presents the results of laboratory tests on the coiled tube specimens to determine the fatigue life and to verify the shape and scale parameters of the Weibull correlation method.

3.2 Introduction

One of the major failures in the use of coiled tubes (almost 30% of total failures) has been caused by the elastoplastic fracture mechanism resulting from low-cycle fatigue in the steel structure of the coiled tube body (J. Li *et al.*, 2008). This kind of failure happens when a coiled tube undergoes repeated bending and straightening cycles, as it passes over curved surfaces (reel and/or gooseneck) while it is running in or out of the hole. The coiled tube structure can be affected by the concentration of stresses and strains, leading to create micro-cracking and finally fatigue failure.

One of the ways to reduce the likelihood of coiled tubing mechanical failures and improve reliability is to understand the fatigue life mechanism and utilize a proper statistical analysis method to process failure results. The standard experimental fatigue test on coiled tube should be conducted using a low-cycle fatigue test method (Sisak & Crawford, 1994).

Repeated bending causes plastic deformation in the coiled tube body as it passes its elastic limit to the plastic region. The plastic deformation imposes a strain concentration to the high stress zones. Consequently, the cumulative strain causes an irreversible strain hardening (or strain softening) to the affected area and finally mechanical failure of the structure of the coiled tube. Internal pressure in the coiled tube during bending accelerates fatigue due to a ballooning effect resulting in an increase in the coiled tube diameter (decreasing wall thickness) (Newman, 1991).

According to the accepted standard in the coiled tubing industry, the working history of mechanical behaviour and geometric parameters along with internal pressure changes of coiled tube specimens should be monitored and recorded at the straightening and curved side of the blocks during bending on the test machine. The test information helps to determine the fatigue life distribution of the coiled tube specimen. Then, through a mathematical correlation, the fatigue life relationship can be obtained from applied bending and hoop stresses and lab experiment results.

The problem of fatigue failure in steel coiled tubes subjected to internal pressure have been studied using cyclic bending fatigue experiments. The mathematical model

determines whether a specific length of the coiled tube would need to be cut off to increase the life of the remaining coiled tube, or whether it should be retired to decrease the possibility of failure in the coiled tube string during well site operations.

The aim of this chapter is to investigate the fatigue failure life of HS-90 steel coiled tube subjected to bending cyclic loading. A statistical method analyses the test results using the Weibull distribution. The Weibull plot results can thereafter be utilized at the various reliability levels for practical coiled tubing applications.

3.3 Stress-Strain behaviour of steel coiled tube

During operations, a coiled tubing string deforms elasto-plastically and undergoes six bending and straightening events on every trip in and out of a well. However, due to negligible coiled tubing string weight, axial load was not applied during the experiment test. Thus, the hoop stress, resulting from internal pressure, and the complex bending stresses provided the necessary data for calculating the accumulated low-cycle fatigue damage along the length of coiled tube.

During the bending cyclic events, the internal pressure imposes additional circumferential stress on the coiled tube. When the coiled tube bends on the curved surface, the material is exposed to elastoplastic deformation along both sides of the neutral axis. This results in the thinning of the wall of the coiled tube on the inside bending zone. Higher internal pressure of tube causes increased hoop stress and hence ballooning along the length of the coiled tube. Thus cyclic bending of the tube at higher internal pressure results in decreased fatigue life of the tube (Sisak & Crawford, 1994).

The stress and strain behaviour of the steel coiled tube during cyclic bending is completely different from that of a unidirectional experiment. The observed response of cyclic bending of a coiled tube specimen is fairly dependent on the state of the material in the steel structure and conditions of the experiment.

In a soft metal, the initial structural dislocation density (cyclic hardening) is low. This starts to increase during cyclic elastoplastic deformation. In a hard metal, the initial structural dislocation density is equally low, but cyclic elastoplastic deformation causes the dislocation density to decrease (cyclic softening). Therefore, the hardening or softening of a metal during elastoplastic cyclic loading is related to the nature of the structural dislocation density in metallic properties (Bannantine, 1990).

There are two hardening rules to describe the changes (size, centre, and shape) in surface yield strength under elastoplastic deformation:

Isotropic hardening: The yield surface strength remains the same shape but expands uniformly, as shown in Figure 3-1, in all directions as the stress and plastic flow increases. This implies that if the same tension and compression yield strength was applied to the metal, the yield surface changes during plastic deformation. Isotropic hardening states that during elastoplastic deformation, the surface of the yield strength expands uniformly around the centre axes of stress (Figure 3-2). Isotropic hardening is often used for large strain or proportional loading simulations. It is usually not applicable for cyclic loading.

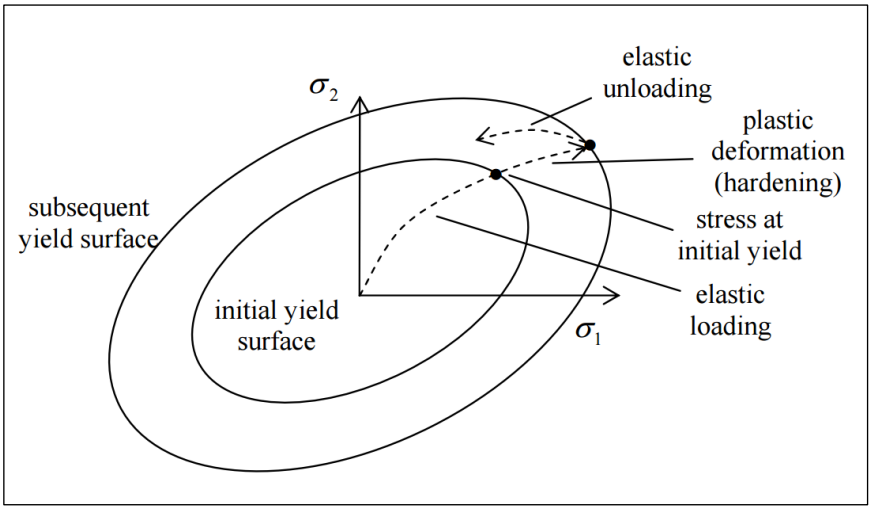

Figure 3-1: Isotropic hardening (Kelly, 2008).

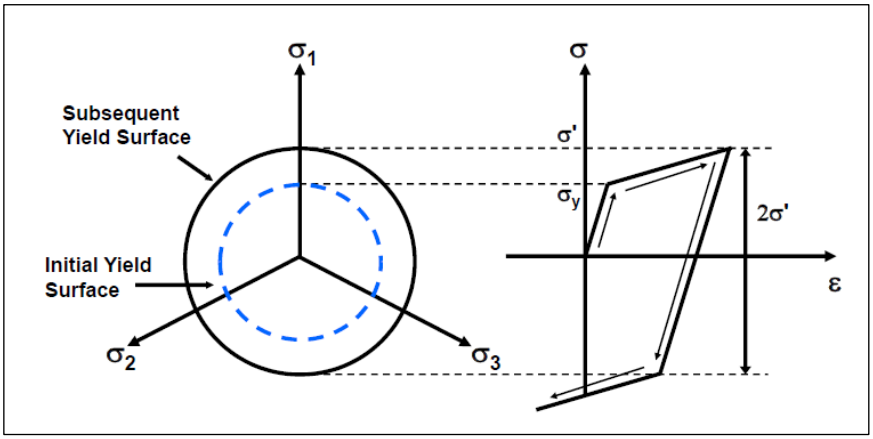

Figure 3-2: Stress-strain behaviour in isotropic hardening (Kelly, 2008).

- Kinematic hardening: The yield surface strength remains constant but its direction shifts, as shown in Figure 3-3, relative to the stress axis. In the case of cyclic loading, most of the metals exhibit kinematic hardening behaviour during elastoplastic deformation conditions. It is normally applicable to cyclic loading conditions with a small strain rate.

  The stress-strain behaviour for kinematic hardening is shown in Figure 3-4. The subsequent surface of the yield strength movement shows a decrease in the amount of yield strength in the compression side while the yield strength value in the tension side increases, in a way that a $2\sigma_y$ (where σ_y is initial yield strength) difference between the maximum and minimum yields is not changing. This phenomenon is dependent on the direction and path of yield strength and is known as the Bauschinger effect (Bauschinger, 1886; Yoshida & Uemori, 2002). It can be commonly observed when the direction of strain work is reversing. The Bauschinger effect occurs when yield strength reduces without a significant change in tensile strength, cross sectional area, and elongation in coiled tube (Newman, 2015).

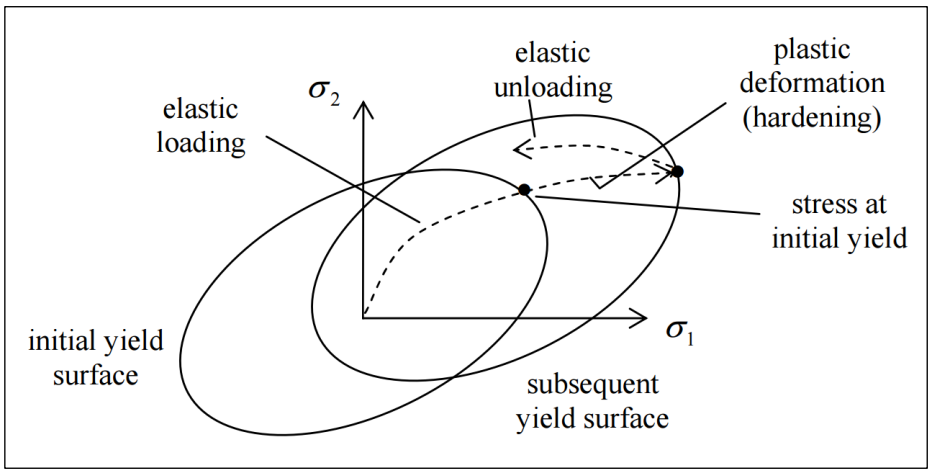

Figure 3-3: Kinematic hardening (Kelly, 2008).

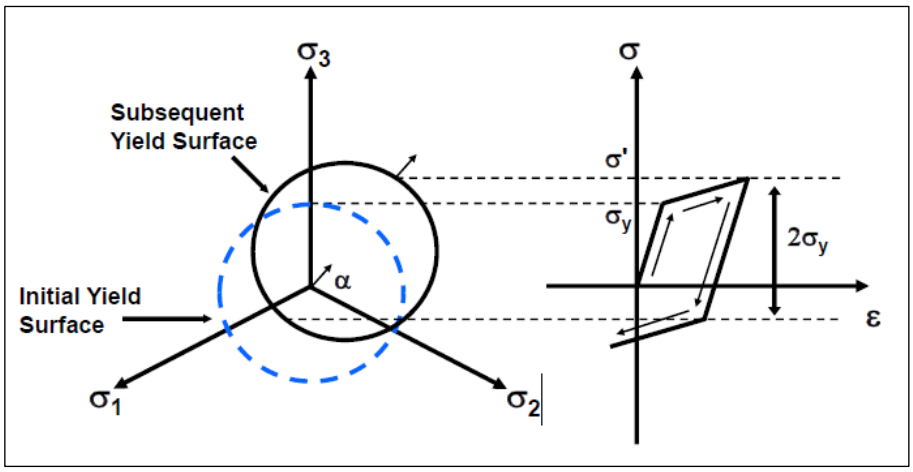

Figure 3-4: Stress-strain behaviour in kinematic hardening (Kelly, 2008).

The Bauschinger effect mechanism is related to the dislocation in most of the polycrystalline metallic structure during the cold work process. Moreover, because of the Bauschinger effect, kinematic hardening is not an appropriate modelling method for very large strain rates. Therefore, the possibility of fatigue failure, resulting from cyclic load bending in coiled tubing experiments is more likely to happen on the compressional side than in the tension side of the tube body.

3.4 Ovality and ballooning

The steel coiled tube is manufactured with almost perfect roundness (with an ovality of less than or equal to 5%). During normal bending cyclic operations, ballooning in the bending zone occurs and the steel coiled tube becomes oval. The outer diameter and ovality usually increase, as the bending cycling continues (Newman, 1991). Increase in ballooning and ovality, increases the possibility of failure in steel coiled tube in comparison to a round one (Boles *et al.*, 2008).

When a steel coiled tube experiences ballooning, the average wall thickness of the tube reduces. Every bending event imposes tensile and compressive stresses on the inner and outer faces of the tube, respectively. Therefore, the stress level is not uniform around the circumference of the tube being bent and consequently, the wall thickness about the circumference of the tube is not equal. Experimental data obtained from lab testing shows that 3% increase in the outer diameter of steel coiled tube decreases the average wall thickness by 7.5% (Sas-Jaworsky & Williams, 1993).

At the end of each experiment at the proximity of the failure point, the steel coiled tube diameter was measured on two axes, the failure axis and neutral axis. The diameter growth rate for each section tested was calculated using the ovality percentage (API Standard 5ST- 2015 - Specification for Coiled Tubing) from the following formula:

$$\text{Ovality}(\%) = \frac{100 \times 2 \times (\mathrm{D_{max}} - \mathrm{D_{min}})}{(\mathrm{D_{max}} + \mathrm{D_{min}})} \tag{3.1}$$

where:

D_{max} Maximum coiled tube outer diameter

D_{min} Minimum coiled tube outer diameter

The ovality together with axial tensile force reduces the collapse pressure of the steel coiled tube. Newman (1991) suggested that the steel coiled tube should be replaced when the ovality reaches 5%.

3.5 Standard fatigue testing machine

For a safe down-hole coiled tubing operation, the cumulative stresses (tensile and hoop) should be kept within 60% of the uni-axial yield strength of the coiled tube (Tipton, 1996). The coiled tube experiences the most stress when it passes onto the reel and gooseneck and the stress level goes beyond the yield strength into the plastic range. Counting the number of bending and straightening events helps in tracking the failure progression.

As a standard method, the CT fatigue data is generated from a cantilever style of bending events (depicted in Figure 3-5). The lower end of the coiled tube specimen is fixed with at least 12 inches of tubing extending below the bending point, in such a way that the clamping pressure of the fixed-end is not affecting the bending stress zone. The test specimen is sealed using purpose-built end-caps and then filled with water. Any trapped air is bled off through the top end connector. Once the set-up tubes are tested using 3,500 psi internal pressure (which is the hole pressure for a down hole motor and hammer) and also at 1,000 psi internal pressure (the pull-out pressure of hole for fluid circulation). The tube pressures were maintained constant throughout the experiments.

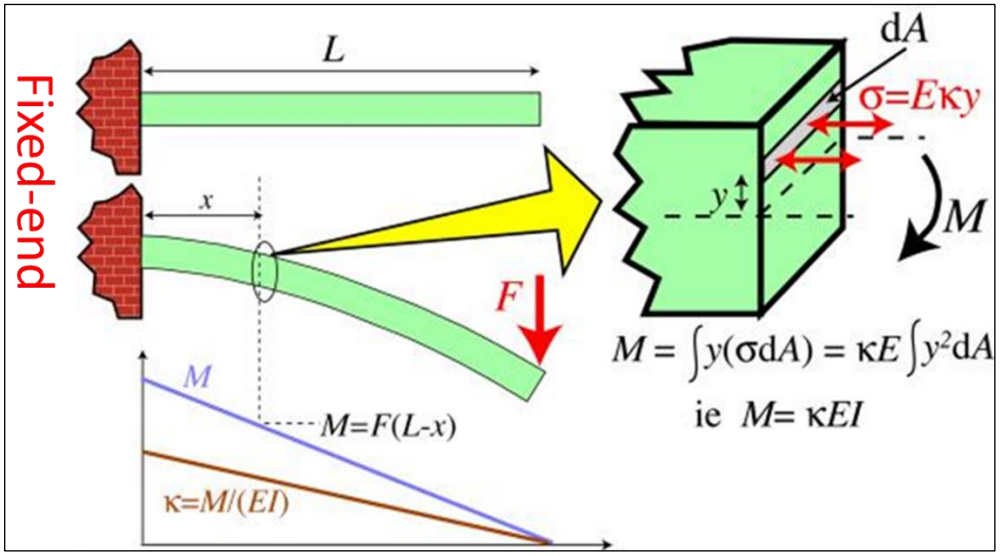

Figure 3-5: Cantilever bending load on coiled tube.

For better understanding of the operational limits to delineate fatigue life, coiled tubing experiments were carried out using a purposely-built bending fatigue testing machine (as shown in Figure 3-6). The most commonly used coiled tube fatigue testing machine was developed by Newman and a group of sponsors including major oil companies, equipment manufacturers, and material suppliers as part of Joint Industry Project in 1993 (Newman & Brown, 1993).

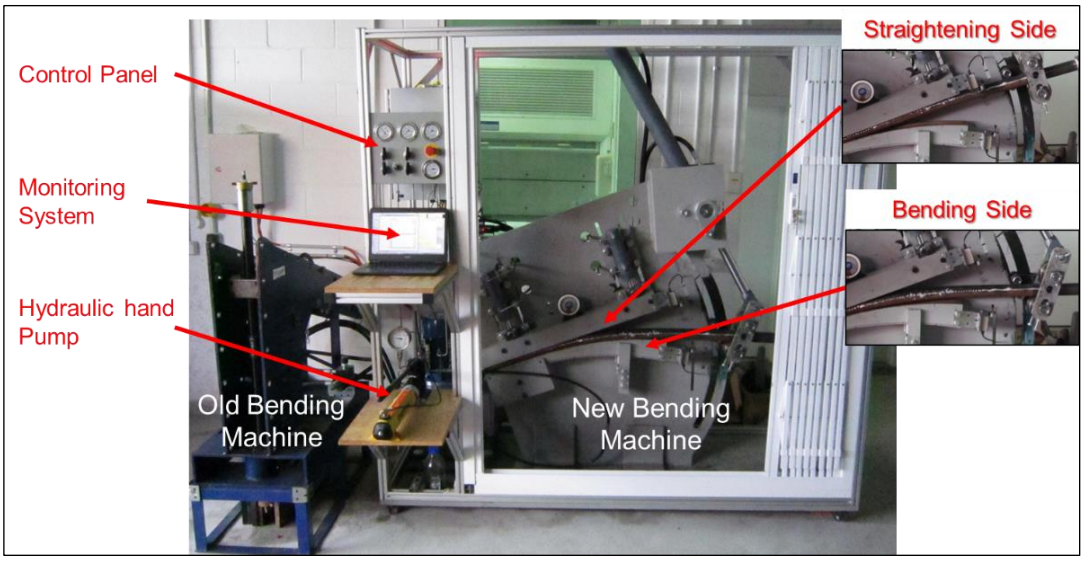

Figure 3-6: Old and new bending machines at Curtin University.

During testing, the internal pressure of the coiled tube specimen was held constant throughout the test. A sample is fixed between a curved and a straight block. The sample is moved back and forth at the free end until a crack initiates, resulting in a pin hole and consequently internal water pressure reduces. The new fatigue life testing machine illustrated in Figure 3-6 was used to characterize the behaviour of fatigue failure and to develop a better understanding of cyclic life in coiled tube specimens for drilling proposes.

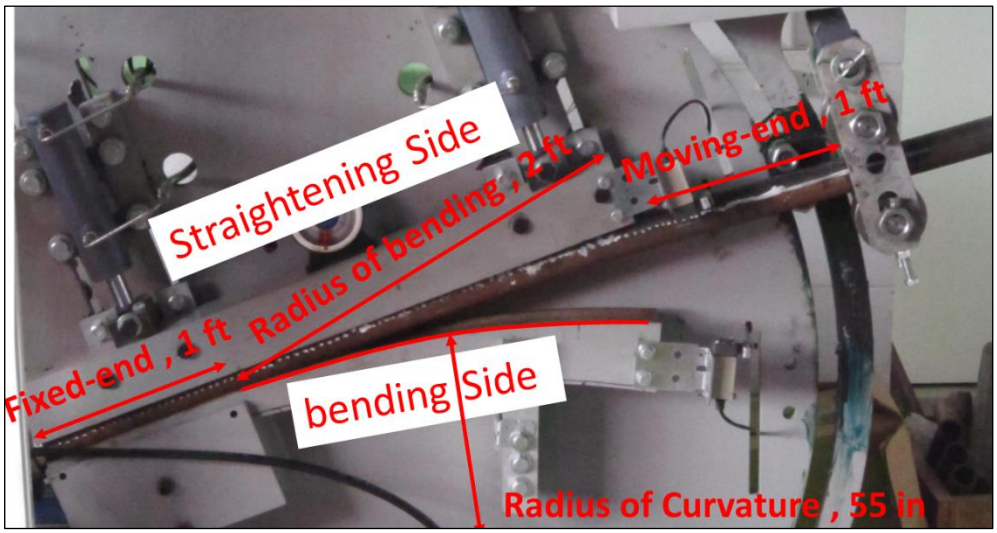

Figure 3-7: Purposely-built fatigue life testing machine at Curtin University.

The test pipe specimen is placed into the bending machine between the bending and straightening blocks and the experiments performed with tubes with different welding seam orientations. During the sequences of an experiment, the orientation of the welding seam may be aligned with the bending block and straightening block and positioned in the neutral axis. The welding seam is marked on the tubes prior to testing. The mark is used as the reference datum for reporting the crack and failure locations on coiled tube specimens.

3.6 Coiled tubing fatigue testing procedure

A total of twelve cyclic bending experiments were performed using HS-90 (90 Kpsi minimum yield strength) coiled tube specimens, supplied by Tenaris Co. which were 6 feet in length, 2 inches outer diameter, and of 0.190 inches wall thickness. Each of the three possible weld line positions were tested, namely the weld line located toward

the curved block side, towards the straightening block side, and positioned on the neutral axis.

The set-up of the cyclic bending experiments is as follows:

- A coiled tube specimen is fixed into the bending machine between two parts of the curved and straightening blocks,
- The free end of the coiled tube specimen is pushed and pulled via two rollers to impose bending and straightening, significant force load being imposed. This simulates the cantilever bending mechanism of a real coiled tubing operations,
- The coiled tube specimen is under internal pressure of 1,000 psi or 3,500 psi during these bending and straightening events,
- A 2 ft segment in the middle of a 6ft piece of the coiled tube specimen is pushed onto a block with a given fixed radius of curvature (55 inches in this experiment) and subsequently pulled back to the straightening block to complete one bending cycle,
- The curved and flat blocks have V-shape groves (Figure 3-8) with 120 degree groove angle. This simulates the contact points of laying the upper layers on the lower layers of coiled tubes during spooling operations,

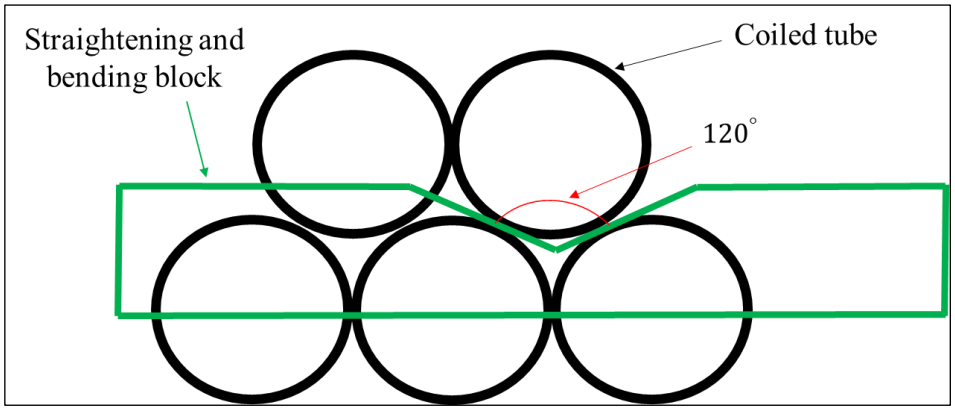

Figure 3-8: Straight and bend surface groove.

- The fatigue bending machine is designed so as to allow the use of lower and upper blocks with different radius of curvature (for reverse bending experiments),

- The bending experiment is performed at a constant speed of approximately 30 seconds per bending cycle,
- The pressure is maintained inside the coiled tube specimen within ±200 psi or ±5% - whichever is larger - of the set pressure value throughout the experiments,
- The coiled tube specimen is filled with water through the lower connection, and its air purged through a valve in the upper connection. Internal pressure inside the coiled tube is applied and fixed at the desired pressure using hydraulic hand pump,
- The coiled tube internal pressure simulates the coiled tubing operation while fluid is pumped into the coiled tube,
- The number of bending cycles are counted until there is a sudden reduction in internal pressure resulting from a pin hole or crack propagating through the wall. Subsequently, the testing operation is automatically stopped by software in-built into the bending machine,
- At the end of the experiment, the diameter of the coiled tube specimen across the longitudinal weld seam and perpendicular to the weld seam is measured for proximity of the ballooned region of the specimen,
- The longitudinal location and angular orientation is also measured -based on the weld line position- of the failure zone measured.

3.7 Numerical modelling

The finite element method was used to simulate the fatigue failure phenomena of a pressurized steel coiled tube specimen in the bending machine. A non-linear three dimensional numerical model was utilized to generate a simulation of cantilever tube bending and the boundary conditions consisted of node sets fixed at one end of the tube and restricted in two degrees of freedom at the other end using WORKBENCH ANSYS 15.0 software.

The focus on equivalent stress and strain in ANSYS-FE model provides useful information to assess fatigue failure. A strain-life approach was adopted for conducting a low-cycle fatigue analysis. The elements were second order, with hexagonal eight node continuum elements and the program applied a uniform constant pressure to the elements on the inside surface of the coiled tube model.

Poor non-linear contact may cause unstable contact conditions with poor convergence to a solution. A proper definition of the contact conditions, size and shape of the meshes contributes to quicker convergence and smoother results. This is especially important when in contact with a curved surface. In this case, it was essential to have similar element sizes (6mm edge size) and shapes (Hexagonal mesh) for the target and source sides.

An appropriate bending displacement was selected, based on the data from the full lab experiments and also from a calculation based on the bending radius of a curved block. The geometrical model assumes that the cross-sectional area of a coiled tube specimen remains circular, which is far from the results of actual experiments. Cyclic bending and straightening causes a coiled tube to become more oval (Shaw & Kyriakides, 1985).

The strain-life method is used to calculate fatigue life. The strain life equation requires a total of 6 parameters to define the material properties; four strain-life parameters ($\sigma'_f, \varepsilon'_f$, b and c) from the Basquin-Coffin-Manson's expression (Equation (2.18)) and the two cyclic stress-strain parameters (K' and n') from the Ramberg-Osgood expression (Equation (3.2)).

$$\varepsilon_a = \frac{\sigma_a}{2E} + \left(\frac{\sigma_a}{2K'}\right)^{1/n'} \tag{3.2}$$

Six strain-life parameters for HS-90 conventional steel coiled tube are shown in Table 3-1:

Table 3-1: Strain-life parameters (Tipton, 2003).

Property	QT-700	QT-800	QT-900	QT-1000	QT-1200	HS-90	HS-110
$S_{y,nom}$ (ksi)	70	80	90	100	120	90	110
E (ksi)	22,910	22,513	25,487	23,318	24,963	24,297	24,242
K' (ksi)	76.57	111.02	109.62	116.67	150.58	95.48	130.29
n'	0.06734	0.09537	0.08042	0.05326	0.070969	0.06227	0.07496
σ_f' (ksi)	148.77	140.19	155.24	199.32	241.50	174.74	187.37
b	-0.14305	-0.1064	-0.11755	-0.1268	-0.13275	-0.136	-0.12055
ε_f'	1.09019	0.78574	0.34656	0.82356	0.81532	1.04388	0.50013
c	-0.7566	-0.7549	-0.6429	-0.82135	-0.8782	-0.7914	-0.74995
σ_f' (ksi)	153.75	142.88	158.84	205.44	248.88	178.91	191.38
b	-0.14305	-0.1064	-0.11755	-0.1268	-0.13275	-0.136	-0.12055
ε_f'	1.30490	0.90567	0.39288	1.00178	0.99484	1.19754	0.57065
c	-0.7566	-0.7549	-0.6429	-0.82135	-0.8782	-0.7914	-0.74995

where:

$S_{y,nom}$	Nominal yield strength
E	Young's modulus of elasticity
K'	Cyclic strength coefficient
n'	Cyclic strain hardening exponent
σ'_f	Fatigue strength coefficient
b	Fatigue strength exponent
ε'_f	Fatigue ductility coefficient
c	Fatigue ductility exponent
ε_a	Total strain amplitude
σ_a	Stress range

Numerical simulations were performed using an ANSYS model for comparison with the experimental results. The model was generated to illustrate the maximum residual strain in a specimen after bending onto a curved surface and removing the bending load (Figure 3-9). The numerical model simulated the applied and released force on the coiled tubing sample in four sequences:

(a) Pushing roller in no-load condition,

(b) Steel coiled tube bent on the curve surface,

(c) Pushing roller return back until the pushing force became zero,

(d) Pushing roller return back to first position.

The model shows that the steel coiled tube undergoes plastic deformation when the bending load is applied. When the bending load is released, the tube does not return to its original straight shape, it stayed in a bent shape, as shown in Figure 3-9. This is attributed to structural dislocation of the steel tube body.

Sample FE-models of a coiled tube specimen at zero psi (Figure 3-10), 1,000 psi (Figure 3-11) and 3,500 psi (Figure 3-12) internal pressure were examined for further analysis of the residual strain and bending mode. As shown in Table 3-2, the high internal pressure shows higher residual strain and more residual bending.

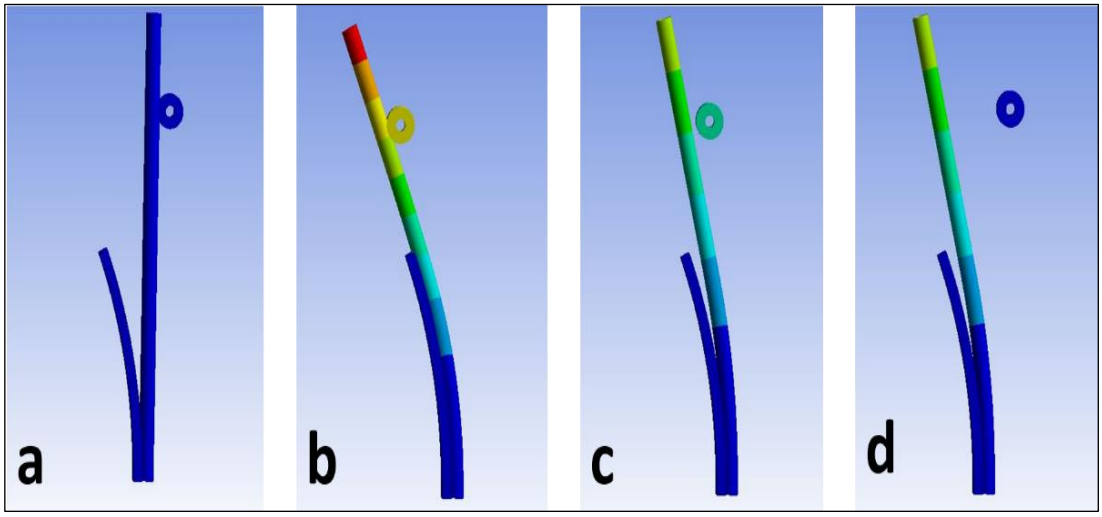

Figure 3-9: Bending sequences.

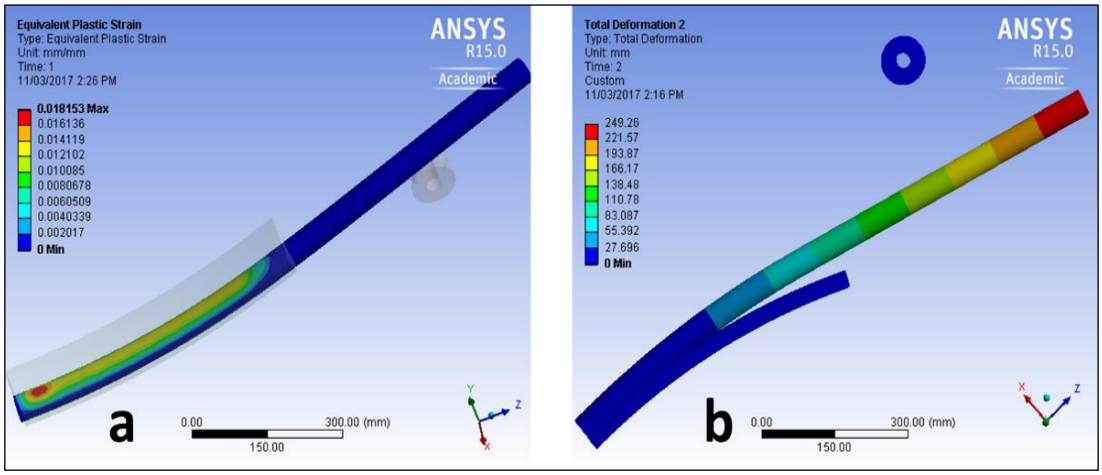

Figure 3-10: Maximum strain and deformation at zero psi.

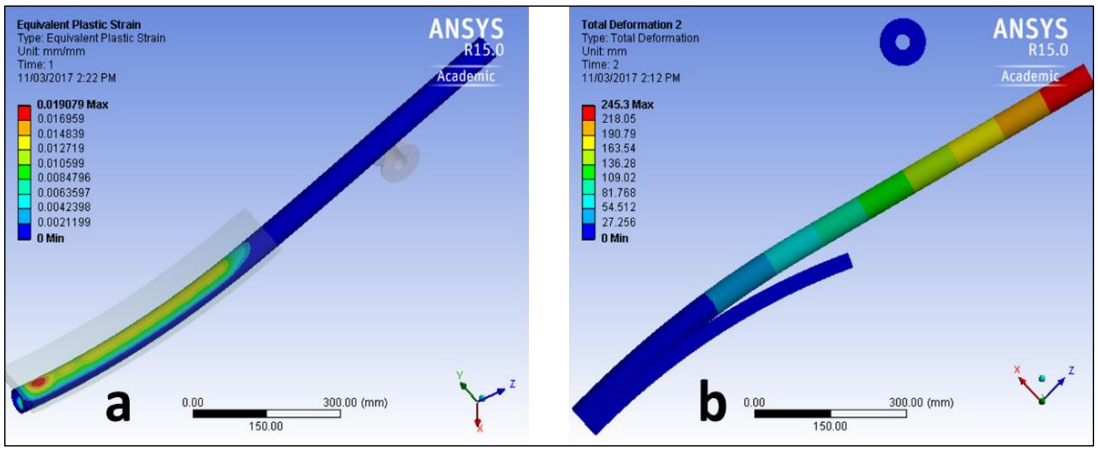

Figure 3-11: Maximum strain and deformation at 1,000 psi.

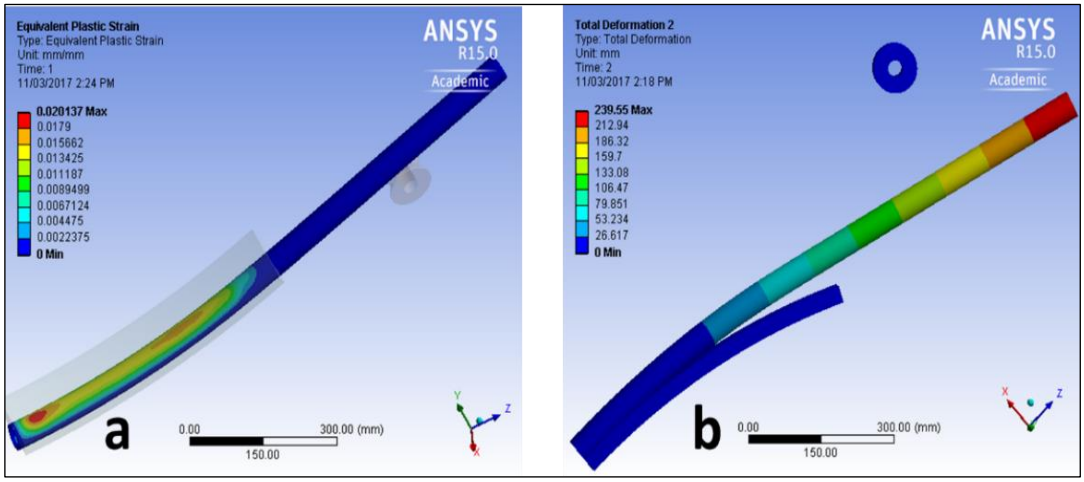

Figure 3-12: Maximum strain and deformation at 3,500 psi.

Table 3-2: A comparison between maximum strains and deformations.

	Internal pressure (psi)	Equivalent Plastic Strain (mm/mm)	Max Deformation (mm)
Coiled tube specimen #1	0	1.81	249.3
Coiled tube specimen #2	1000	1.91	245.3
Coiled tube specimen #3	3500	2.01	239.5

The numerical model simulated the actual experimental specimen, as shown in Figure 3-13. In the FE-model, the coiled tube specimen started from no-load position (a), then it was pushed to complete the bend position on the curved surface (b) and finally returned back to the initial position of a straight shape (c). The force versus the position of the tube (Figure 3-13) illustrates that the coiled tube with specific tube geometries and material properties, pushing roller needs almost 12,000 N force to lay the tube specimen completely on the curved surface. When the pushing force is released, the coiled tube tends to return back to a stable position, therefore it exerts a reaction force on the pushing roller. The coiled tube sample moves back from the curved surface and around 35% of the path towards the straight surface, and the coiled tube becomes stable (no-load position) with a residual bending strain in the tube body. The numerical model simulates this residual bending of the tube. The pulling roller need to apply more than 10,000 N force to return the bent tube sample to the straight shape.

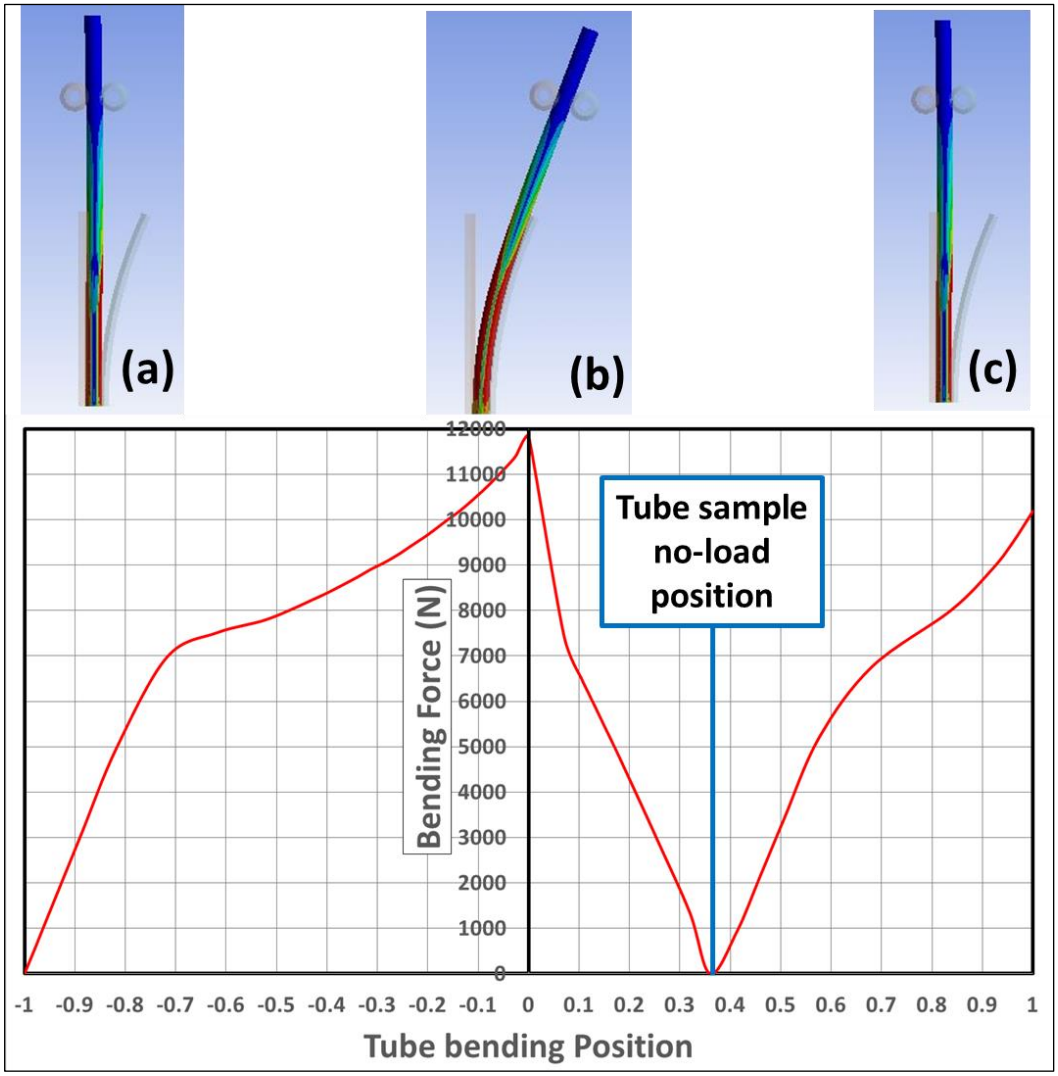

Figure 3-13: Force versus tube bending position.

During bending and straightening modes of the FE-model, the maximum equivalent plastic strain occurs on the bending side of the tube face. In the bending position, the maximum equivalent plastic strain occurs closer to the fixed end of the tube (Figure 3-14) and the maximum value of strain is approximately 1.75%. When the coiled tube returns back to the straightened position, the maximum equivalent plastic strain, which is approximately 1.09%, occurs more close to the edge of the curved surface (Figure 3-15). This proves that there is high likelihood of fatigue failure of the coiled tubing during spooling onto the work reel or bending onto the gooseneck than during the coiled tube straightening.

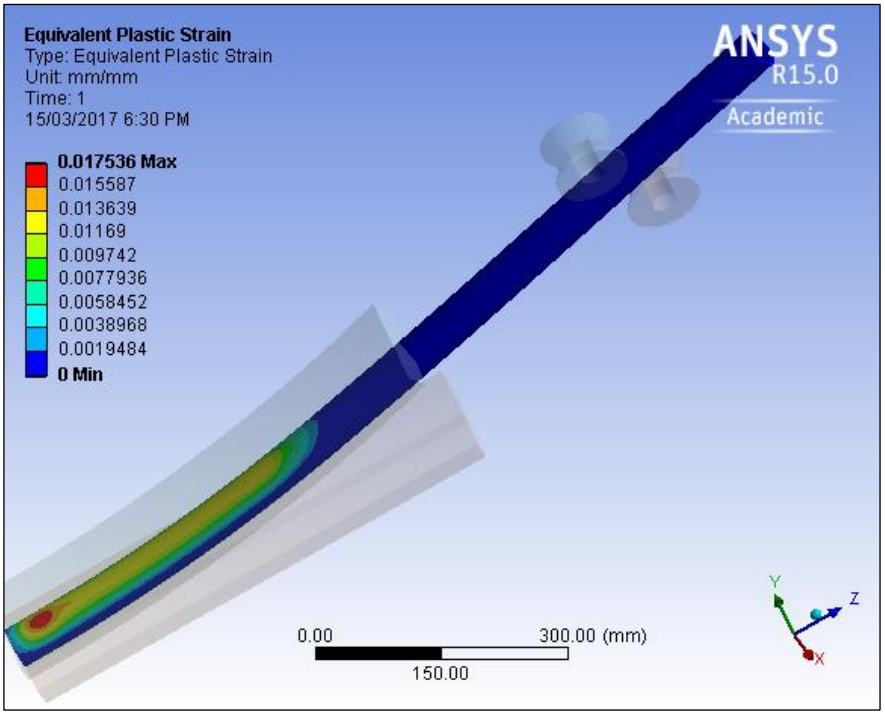

Figure 3-14: Equivalent plastic strain on bending side

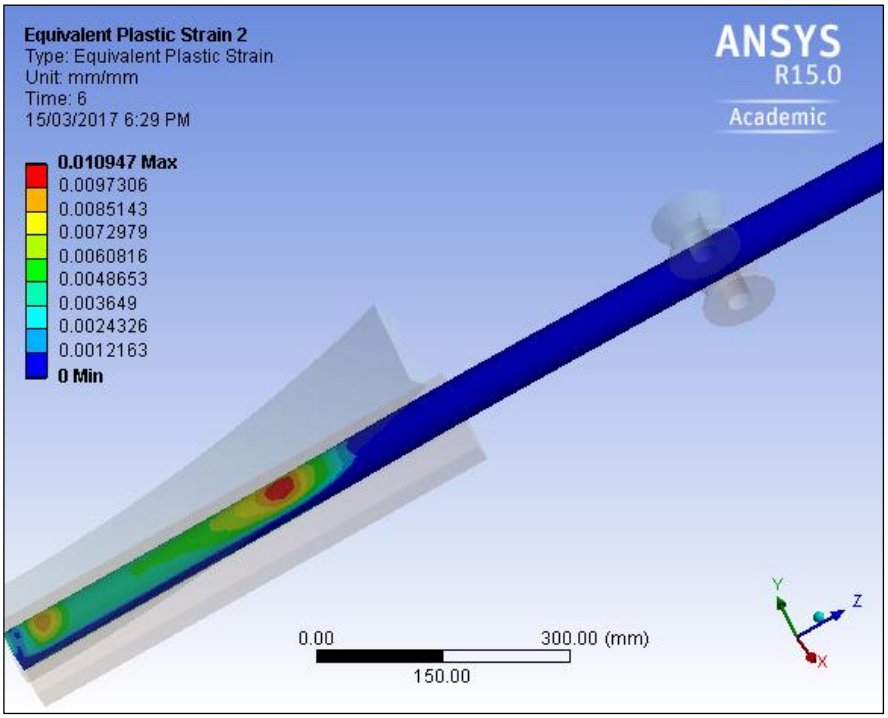

Figure 3-15: Equivalent plastic strain on straightening side.

The strain-life parameters in Table 3-10 were incorporated in the ANSYS fatigue tool. The FE model results indicated that the minimum expected cyclic life

(Figure 3-16) of the coiled tube is estimated to be 522 bending cycles (Figure 3-17) without imposing any internal tube pressure. The numerical modelling result was validated by experimental results performed on six steel tube samples with 1,000 psi internal pressure, as shown in Table 3-10. The average fatigue life for the six samples at 1,000 psi internal pressure was 464 bending cycles. As expected, this is slightly less than the fatigue life at the modelled zero-internal pressure condition.

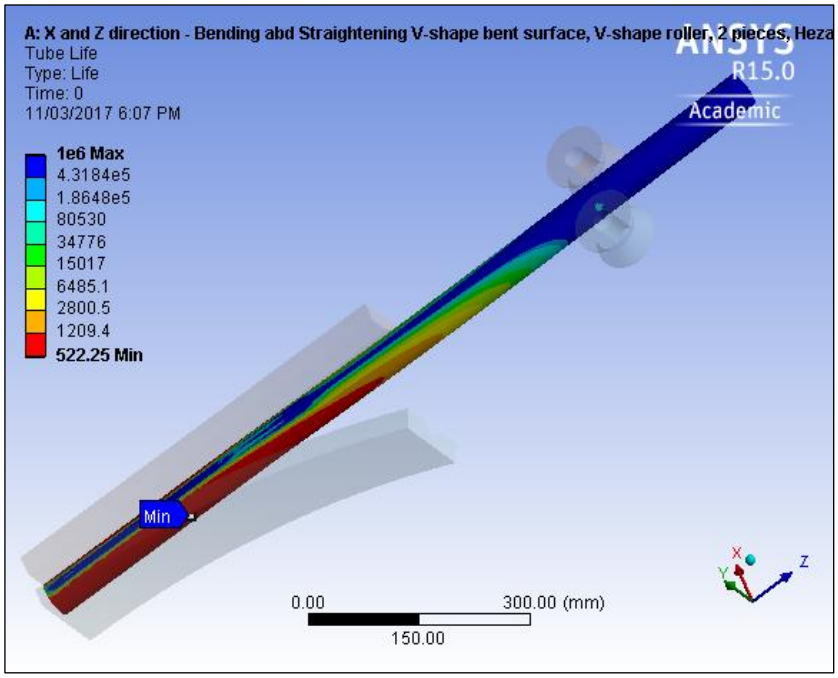

Figure 3-16: Fatigue life of HS-90 steel coiled tube.

Test No	Welding position	Internal Pressure (psi)	
		3500	1000
1	Streighting Side	259	-
2	Streighting Side	279	-
3	Bending Side	191	-
4	Bending Side	191	-
5	Neutral axis	279	-
6	Neutral axis	272	-
7	Streighting Side	-	274
8	Streighting Side	-	352
9	Bending Side	-	436
10	Bending Side	-	448
11	Neutral axis	-	522
12	Neutral axis	-	506

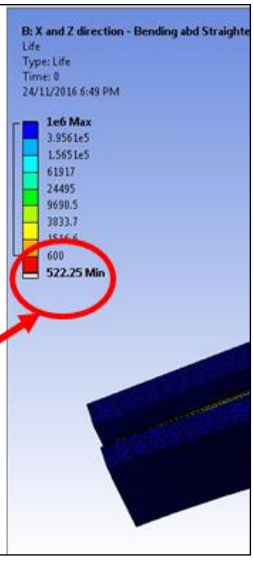

Figure 3-17: Comparison between experimental work and FE modelling results.

A graphical representation of the equivalent stress versus the number of bending and straightening events is shown in Figure 3-18. The trend of the equivalent stress illustrates that after every event (bending or straightening) the maximum equivalent stress is increasing. Hence the increasing number of bending events tend to increase the maximum equivalent stress until the ultimate stress level is reached when the coiled tube body fails. This can be very useful in understanding the cyclic life to fatigue failure and possible effects of the equivalent stress.

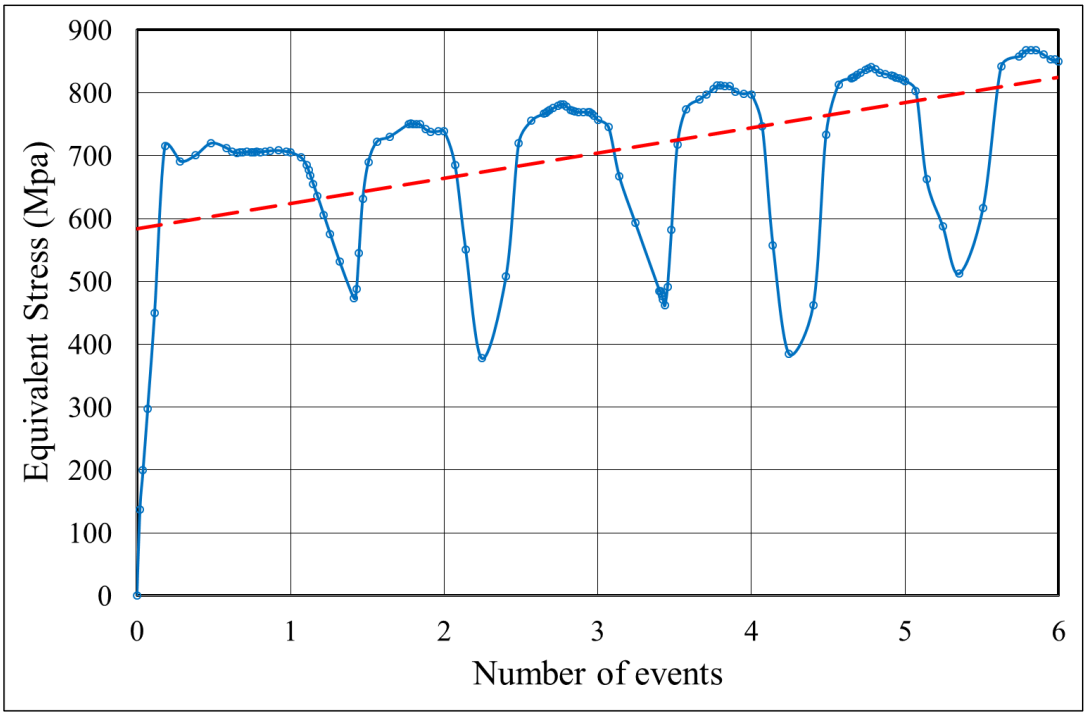

Figure 3-18: Variation of equivalent stress in cyclic events.

3.8 Number of experiments

Coiled tube specimens without any transverse structural discontinuities (e.g. bias or butt welding) were used in the bending fatigue experiments. The bending fatigue standard suggests that the coiled tube specimens be placed into the bending machine with the welding seam position located towards the curved block surface. This mimics the initial situation when the coiled tube is spooled into the reel at the manufacturing yard. The welding seam is originally laying on the reel in factory. While simulating real well conditions, it is necessary, however, to consider all possible positions of a welding seam during spooling and unspooling.

It is obvious that for a specific material grade, the more bending fatigue experimental data, the more reliable the fatigue life results. Table 3-3 shows the typical preferred total number of tests for fatigue failure data, for a particular material grade of coiled tube, according to the coiled tube manufacturer's testing procedure.

Table 3-3: Preferred number of bending experiment.

Test Parameter	**Parameter bins**	**No . Of Experiments**
$\frac{D}{t}$	8-10 , 10-12 , 12-14 , 14-16 , 16-18	5
$\varepsilon_x(\%)$	1.0-1.5 , 1.5-2.0 , 2.0-2.5 , 2.5-3.0 , 3.0-3.5	5
$\frac{\sigma_h}{\sigma_{ys}}(\%)$	Low , 7 , 25 , 40 ,50	5
Total suggested tests for specific material grade		125
Repeating each condition 4 times		500

Tenaris, one the major coiled tube manufacturers, suggested a test plan for fatigue analysis experiments consisted of 125 tests repeated four times totalling 500 experiments for a given grade of steel coiled tube. Due to the unavailability of such a high number of steel tube samples, only 12 tubes were tested. Thereafter a suitable statistical analysis method was applied. A weighting factor for different heat affected zone positions on the welding seam (the weakest region to cyclic loading on a steel coiled tube body) was also utilized.

Instead of performing bending experiments with the welding seam placed at random during testing, the tube sample was installed on the bending machine in a pre-determined order. The cross-sectional area of the steel coiled tube was divided into four sectors; the welding seam against the straightening block; the welding seam laying on the bending block; and the other two with the welding seam located on the neutral axis, as shown in Figure 3-19.

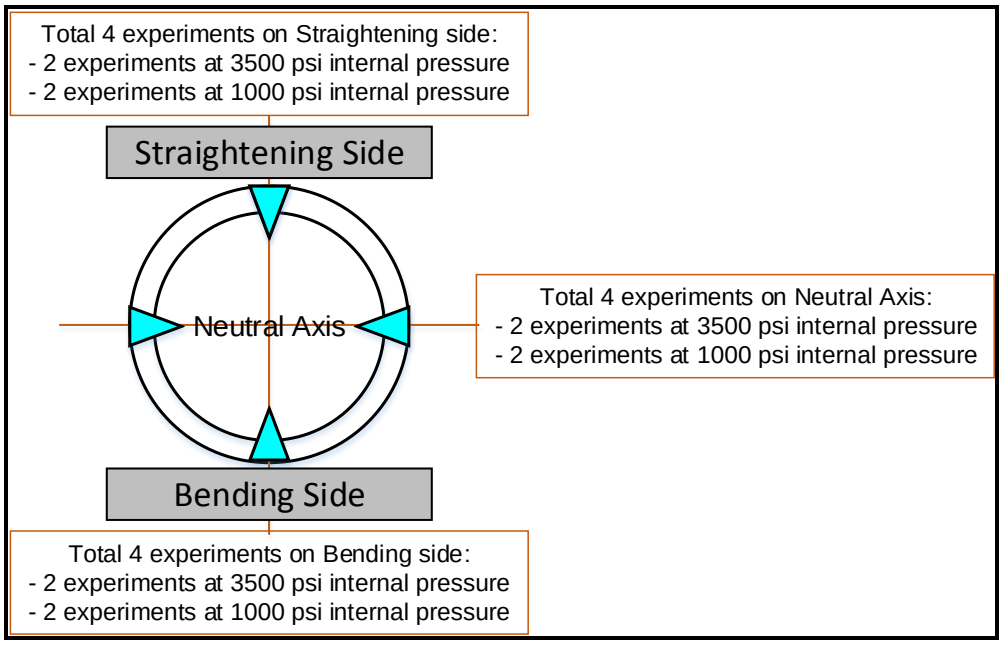

Figure 3-19: Bending experiment arrangement.

Table 3-4 shows the possibility of the welding seam facing the different directions indicated in Figure 3-19 and their related weighting factors.

Table 3-4: Weighting factors for welding seam position.

Item	Welding seam position	Possibility	Weighting factor
1	Straightening side	1/4	0.25
2	Bending side	1/4	0.25
3	Neutral axis	1/2	0.5

3.9 Test results

In order to investigate the fatigue failure and to determine bending cyclic life in steel coiled tube, 12 samples of unused and straight steel coiled tubes with 90 Kpsi yield strength, approximately 6 feet in length each, 2 inches outer diameter and 0.190 inch wall thickness (shown in Figure 3-20) were used for conducting the bending fatigue experiments. The tubes were supplied by Tenaris in the USA. The outside diameter and wall thickness of each sample were measured and recorded before and after each experiment. A steel coiled tube specimen was placed in the bending cyclic

machine (Figure 3-7) against a bending block having 55 inches radius of curvature and a straight block.

Figure 3-20: New steel coiled tubes received from Tenaris.

For each of the welding seam positions given in Figure 3-19, four coiled tube samples were tested, two with 3,500 psi and two with 1,000 psi internal pressure. A total of 12 steel coiled tube specimens were tested as shown in Figure 3-21.

Figure 3-21: Tested steel coiled tube specimens.

The experiment results were divided into three groups, with the welding seam held against the straightening surface (Table 3-5), welding seam against the bending surface (Table 3-6) and the welding seam positioned on the neutral axis (Table 3-7). The fatigue cyclic-life for the twelve tube samples and their welding seam positions are shown in Figure 3-22.

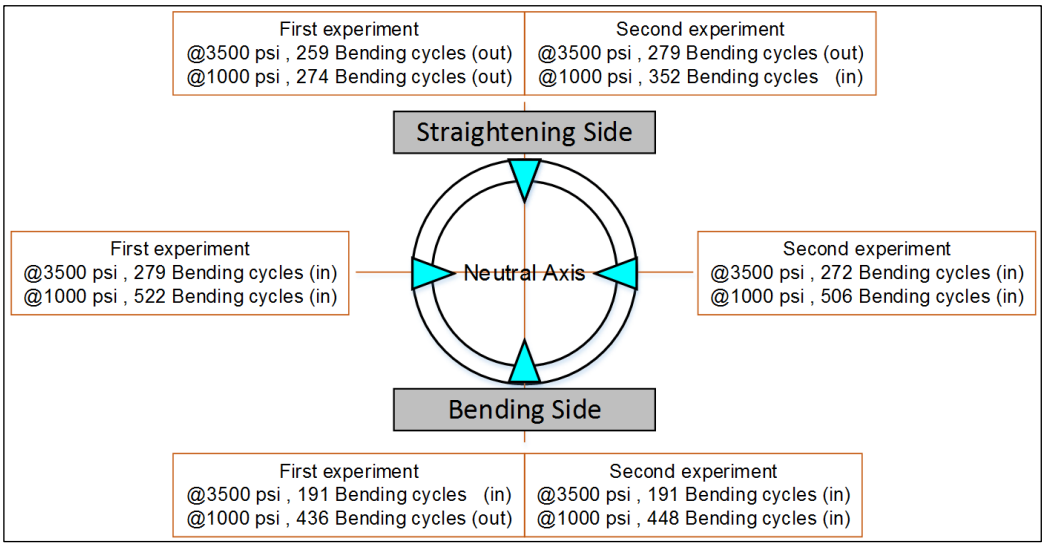

Figure 3-22: Bending experiment results.

Table 3-5: Experiment results - straightening side.

Sample No.	Internal pressure (psi)	Cyclic life (2-ending events)	Specimens
1	3500	279	
2	1000	352	
7	3500	259	
8	1000	274	

Table 3-6: Experiment results - bending side.

Sample No.	Internal pressure (psi)	Cyclic life (2-bending events)	Specimens
3	3500	191	
4	1000	436	
9	3500	191	
10	1000	448	

Table 3-7: Experiment results – neutral axis.

Sample No.	Internal pressure (psi)	Cyclic life (2-bending events)	Specimens
5	3500	279	
6	1000	522	
11	3500	272	
12	1000	506	

The average cyclic-life results of the steel coiled tubes with different welding seam positions on the fatigue test machine are shown in Table 3-8. The best fatigue cyclic-

life of steel coiled tube having a 90 Kpsi yield strength was obtained when the welding seam was placed at the neutral axis. At high internal pressure (3,500 psi), the cyclic fatigue life of the tube was found to be lower when the welding seam was positioned against the bending surface compared to when it was positioned against the straightening surface. However, at lower internal pressure (1,000 psi), the cyclic fatigue life of the tube was significantly higher when the welding seam was positioned against the bending surface.

The geometry of the coiled tube specimens was investigated before and after every fatigue experiment. There was notable variation in tube diameters at the failure zones, referred to as the "ovality" of the tube. The recorded tube diameters at the failure zone for the 12 samples are shown in Table 3-9. The ovality was computed using Equation (3.1). Greater ovality was observed on the steel coiled tubes samples tested at the lower pressure (1,000 psi internal pressure).

Table 3-8: Average cyclic-life in different welding line position.

Average cycilc life	**Straightening Side (Cyclic-life)**	**Bending Side (Cyclic-life)**	**Neutral Axis (Cyclic-life)**
Internal Pressure at 3,500 psi	269	191	275
Internal Pressure at 1,000 psi	313	442	514

Table 3-9: Steel coiled tube fatigue failure data.

Test No	**Welding line position**	**fatigue life**		**Diamater (mm)**		**Ovality (%)**
		at 3500 psi	**at 1000 psi**	**Failure side**	**Neutral axis**	
1	Straightening Side	259	-	56.2	55.4	1.43
2	Straightening Side	279	-	53.8	49.9	7.52
3	Bending Side	191	-	55.5	54.9	1.09
4	Bending Side	191	-	52.5	50.7	3.49
5	Neutral axis	279	-	54.4	51.7	5.09
6	Neutral axis	272	-	51.7	49.9	3.54
7	Straightening Side	-	274	55.2	53.6	2.94
8	Straightening Side	-	352	53.3	52	2.47
9	Bending Side	-	436	56.5	53.5	5.45
10	Bending Side	-	448	54.3	50.1	8.05
11	Neutral axis	-	522	56.9	54.3	4.68
12	Neutral axis	-	506	53.5	49.9	6.96

The distances of the failure zone from the bending point were measured and recorded in Figure 3-23. The results show that for more than 90% of the coiled tubes, failures occurred close to the fixed end and more than 65% against the curved surface. These experimental results validate the results of the numerical model (shown in Figure 3-14). The model indicates that the maximum equivalent strain occurs close to the bending point and against the curved surface.

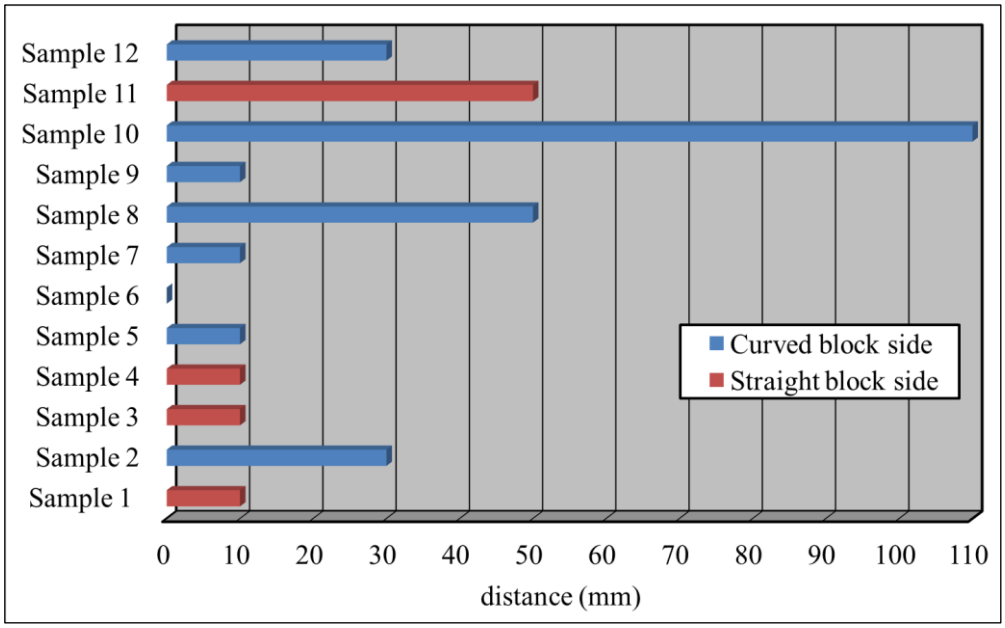

Figure 3-23: Failure zone distance from bending point.

3.10 Weibull distribution method

During tube manufacture, a flat steel strip converts into the shape of a tube. Different parts of the steel coiled tube are exposed to a continuous longitudinal high-frequency induction welding process during forming. This process affects the coiled tube structure with different strain rates having different mechanical properties. Therefore, the steel structure presents different yield strengths, which means that there is no specific yield strength value to represent the mechanical behaviour of a coiled tube sample. In the absence of non-destructive inspection methods, a fatigue life analysis model had to be developed to track this accumulated mechanical damage and predict safe working failure conditions for coiled tubing operations. Hence the development of a statistical analyses method used to specifically predict fatigue failure and to achieve a reasonable safety margin during field operations.

The Weibull distribution is one of the most reliable methods for fatigue life time distribution analysis and material strength evaluation (Weibull, 2013). By using appropriate parameters, the Weibull distribution is used for the determination of fatigue failure properties and modelling the failure behaviours of steel coiled tubes which is based on laboratory experiments using a standard coiled tubing bending test machine (Abernethy, 2006).

The general expression for the three-parameter Weibull Probability Density Function (PDF) is given by (Lai, 2014):

$$f(t) = \frac{\beta}{\eta}\left(\frac{t-\gamma}{\eta}\right)^{\beta-1} e^{-\left(\frac{t-\gamma}{\eta}\right)^{\beta}} \tag{3.3}$$

where:

$f(t) \geq 0$, $t \geq 0$ or γ

$\beta > 0$

$\eta > 0$

$-\infty < \gamma < +\infty$

and:

t	Life time
η	Scale parameter, or characteristic life
β	Shape parameter, or Weibull slop
γ	Location parameter, or failure free life

If the location parameter is not used, the Weibull PDF equation reduces to a two-parameter Weibull distribution. By setting $\gamma = 0$, it gives:

$$f(t) = \frac{\beta}{\eta}\left(\frac{t}{\eta}\right)^{\beta-1} e^{-\left(\frac{t}{\eta}\right)^{\beta}} \tag{3.4}$$

The formula for the cumulative distribution function of the Weibull distribution is given as follows (Rinne, 2008):

$$F(t) = 1 - e^{-\left(\frac{t}{\eta}\right)^{\beta}} \tag{3.5}$$

The reliability function of a Weibull distribution is one minus the probability density function and given by:

$$R(t) = 1 - F(t) = -e^{-\left(\frac{t}{\eta}\right)^{\beta}} \tag{3.6}$$

By taking the double logarithms of both sides of Equation (3.5), a linear regression model in the form of $(Y = aX + b)$ is obtained as follows:

$$\ln\left(\ln\left(\frac{1}{1-F(t)}\right)\right) = \beta\ln(t) - \beta\ln(\eta) \tag{3.7}$$

hence:

$$Y = \ln\left(\ln\left(\frac{1}{1-F(t)}\right)\right) \tag{3.8}$$

$$X = \ln(t) \tag{3.9}$$

and:

$$Y = \beta X - \beta\ln(\eta) \tag{3.10}$$

Weibull used mean ranks for plotting positions. Johnson (Johnson, 1950) suggested analysis using the median rank, which is more accurate than the mean rank.

$$\text{Median Rank (MR)} = \frac{j-0.3}{N+0.4} \tag{3.11}$$

where:

j	Total number of failures
N	Failure order number

The slope of the Weibull distribution line (β) is a particularly significant parameter. It provides the physical behaviour of the failure and determines which part of the Weibull failure distributions describes the data. The β parameter indicates the shape of the failure plot as below:

- $\beta < 1.0$ Infant mortality,
- $\beta = 1.0$ Random failures (independent of age),
- $\beta > 1.0$ Wear out failures.

The shape factor (β) parameter indicates also the width of the distribution of data. The larger the shape factor, the more concentrated the data (Abernethy, 2006).

The characteristic life (scale parameter, η) is related to the mean time to failure. The characteristic life η (by replacing t=η in Equation (3.5)) which is defined as the life of failure occurring at 63.2% of the age of the failure of the material (which is called B63.2 life) is shown in Equation (3.12):

$$F(t) = 1 - e^{-\left(\frac{\eta}{\eta}\right)^{\beta}} = 1 - e^{-1} = 0.632 = 63.2\% \tag{3.12}$$

One of the advantages of using the Weibull distribution is its ability to provide an accurate analysis of the failure and predict the possibility of failure with a few samples or even with inadequate data. The Weibull distribution is the best method for failure analysis with less than 20 samples (Abernethy, 2006) and its plot is shown in Figure 3-24 and

Figure 3-25 illustrates another advantage of the Weibull distribution, in that it can analyse the failure data using a simple and useful graphical method (the Weibull Plot).

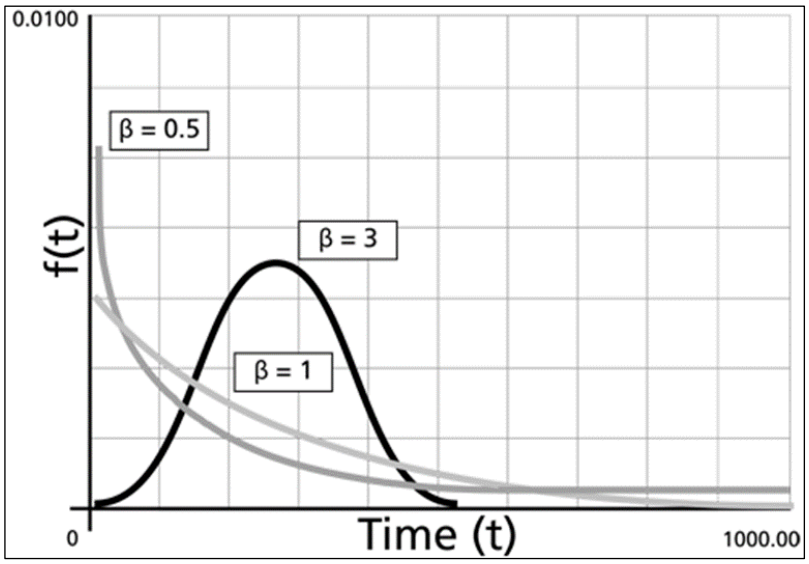

Figure 3-24: Typical Weibull PDF plot (ReliaSoft, 2015).

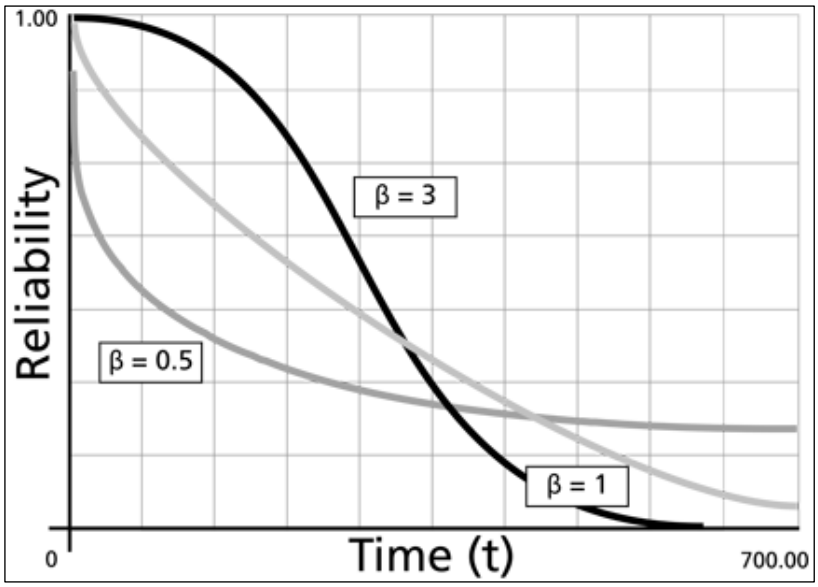

Figure 3-25: Typical Weibull Reliability plot (ReliaSoft, 2015).

3.11 Constructing a Weibull plot

In order to extract a clear safety margin for the cyclic life of a coiled tube specimens (given in Table 3-9), the results need to be analysed using the Weibull distribution as the statistical method. Data processing using the Weibull distribution analysis requires some preparation:

1. Order the fatigue data from the shortest to the longest fatigue cyclic life for every specific test at the same internal pressure.
2. Calculate the median rank (see Equation (3.11)) for each cyclical life value which is between zero and one. The median rank represents the distribution of the specific life value.
3. Apply the Equation (3.8) for "Y" values by calculating the double logarithm of [1/ (1-median rank)].
4. Conduct the linear regression analysis using shape parameters (β), scale parameters (η) and calculate via Equation (3.10) at 3,500 psi and 1,000 psi internal pressure, respectively, as shown in Table 3-10 and
5.
6. Table 3-11. In both bending experiments, the shape factors are more than one ($\beta > 1$) which indicates that the rate of fatigue failure is increasing. This type of fatigue failure is called "wear out failure".

Table 3-10: Bending cyclic life at 3,500 psi from fatigue testing machine.

Cyclic life @ 3500 psi	Rank	Median Ranks	1/(1-Median Rank)	ln(ln(1/(1-Median Rank)))	ln(Cyclic life)
191	**1**	**0.11**	**1.12**	**-2.16**	**5.25**
191	**2**	**0.27**	**1.36**	**-1.18**	**5.25**
259	**3**	**0.42**	**1.73**	**-0.60**	**5.56**
272	**4**	**0.58**	**2.37**	**-0.15**	**5.61**
279	**5**	**0.73**	**3.76**	**0.28**	**5.63**
279	**6**	**0.89**	**9.14**	**0.79**	**5.63**

β	**5.16**
η	**266.44**

Table 3-11: Bending cyclic life at 1,000 psi from fatigue testing machine.

Cyclic life @ 1000 psi	Rank	Median Ranks	1/(1-Median Rank)	ln(ln(1/(1-Median Rank)))	ln(Cyclic life)
274	1	0.11	1.12	-2.16	5.61
352	2	0.27	1.36	-1.18	5.86
436	3	0.42	1.73	-0.60	6.08
448	4	0.58	2.37	-0.15	6.10
506	5	0.73	3.76	0.28	6.23
522	6	0.89	9.14	0.79	6.26

β	4.25
η	464.52

7. Plot the double logarithm of [1/ (1-median rank)] indicated by "Y" in Equation (3.8) versus the logarithm of the bending cyclic life indicated by "X" in Equation (3.9). Draw a trend line for the linear regression through the data points at both operating pressures (1,000 psi and 3,500 psi). The shape parameter (β) is the slope of the trend lines which are equal to "4.25" and "5.16" for 1,000 psi and 3,500 psi internal pressure, respectively.

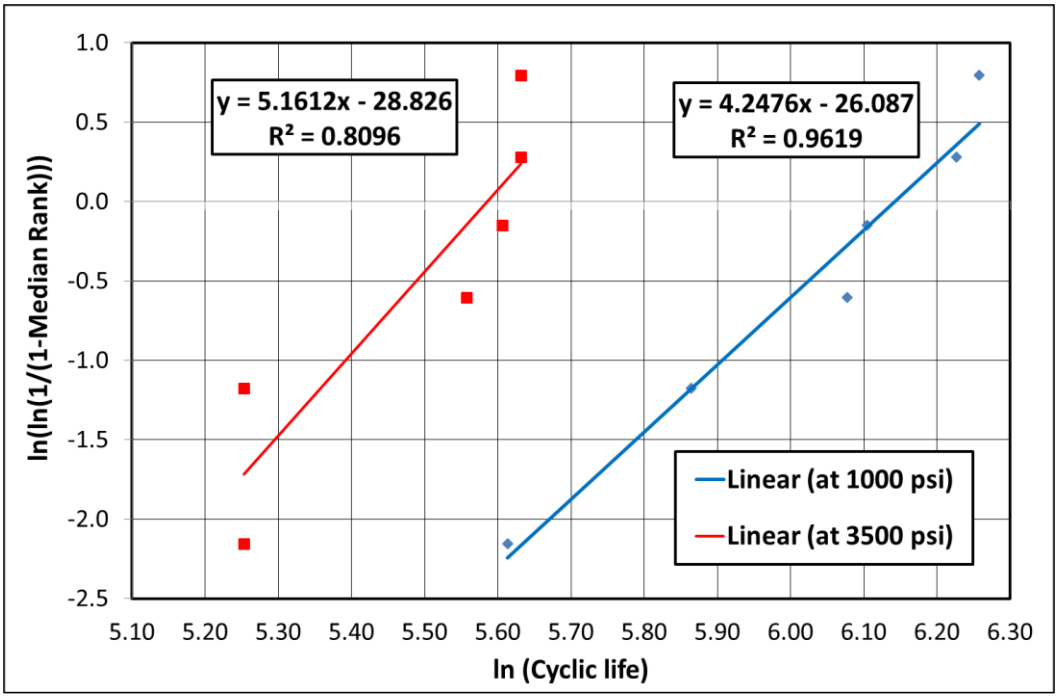

Figure 3-26: Weibull plot with fitted regression line at 1,000 psi and 3,500 psi.

8. Construct the Weibull plot for both groups of data on a log-log axis. In a 2-parameter Weibull distribution analysis, the Weibull plot is a graphical method to determine scale parameters (η). Plot a horizontal line at value of 63.2%. The characteristic life is the cyclic life equal to the scale parameter. The bending cyclic life at the intersection of the characteristic life line and the trend line through the data points for 1,000 psi and 3,500 psi internal pressures are equal to 266 and 464 bending cycles, respectively.

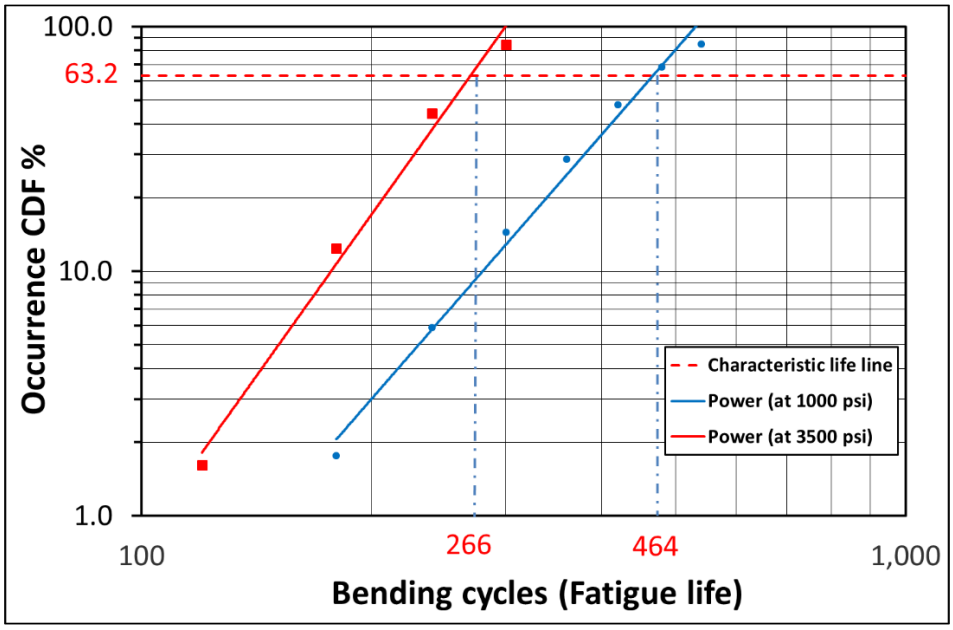

Figure 3-27: Weibull probability plot (log-log).

9. The experimental data was used for five reliability levels (R= 1%, 10%, 50%, 90%, and 99%) under the same operating conditions at 1,000 psi and 3,500 psi internal pressure in Table 3-12. For a better assessment, consider 50% (the middle of the fatigue test failure data) and 99% (almost pure fatigue failure) confidence levels at 1,000 psi and 3,500 psi operation. When these values are put in Equation (3.6) to solve for "t", the cyclic fatigue life values 426 and 157 at 1,000 psi and 248 and 109 at 3,500 psi are obtained for 50% and 99% confidence levels respectively. In other words, the HS-90 steel coiled tube with 2 inch OD and 0.190 inch wall thickness would fail with 50% probability at 426 and 248 bending cycles or more at 1,000 psi and 3,500 psi internal pressure respectively, and similarly will fail with 99% probability at 157 and 109

bending cycles or more at 1,000 psi and 3,500 psi internal pressure, respectively.

Table 3-12: Reliability with 1,000 psi and 3,500 psi internal pressure.

at 1000 psi		
Reliability	**Reliability percentage**	**Cyclic Life**
0.01	**1**	**665**
0.1	**10**	**565**
0.5	**50**	**426**
0.9	**90**	**273**
0.99	**99**	**157**

at 3500 psi		
Reliability	**Reliability percentage**	**Cyclic Life**
0.01	**1**	**358**
0.1	**10**	**313**
0.5	**50**	**248**
0.9	**90**	**172**
0.99	**99**	**109**

10. The fatigue cyclic-life of the steel coiled tube with 90 Kpsi yield strength, 2 inches outer diameter and 0.190 inch wall thickness for three different reliability levels (10%, 50% and 90%) is shown in Figure 3-28. The operating conditions and safety policies dictate the reliability level of the coiled tubing operations. Therefore, knowledge about the effect on reliability changes from the plot of the cyclic life versus internal pressure will help engineers have a better view of coiled tube string design.

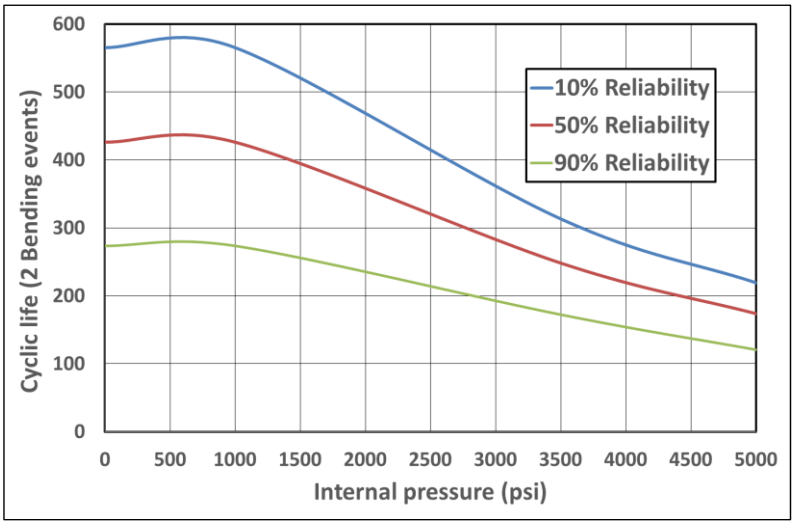

Figure 3-28: Fatigue cyclic-life versus internal pressure.

11. Figure 3-29 and Figure 3-30 illustrate a comprehensive comparison of the cyclic fatigue life of the steel coiled tube specimens at 1,000 psi and 3,500 psi

internal pressures. These graphs depict the Weibull reliability and probability density with each operating pressure at various numbers of bending cyclic life. As an example after 300 bending cycles, the possibility of the steel coiled tube specimens to survive at 1,000 psi and 3,500 psi internal pressure is 15% and 85%, respectively. Therefore, the reliability goal of R (300) is 0.85 at 1,000 psi and 0.15 at 3,500 psi internal pressure. This plot helps engineers to choose proper reliability factor in order to satisfy the best design requirement.

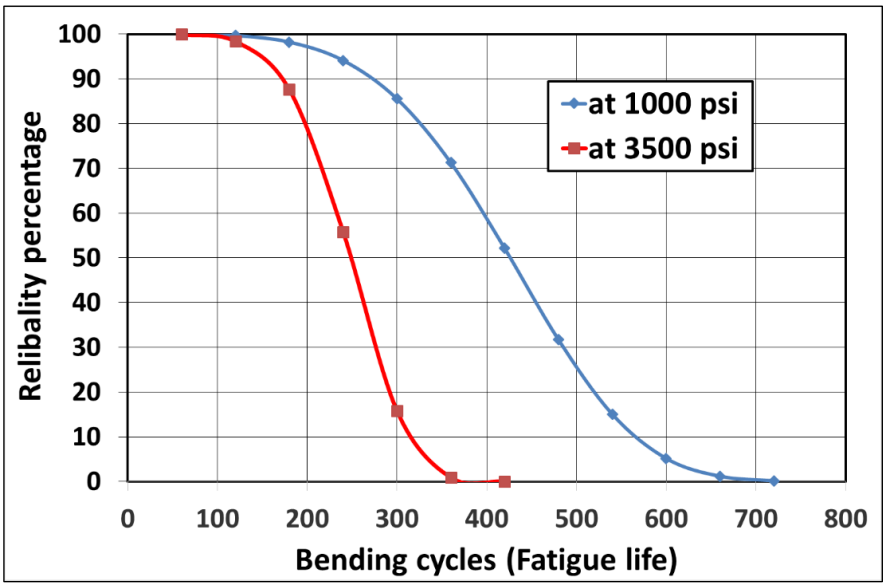

Figure 3-29: Weibull reliability distribution plot at 1,000 psi and 3,500 psi.

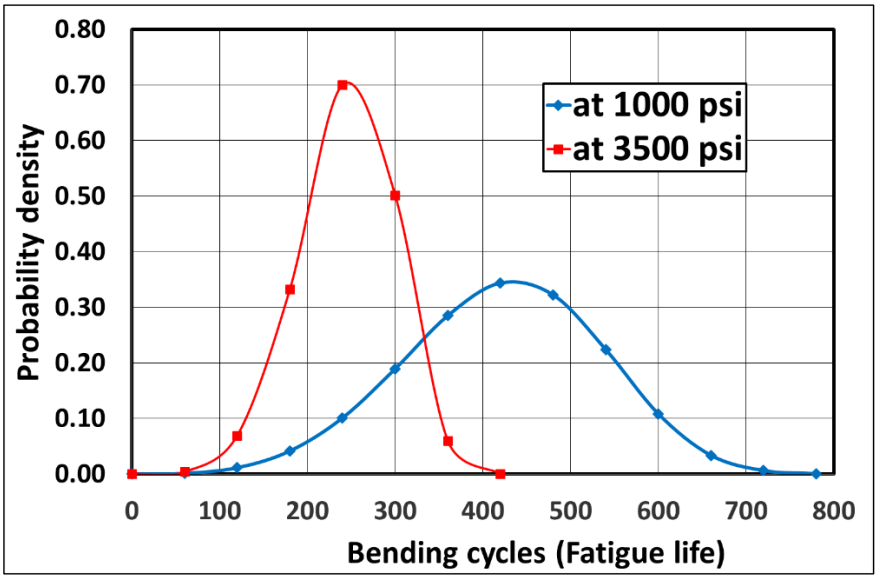

Figure 3-30: Weibull probability density plot at 1,000 psi and 3,500 psi.

3.12 Coiled tubing life management

During a conventional running trip cycle, the coiled tubing string is injected into and retrieved out of the hole, three times. In every bending cycle, the strain rate imposes micro-crack initiation (Tipton, 2003). The crack then spreads within the coiled tube structure to create fatigue failure. Fatigue is not a measurable characteristic of material. Therefore, to avoid a catastrophic failure, it is vital to track the fatigue occurring within the coiled tube and replace it if the cyclic life approaches the estimated fatigue life (Newman, 1991). Hence, the fatigue development needs to be monitored to develop a service working history of the string throughout its service life (Behenna *et al.*, 2003).

In accordance with operational standards, when the total "running meters" approaches 100,000 meters, the coiled tube should be retired (Ackert *et al.*, 1989). In this case, the "running meters" was defined as the distance run in and out of a well (both directions), rather than one directional run. This means a coiled tube must be retired after it reaches the value of "running meters", rather than total failure. In my next approach, I measured the internal pressure and bending radius of the curved surfaces, which are the most important factors that push the stress levels further into the plastic range. Tracking the parameters allows the prediction of the weakened section of the tube before it fails.

The fatigue behaviour of coiled tubes is influenced by the cumulative stresses (bending, axial and hoop stresses) of the structure of the coiled tube (Thomeer & Newman, 1991). For a coiled tube with a constant geometry and specification, and regardless of axial loading, the fatigue cyclic life depends on the number of bending events imposed by spooling on and off the gooseneck and reel, and internal pressure of the coiled tube.

A safe coiled tube operating condition requires an analysis method or organized data gathering system to evaluate the progress of damage and prediction of fatigue life of the coiled tubing string. One of the basic and practical methods of monitoring of quality of a coiled tube is the fatigue life cycle tracking model. An accurate monitoring model increases the reliability of coiled tubing operations.

HS-90 coiled tube with 2 inches outer diameter and 0.190 inches wall thickness was bent while the weld seam was positioned in the neutral axis. In the first experiment, a coiled tube (as shown in Figure 3-31) was tested with 3,500 psi internal pressure to

138 bending cycles and then the test was continued at 1,000 psi internal pressure until the coiled tube failed after 177 bending cycles (total of 315 bending cycles). In the second experiment (as shown in Figure 3-32), the tube was tested first to 177 bending cycles with 3,500 psi internal pressure and then 163 bending cycles at 1,000 psi internal pressure (total of 340 bending cycles).

The test results illustrate that internal pressure based on subdivision of the fatigue life history to specific coiled tube material and sizes, bent on a surface with a constant radius of curvature, is an applicable method for accumulating the tube running calculation. The experimental data validate the operational tube management method with almost 93% accuracy.

Failed CT Specimen 1

Cyclic life (2-bending events)	
First at 3500 psi Internal pressure	Then at 1000 psi Internal pressure
133	177

Figure 3-31: Steel tube test first at high pressure then low pressure.

Failed CT Specimen 2

Cyclic life (2-bending events)	
First at 1000 psi Internal pressure	Then at 3500 psi Internal pressure
177	163

Figure 3-32: Steel tube test first at low pressure then high pressure.

3.13 Conclusions

This chapter presents the results of laboratory fatigue testing on conventional coiled tube specimens, obtained from a purpose-built fatigue test machine. The experimental results of cycles to failure of coiled tubing specimens validate the predictions of the finite element model. The following results were obtained:

- I developed a bending fatigue numerical model using the ANSYS-FE software to accurately predict the fatigue life of a conventional steel coiled tube (HS-90) with 2 inches outer diameter and 0.190 inch thickness bent on a 55 inch radius bending block at uniform internal pressures of 3,500 psi and 1,000 psi.
- The cumulative fatigue life of the HS-90 steel coiled tube resulted from FE modelling validated the "running meters" fatigue life prediction method.
- The finite element analysis method demonstrated a force of load 10,000 N was required for straightening the bent coiled tube. This showed the tendency of the steel coiled tube string to be curved, resulting in pushing against the well bore during running and pulling out of the hole.
- Visual inspection of the tube samples following a laboratory fatigue test indicated a failure position consistent with expectations from numerical modelling. In low and high internal pressure cases the failures were distributed along the curved block, on the inside radius of the tube specimens rather than on the outside radius.
- In conventional steel coiled tube (HS-90) significant ovality was observed for cases involving the low internal pressure (1,000 psi). The average ovality was 5.09% at low internal pressures and 3.69% at high internal pressures (3,500 psi).
- The Weibull distribution plot showed that the larger the probability of failure, the less the fatigue life of the steel coiled tube.
- Linear finite element modelling tends to give an over-estimated prediction of the fatigue life of the materials, whereas using the non-linear finite element model gives results very close to the predicted fatigue life.
- The Weibull distribution analysis depicts a plot which illustrates the relation between the cyclic life and expected reliability of a specific coiled tubing string. This plot can help engineers to predict the fatigue life of the steel coiled tube for different operations with a higher level of confidence.

- The maximum equivalent stress in steel coiled tube increases as the number of the cyclic life value (bending and straightening) increases. This provides a reason for failure during low-cyclic fatigue phenomena while the maximum stress is less than the ultimate stress level in the material.
- Changes in the welding seam positions against the curved surface changes the cyclic life of the steel coiled tube.

References

Abernethy, R. B. (2006). *The new Weibull handbook, Fifth edition*. North Plam Beach, Florida: Dr. Robert B. Abernethy.

Ackert, D., Beardsell, M., Corrigan, M., & Newman, K. (1989). The coiled tubing revolution. *Oilfield Review, 1*, 4-16.

Avakov, V., Foster, J., & Smith, E. (1993). *Coiled tubing life prediction*. Paper presented at the Offshore Technology Conference, houston ,Texas.

Bannantine, J. (1990). *Fundamentals of metal fatigue analysis*. Englewood Cliffs, New Jersey: Prentice Hall.

Bauschinger, J. (1886). On the change of the position of the elastic limit of iron and steel under cyclic variations of stress. *Mitt. Mech.-Tech. Lab., Munich, 13*(1).

Behenna, F., Myrick, D., Stanley, R., Tipton, S., & Hammond, W. (2003). *Field validation of a coiled tubing fatigue model.* Paper presented at the SPE/ICoTA Coiled Tubing Conference and Exhibition, Houston, texas.

Boles, J. A. B., Burgos, R., & Ballesteros Medina, J. A. (2008). *A field study of coiled-tubing material loss and ovality.* Paper presented at the SPE/ICoTA Coiled Tubing and Well Intervention Conference and Exhibition, The Woodlands, Texas.

Johnson, L. G. (1950). *The median ranks of sample values in their population with an application to certain fatigue studies.* Paper presented at the Bulletin of the American Mathematical Society.

Kelly, P. (2008). *Solid mechanics* Vol. 1. A. University (Ed.) *Part* (pp. 301-313).

Lai, C.-D. (2014). *Generalized Weibull Distributions*. Palmerston North, New Zealand: Springer.

Li, J., Crabtree, A. R., Kutchel, M., Diaz, J. D., Reyes, W., Dugarte, R., & Pena, L. (2008). *Sand/Well Vacuuming Technology With Concentric Coiled Tubing: Best Practices and Lessons Learned from Over 600 Operations.* Paper presented at the SPE Asia Pacific Oil and Gas Conference and Exhibition.

Newman. (1991). Determining the working life of a coiled tubing string. *Offshore, incorporating the Oilman, 51*, 31-32.

(2015). *Residual curvature and moments in CT due to bending.* Paper presented at the SPE/ICoTA Coiled Tubing & Well Intervention Conference & Exhibition, The woodlands, Texas.

Newman, & Brown. (1993). Development of a standard coiled-tubing fatigue test. *paper SPE, 26539*, 3-6.

ReliaSoft. (2015). *Life Data Analysis Reference*. Tucson, Arizona: ReliaSoft Corporation.

Rinne, H. (2008). *The Weibull distribution: a handbook*. Boca Raton, FL: CRC Press.

Sas-Jaworsky, A., & Williams, J. G. (1993). *Development of composite coiled tubing for oilfield services*. Paper presented at the SPE Annual Technical Conference and Exhibition, Houston, Texas.

Shaw, P., & Kyriakides, S. (1985). Inelastic analysis of thin-walled tubes under cyclic bending. *International Journal of Solids and Structures, 21*(11), 1073-1100.

Sisak, W., & Crawford, D. (1994). *The fatigue life of coiled tubing.* Paper presented at the SPE/IADC Drilling Conference, Dallas ,Texas.

Thomeer, H., & Newman, K. (1991). *Safe Coiled-Tubing Operations.* Paper presented at the SPE Health, safety and environment in oil and gas exploration and production conference, The Hague, The Netherlands.

Tipton. (1996). *Coiled tubing deformation mechanics: Diametral growth and elongation.* Paper presented at the SPE Gulf Coast Section/ICoTA North American Coiled Tubing Roundtable, Richardson, Texas.

(2003). Achilles 4.0 CT fatigue life prediction algorithm. *CTES Technical Note, Conroe, TX*.

Weibull, W. (2013). *Fatigue testing and analysis of results*. The universities press, Belfast: Pergamon Press.

Yoshida, F., & Uemori, T. (2002). A model of large-strain cyclic plasticity describing the Bauschinger effect and workhardening stagnation. *International Journal of Plasticity, 18*(5), 661-686.

Chapter 4 Fatigue failure analysis of improved fatigue performance steel coiled tubes (BlueCoil)

4.1 Background

Coiled tubing technology has been developed for work-over well operations in the oil and gas industry (Newman, 1991). The technology is becoming more popular for drilling operations due to the rigs lower operational cost and ease of transportation (Wu, 1995). The coiled tubing material needs to have good flexibility and high strength. There is a need for a higher strength coiled tube grade that has more resistance to high strain rates and also higher fatigue life in both the tube body and around the weld line areas (Valdez *et al.*, 2015).

In this chapter, the HT-125 coiled tube specimens were subjected to laboratory scale cyclic life testing using a fatigue bending machine under 1,000 psi and 3,500 psi internal tube pressure. The outer diameter of HT-125 BlueCoil was measured and recorded before and after experiments. The interaction force between the bending loads, axial load and internal pressure produces a severe strain rate on the body of the coiled tube string. This can be intensified when the tube is under high internal pressure (more than 3,000 psi). This increases the tube diameter, especially around heat affected zones. The growth of plastic deformation in a coiled tube body make it susceptible to fatigue failure under cyclic load conditions.

4.2 Introduction

The maximum stress and strain values in the structural body of a coiled tube string is more than that found in drill pipes. This can emerge as a limitation to the fatigue life performance of the conventional steel coiled tube. One of the major limitation of steel coiled tube is the capability of the material of the tube body to withstand a combination

of axial and hoop stresses (Zhu & Zehnder, 2016). The hoop stress results from internal and external pressure. This problem has been recently resolved by using higher strength steel coiled tubes. Another limitation is the weakness of the heat treated zones either side and along the weld seam areas. The cyclic fatigue life on the weld seam is lower than the rest of the tube body (Stanley, 1998), especially in the coiled tube with higher material grade. Consequently, higher material grade increases the strength of the coiled tube but weakens the heat treated areas along a welding seam. Therefore, it is necessary to have a comprehensive understanding of structural behaviour of the HSLA steel (Wainstein & Ipiña, 2012) and its metallurgical properties to identify what improvement there has been in the manufacturing process.

4.3 New coiled tubing technology (BlueCoil)

During bending and straightening events in the field operations, coiled tube undergoes plastic deformation and residual strain in its steel structure (Bridge, 2011). Accumulation of residual strain in addition to the effect of internal pressure imposes fatigue damage into the coiled tube material after limited bending cycles. The well services market demands that a coiled tubing string is manufactured from a high strength material and has greater durability at high pressures and higher stress working conditions than normal steel throughout the entire coiled tube string. Stronger grades of steel tube improves the reliability and fatigue performance while decreasing the ballooning effect.

An increase in yield strength of conventional coiled tube should result in increased cyclic life. However, weld seam areas have less cyclic fatigue life in comparison with the base tube. Consequently, this reduces the overall fatigue life of the tube. The higher yield strength of steel material, however, has more sensitivity to sour gas corrosion (H_2S environment), especially along the weld seam areas, which fail at lower cyclic fatigue life than the conventional steel tube material.

In order to improve these welding drawbacks, a new steel coiled tube manufacturing process has recently been developed by Tenaris. They have produced a new coiled tubing technology (BlueCoil) by using (Valdez *et al.*, 2015) new steel chemistries and new heat-treatment processes along the weld seam areas. This new coiled tube is obtained by producing a tempered martensite microstructure, which improves fatigue

performance and corrosion resistance compared to the conventional (HS-90) coiled tube (Feechan *et al.*, 2003).

This new technology shapes the microstructure of the metal material into a more uniform and homogeneous structure along the tube body and weld seam areas. This process improves the performance of coiled tube by re-imaging the microstructure of the tube material and consequently increasing the cyclic life of the coiled tube.

4.4 Ovality and ballooning effect

Coiled tube is produced with an approximate circular cross-section with an ovality not more than 5% (Liessem *et al.*, 2006). The ovality changes over time when the tube is running into and pulling out of the well bore (Newman, 1991). Any increase in the percentage of ovality, decreases the fatigue life of the coiled tube. The amount of the ovality can be calculated using API Standard 5ST (Equation (4.1)) or the Newman method (Equation (4.2)), as shown below:

$$\text{API Ovality}(\%) = \frac{100 \times 2 \times (\mathrm{D_{max}} - \mathrm{D_{min}})}{(\mathrm{D_{max}} + \mathrm{D_{min}})} \tag{4.1}$$

$$\text{Newman Ovality}(\%) = \left[\frac{\mathrm{D_{max}}}{\mathrm{D_{min}}} - 1\right] \times 100 \tag{4.2}$$

where:

D_{max} Maximum coiled tube outer diameter

D_{min} Minimum coiled tube outer diameter

Coiled tube specimens with 2 inches outer diameter and 0.190 inch wall thickness were inserted into the bending machine with the weld seam position against the bending surface. The variation of the diameters along the bending axis (weld seam axis) and counter bending axis (neutral position axis) at low and high pressures were measured and recoded every 5 cm from the fixed end after failure during the bending cyclic tests. The measured diameters and related percentage ovalities based on the API standard and Newman method were listed in Table 4-1 with 1,000 psi internal pressure and Table 4-2 with 3,500 psi internal pressure.

Table 4-1: Ovality at 1,000 psi internal pressure.

Distance from fixed end (mm)	Diameter (Weld line side)	Diameter (Counter weld line side)	% Ovality (Newman Method)	% Ovality (API 5ST Method)
5	50.41	51.37	1.90	1.89
10	50.44	51.31	1.72	1.71
15	50.43	51.31	1.74	1.73
20	50.49	51.30	1.60	1.59
25	50.49	51.30	1.60	1.59
30	50.53	51.32	1.56	1.55
35	50.40	51.34	1.87	1.85
40	50.33	51.54	2.40	2.38
45	50.50	52.05	3.07	3.02
50	50.78	51.84	2.09	2.07
52	50.74	51.66	1.81	1.80
55	50.80	51.64	1.65	1.64
60	50.75	51.62	1.71	1.70
65	50.69	51.57	1.74	1.72
70	50.76	51.56	1.58	1.56
75	50.73	51.70	1.91	1.89
80	50.78	51.54	1.50	1.49

Table 4-2: Ovality at 3,500 psi internal pressure.

Distance from fixed end (mm)	Diameter (Weld line side)	Diameter (Counter weld line side)	% Ovality (Newman Method)	% Ovality (API 5ST Method)
5	50.52	51.14	1.23	1.22
10	50.53	51.21	1.35	1.34
15	50.48	51.22	1.47	1.46
20	50.49	51.17	1.35	1.34
25	50.46	51.14	1.35	1.34
30	50.50	51.15	1.29	1.28
35	50.39	51.17	1.55	1.54
40	50.68	51.83	2.27	2.24
45	51.59	53.36	3.43	3.37
50	52.03	54.20	4.17	4.09
52	51.06	53.16	4.11	4.03
55	50.95	52.47	2.98	2.94
60	50.95	52.25	2.55	2.52
65	50.98	52.38	2.75	2.71
70	51.03	52.50	2.88	2.84
75	51.07	52.55	2.90	2.86
80	50.78	51.54	1.50	1.49

The ovality of the coiled tube should be constantly monitored. It has been suggested that the tube be replaced when the ovality approaches 5%. The percentage ovality in Table 4-1 and Table 4-2 shows that tube samples failed with an ovality of 3% and 4% at 1,000 psi and 3,500 psi internal pressure, respectively. Although the ovality values didn't exceed the limit level, the variation of diameters in bending and counter bending axes show that the ballooning rate with 3,500 psi was much more than the tube sample with 1,000 psi internal pressure. This phenomena shows the effect of higher internal pressures on the ballooning rate.

4.5 Test results

Investigation of the fatigue failure behaviour of the new technology steel coiled tube (BlueCoil) was conducted through a standard bending test mechanism. Seven samples with 2 inches outer diameter, 0.190 inch wall thickness and 6 feet in length of HT-125 (125 Kpsi yield strength) straight coiled tubes were utilized to conduct the cyclic bending fatigue experiments. The coiled tube specimens were supplied by Tenaris.

The experiences of running the coiled tubing cyclic life experiments show that the cyclic fatigue life of the tube is highest when the weld seam position is placed on the neutral axis of the bending section. Two coiled tube samples were tested at 1,000 psi and 3,500 psi internal pressure (to represent approximately the worst and least severe operating conditions). Two more coiled tubing sample tests of the above experiments were tested, in order to compare the effect of weld seam position in different directions against the bending surface on the bending machine (as shown in Figure 4-1) using a curved surface of 55 inches radius of curvature. Three more experiments were conducted positioning the weld line against the curved surface and against the flat surface.

Typically, a gas-tight thread was made on both ends of each test sample and a proprietary cap and connector was manufactured to seal each coiled tube sample. This allowed the test specimens to hold an internal pressure of 4,000 psi (tube hydrostatic test pressure). The specified internal pressures were applied through one of the pressure caps while the air was extracted from the other end. After conducting each pressure test, the coiled tube specimens were placed in the cyclic fatigue test machine

(Figure 4-1) to simulate the bending and straightening events onto the working reel and gooseneck.

Coiled tube specimens underwent bending and straightening events along their 2 feet length of each test sample. Each experiment was continued until the tube specimen failed either due to a pinhole or a crack, resulting in the test fluid inside of the tube depleting and the internal pressure dropping to below the setting value.

Figure 4-1: Standard bending machine (Courtesy of Curtin University).

The fatigue test of the HT-125 coiled tube results are presented in three different tables. Table 4-3 shows the fatigue life of the tubes with the welding seam positioned on the neutral axis, Table 4-4 shows the fatigue life of the tubes with welding seam placed against the straightening block and Table 4-5 shows the fatigue life of the tubes with the welding seam placed against bending block. The outer diameter of each specimen on the bending axis and opposite axis were measured and recorded before and after each bending experiment.

Table 4-3: Experiment results – neutral axis.

Sample No.	Internal pressure (psi)	Cyclic life (two bending events)	Specimens
1	3500	705	
2	3500	597	
3	1000	959	
4	1000	955	

Table 4-4: Experiment results – straightening side.

Sample No.	Internal pressure (psi)	Cyclic life (two bending events)	Specimens
1	3500	600	
2	1000	703	

Table 4-5: Experiment results – bending side.

Sample No.	Internal pressure (psi)	Cyclic life (two bending events)	Specimens
7	3500	637	

The experimental results from the cyclic bending test of seven steel coiled tube samples are schematically shown in Figure 4-2. The figure presents the position of the weld seam against the bending and straight blocks to demonstrate the three different stress conditions acting on the steel material in a bending cycle. The straightening side of the tube is in maximum tension, the bending side experiences maximum compressional stress and the neutral axis has the minimum bending stress. The position of the failure points show that, except in the case of the weld seam against the straight block (in which a failure crack occurred on the outer radius of tube bending) in the other weld position, the tube sample failed on the inner radius of bending (against the bending block).

The failure crack locations indicate the weld area fails before any other part of the tube body, when it is under tensile stress (weld placed on the outer radius of tube bending). This means that the structural behaviour of the heat treated zone around welding is more sensitive to tension than compressional stresses.

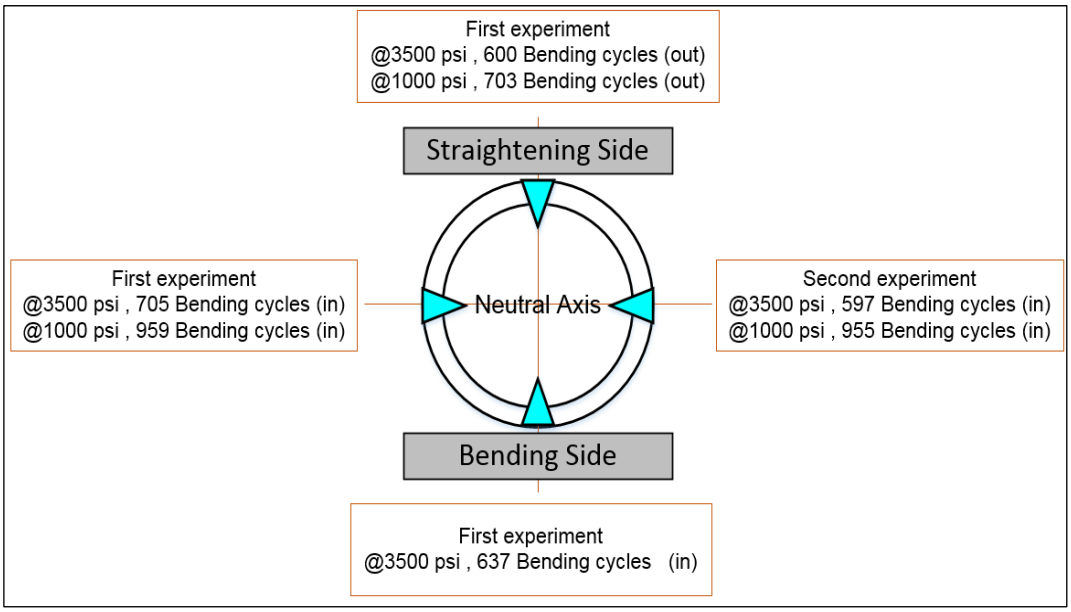

Figure 4-2: Schematic fatigue life and failure positions.

Table 4-6 compares the fatigue life in HT-125 and HS-90 along different weld seam positions for some specific experiments. The average fatigue records indicate that the HT-125 tubes have 2.6 times and 1.91 times more fatigue life than the HS-90 at 3,500 psi and 1,000 psi, respectively. Thus HT-125 steel coiled tubes have a better fatigue performance compared with HS-90 at higher internal pressures.

Table 4-6: HT-125 to HS-90 life ratio table.

Sample No.	Internal Pressure (psi)	Welding Line position	HT-125 Cycles life	HS-90 Cycles life	HT-125 to HS-90 Life ratio
1	3,500	Neutral axis	705	279	2.53
2	1,000	Neutral axis	959	522	1.84
4	3,500	Neutral axis	597	272	2.19
5	1,000	Neutral axis	955	506	1.89
7	3,500	Straightening side	600	259	2.32
8	3,500	bending side	637	191	3.34
9	1,000	Straightening side	703	352	2.00

The ballooning effect and resulting reduction in wall thickness of the coiled tube during cycling bending events is another common phenomenon in cyclic bending caused by tube elongation (Newman *et al.*, 1997). Both of these phenomena cause an increase in the internal volume of the conventional steel coiled tube after every single additional bending event. During internal pressure monitoring of the HT-125 tube under a uniform 3,500 psi pressure, the same process of a decrease in internal pressure (resulting from increasing internal volume of the tube) was observed and recorded as shown in Figure 4-3.

However, the test result shows that for the HT-125 tube under uniform 1,000 psi pressure, the internal pressure of the tube specimen anomalously increased (Tipton, 1996) after every bending event (Figure 4-4). The observed opposite trend of internal pressure variation illustrates a decrease in internal volume of the tube specimen from the cyclic bending effect. The graphs in Figure 4-5 and Figure 5-6 indicate that both the minimum and maximum outer diameters of the HT-125 tube are increasing during its bending life. Therefore, either the wall is thickening or thinning during bending events.

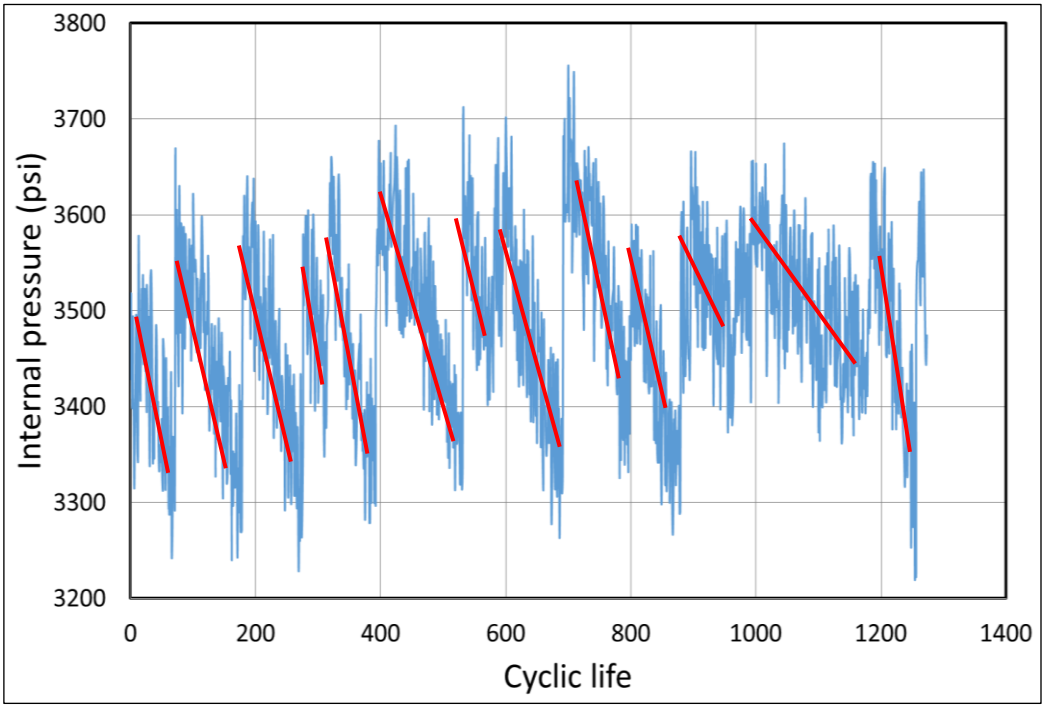

Figure 4-3: Internal pressure vs. cyclic life at 3,500 psi.

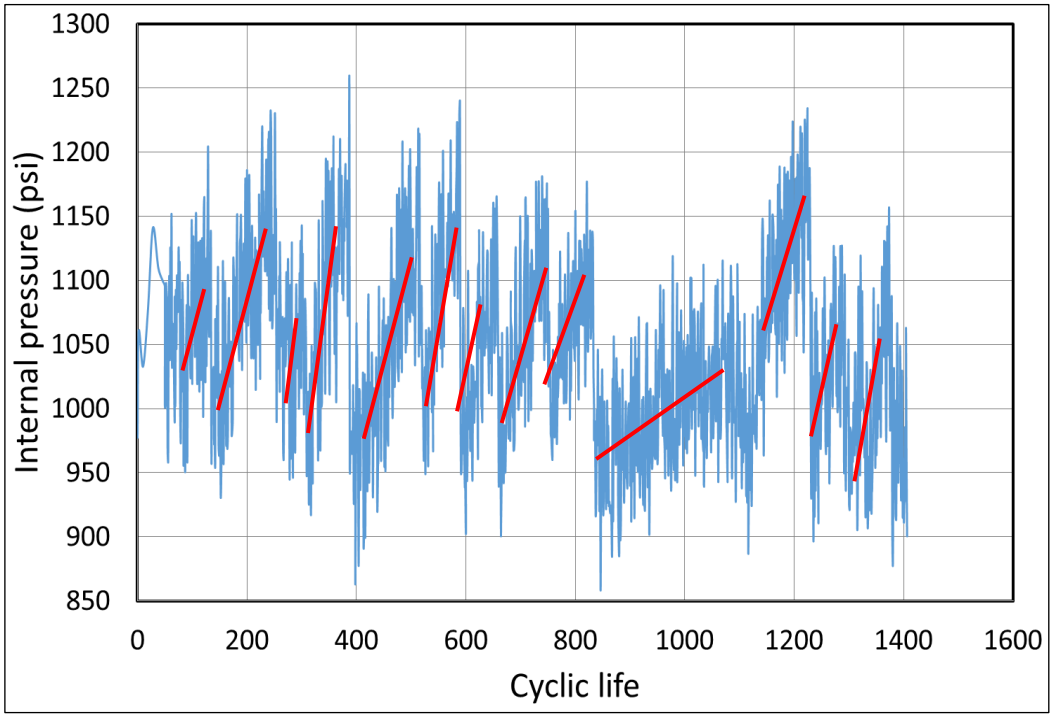

Figure 4-4: Internal pressure vs. cyclic life at 1,000 psi.

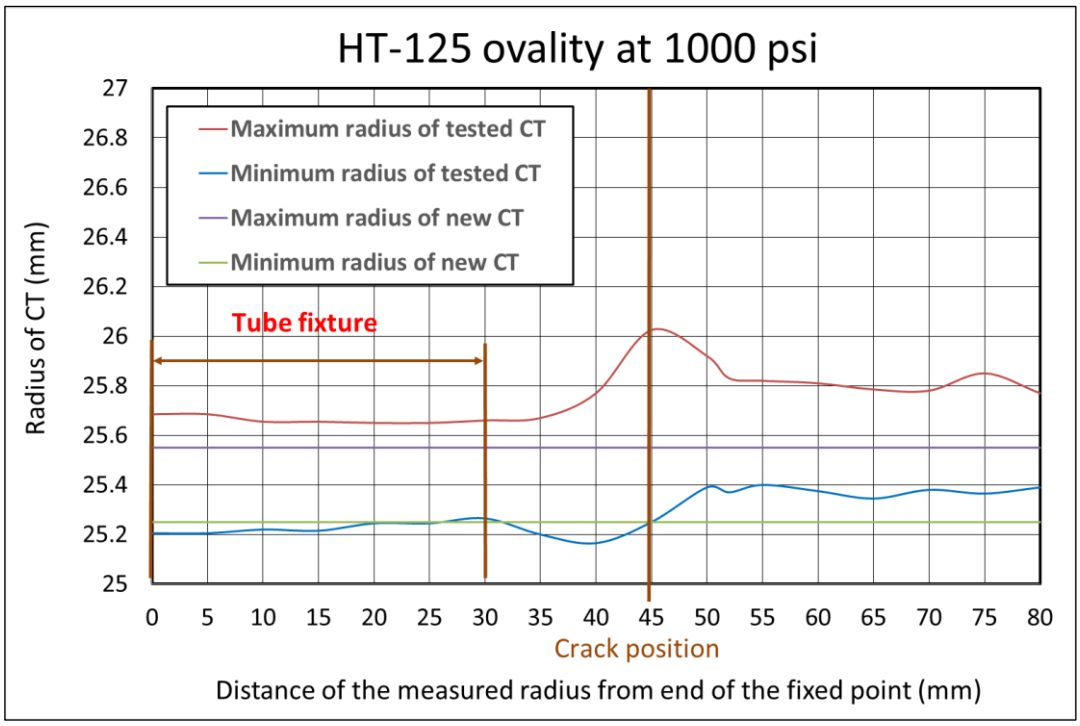

Figure 4-5: Outer diameter variation at low internal pressure.

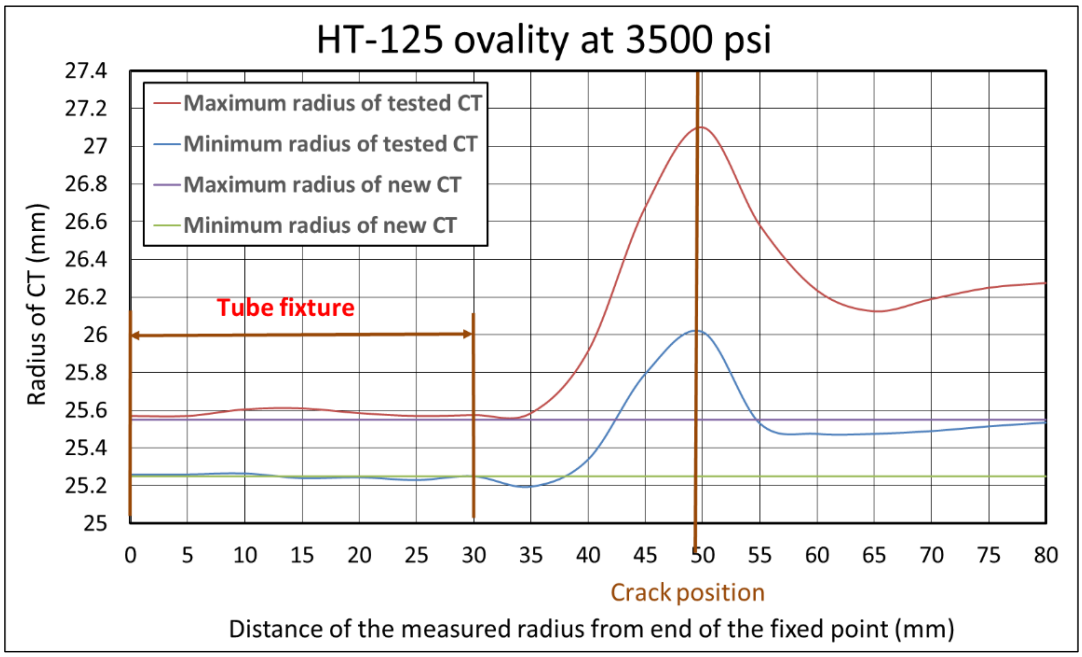

Figure 4-6: Outer diameter variation at low internal pressure.

4.6 Conclusions

This chapter discussed cyclic fatigue tests of the HT-125 (BlueCoil) steel coiled tube specimens testing at purpose-built fatigue bending machine. The outer diameter

of specimens during the beginning and end of experiments alongside internal pressure changes were monitored and recorded. The following results were obtained:

- The tube specimens' measurements showed that variations in the outer diameter of failed tube versus new tube were not significant even at higher test pressures.
- Test results show that the HT-125 BlueCoil tube has 2.6 times and 1.9 times more average working life than HS-90 conventional steel coiled tubes at 3,500 psi and 1,000 psi internal pressure, respectively. This illustrates a greater performance of HT-125 over HS-90 with the higher internal pressures.
- The weld line areas of the HT-125 have almost the same cyclic fatigue life as HS-90 and consequently the same micro-structural behaviour as the rest of the coiled tube body. However, test results show the least cyclic bending life occurs in HS-90 conventional coiled tube when the weld seam is placed under high stress conditions, against the bending block side.
- During the bending experiment of HT-125 Bluecoil at 3,500 psi internal pressure, a continuous reduction in internal pressure was recorded which was similar to the normal behaviour of the conventional steel coiled tubes. Whereas, during the bending experiment at 1,000 psi internal pressure, a continuous increase in internal pressure was recorded which showed an opposite trend with respect to the conventional steel coiled tubes. At the end of the experiments, tube size measurement indicated that the outer diameter of the HT-125 Bluecoil was slightly increasing. Therefore, the increase in internal pressure could have resulted from tube length shortening and/or tube wall thickening.

References

Bridge, C. (2011). *Combining elastic and plastic fatigue damage in coiled tubing.* Paper presented at the SPE/ICoTA Coiled Tubing & Well Intervention Conference and Exhibition, The Woodlands, Texas.

Feechan, M., Makselon, C., & Nolet, S. (2003). *Field experience with composite coiled tubing.* Paper presented at the SPE/ICoTA Coiled Tubing Conference and Exhibition, Houston, Texas.

Liessem, A., Marewski, U., Groß-Weege, J., & Knauf, G. (2006). *Methods for collapse pressure prediction of UOE line pipe.* Paper presented at the 25th International Conference on Offshore Mechanics and Arctic Engineering, , Hamburg.

Newman. (1991). Determining the working life of a coiled tubing string. *Offshore, incorporating the Oilman, 51*, 31-32.

Newman, Sathuvalli, & Wolhart. (1997). Elongation of coiled tubing during its life. *SPE paper, 38408*.

Stanley, R. K. (1998). *An Analysis of Failures in Coiled Tubing.* Paper presented at the IADC/SPE drilling conference, Dallas, Texas.

Tipton. (1996). *Coiled tubing deformation mechanics: Diametral growth and elongation.* Paper presented at the SPE Gulf Coast Section/ICoTA North American Coiled Tubing Roundtable, Richardson, Texas.

Valdez, M., Morales, C., Rolovic, R., & Reichert, B. (2015). The development of high-strength coiled tubing with improved fatigue performance and HS resistance. *SPE/ICoTA Coiled Tubing & Well Intervention Conference & Exhibition*.

Wainstein, J., & Ipiña, J. P. (2012). Ductile Instability Analysis of HSLA Coiled Tubing. *Procedia Materials Science, 1*, 297-304.

Wu. (1995). Coiled tubing working life prediction. *SPE Production Operations Symposium*.

Zhu, & Zehnder. (2016). *Experimental and applied mechanics, Volume 4: Proceedings of the 2016 annual conference on experimental and applied mechanics*. New York, NY: Springer International Publishing.

Chapter 5 Interlaminar modelling to predict composite coiled tube failure

5.1 Background

Fibre-composite coiled tubes offer several advantages compared to steel material, including a reduction in weight, no corrosion and a possible improvement in fatigue life.

During well service operations, the bending stiffness of composite material degrades progressively with increasing number of cyclic loading (Turon Travesa, 2006). The fatigue damage and failure criteria of fibre-reinforced composite coiled tubes is more complex than that of steel; hence, failure predictions are somewhat unreliable.

Among the failures in composite materials, interlaminar delamination is the most common. It leads to a reduction in strength and stiffness especially in cyclic-load conditions (Li *et al.*, 2013). Delamination of the layers causes a redistribution of the load path along the composite structure, which is unpredictable; therefore, delamination in a composite coiled tube in a down-hole operation would eventually lead to failure, which could be catastrophic.

A ply-by-ply mathematical modelling and numerical simulation method was developed to predict the interlaminar delamination of filament-wound composite coiled tubes during a combination of different loading scenarios with a focus on low-cycle fatigue. Filament winding is the composite manufacturing process in which continuous fibres wet by resin are wound onto a supporting form (Harris, 1986).

The objective of this chapter is to explain the interlaminar delamination as an initial crack and source of stress concentration in composite coiled tubes, in the framework of a meso-cracking progression of matrix damage modelling of composite laminates.

5.2 Introduction

Coiled tubes are subjected to cyclic bending and straightening during running in and pulling out of wellbores. Reifsnider (Reifsnider *et al.*, 1983) concluded that the damage index value of composite material follows a non-linear graph for cyclic loading, as shown in Figure 5-1. During the period of fatigue life of a composite tube many modes of damage occur - including matrix cracking, interfacial de-bonding, interlaminar failure (delamination) and fibre breakage can be observed (Ochoa & Reddy, 1992).

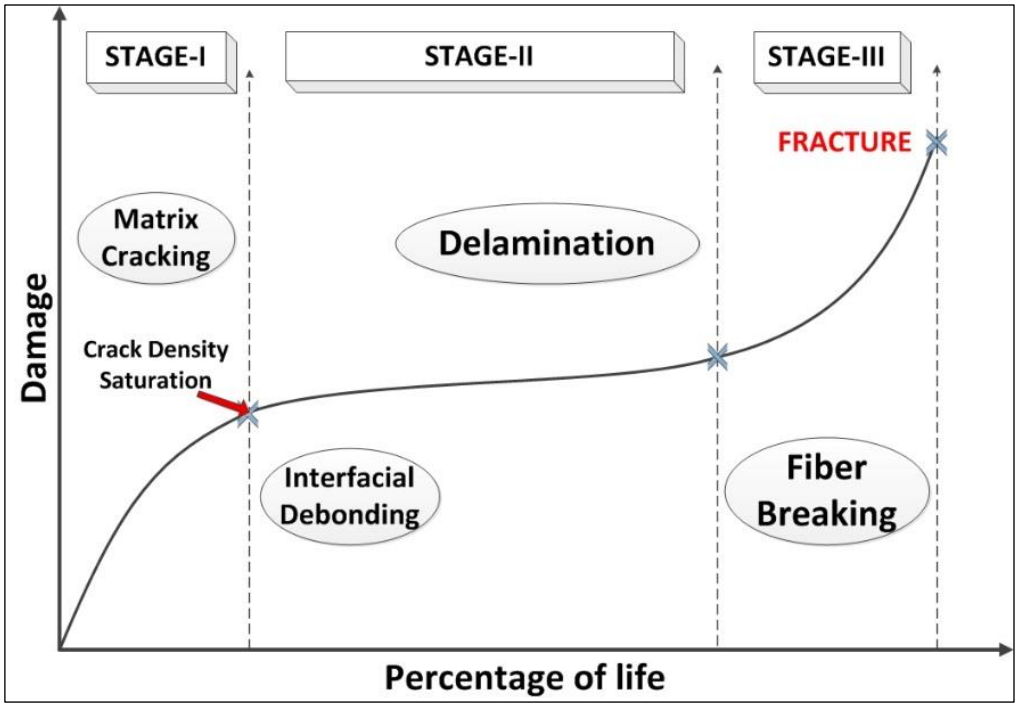

Figure 5-1: Damage index in composite material (Reifsnider *et al.*, 1983)

Delamination is a common failure mode that causes an unpredictable redistribution of the load path along the composite structure and leads to a reduction in the strength and stiffness of the fibre-reinforced composite material (Szekrenyes, 2002). Although delamination occupies the highest percentage of the middle period of the cyclic life, the damage index - as the main design parameter for fatigue life evaluation - does not significantly change. As a result, the investigation of crack propagation between the layers is unclear. Consequently, composite materials often need to be over-designed

with an additional margin of safety to compensate for the deficiency in predicting their lifetime cyclic-load conditions (Degrieck & Van Paepegem, 2001).

The damage index, as a physical parameter that quantifies the degradation of a composite material (Gibson, 2011), can be calculated using Equation (5.1) according to (Wu & Yao, 2010):

$$D_n = \frac{E_0 - E_n}{E_0 - E_f} \tag{5.1}$$

where:

D_n Fatigue damage

E_0 Initial Young's modulus

E_f Failure Young's modulus

E_n Young's modulus of the material subjected to the *n*th cyclic load

According to Figure 5-1, when the Crack Density Saturation (CDS) occurs in the matrix, the tip of the delamination initiates and propagates. Based on the meso-scale damage model, therefore, a composite laminate is defined as a stacking sequence (Jones, 1998) of elementary composite layers and interfaces (Figure 5-2) with different mechanical properties. The meso-scale damage model helps to define the interlaminar delamination phenomenon as interface cracking or loss of cohesion between layers (Burlayenko & Sadowski, 2008).

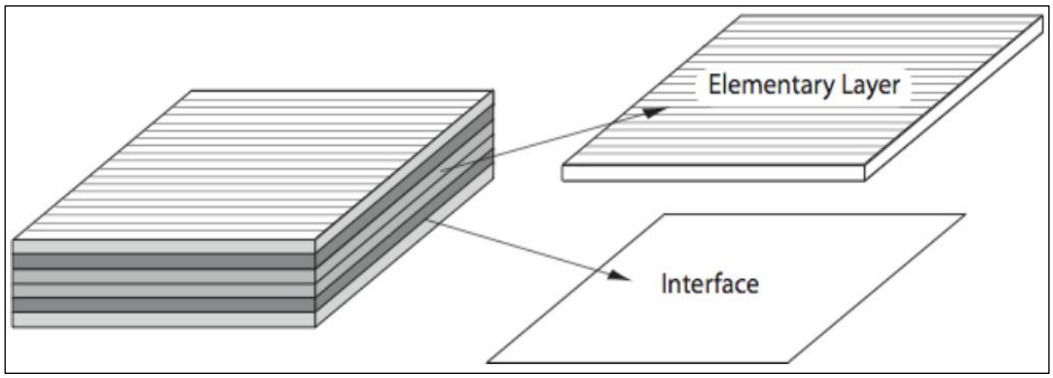

Figure 5-2: Meso-scale damage model of a laminate (Bordeu & Boucard, 2009).

Delamination (inter-ply damage) growth causes a reduction of the load capacity due to tensile and shear stresses at the delaminated interface, which would eventually cause failure to the laminate composite structure (Szekrenyes, 2002). Tensile and shear

stresses in the pre-existing delaminated layer can be measured by Mode-I and Mode-II interlaminar fracture toughness testing methods, respectively. The interlaminar fracture toughness of composite material can be quantified by the strain energy release rate (G_I) in Mode-I testing for pure normal stress, (G_{II}) in Mode-II testing for pure shear stress, and (G_{III}) for pure sliding stress. As shown in Equation (5.2), the total strain energy release rate (G_T) expresses the total pure strain energy release rates from normal, shear and sliding stresses. Interlaminar fracture toughness shows the resistance of composite materials to delamination (Thakur, 2014). Therefore, it is an important composite property and widely acknowledged by designers.

$$G_T = G_I + G_{II} + G_{III} \tag{5.2}$$

Ply-by-ply mathematical modelling and numerical simulations were developed to predict interlaminar delamination of filament-wound composite coiled tubes. Fracture test models such as the Double Cantilever Beam (DCB) and End-Notched Flexure (ENF) models can be used to extract fracture parameters.

Three-dimensional commercial finite element software ANSYS/APDL version 15.0 was used for all simulations. The Virtual Crack Closure Technique (VCCT) and Cohesive Zone Model (CZM) were used to determine delamination growth in an initially delaminated composite model. The finite element model was evaluated under a combination of different loading scenarios. A comparison between the crack propagation in glass-fibre and carbon-fibre in composite material was then performed and Hashin's failure criteria was applied.

5.3 Hashin's failure criteria for unidirectional fibre composites

One of the critical problems in the design and modelling of fibre-reinforced composite material under cyclic loading is to establish meaningful fatigue failure criteria. There are many failure criteria for the design and modelling of composite material (Barbero, 2013).

Hashin (1980) proposed a failure criterion for unidirectional fibre-composite materials based on quadratic stress polynomials. Hashin's failure criteria indicated that there are two independent failure modes in unidirectional fibre composites: fibre failure and inter-fibre failure. In the fibre failure mode, composite material fails due to a rupture resulting from a tension force and buckling from a compressional force. Matrix (inter-fibre) failure occurs in a plane parallel to the fibres (Hashin, 1980).

Unidirectional fibre composites are transversely isotropic in the fibre direction, therefore, fibre-reinforced failure modes consider the uni-axial stress state in the fibre direction, while matrix failure modes consider the tri-axial stress state.

Hashin's failure criteria involves four failure modes (Figure 5-3) for fibres and matrices (Hashin, 1980):

- Tensile fibre failure for $\sigma_{11} \geq 0$,
- Compressive fibre failure for $\sigma_{11} < 0$,
- Tensile matrix failure for $\sigma_{22} + \sigma_{33} \geq 0$, and
- Compressive matrix failure for $\sigma_{22} + \sigma_{33} < 0$.

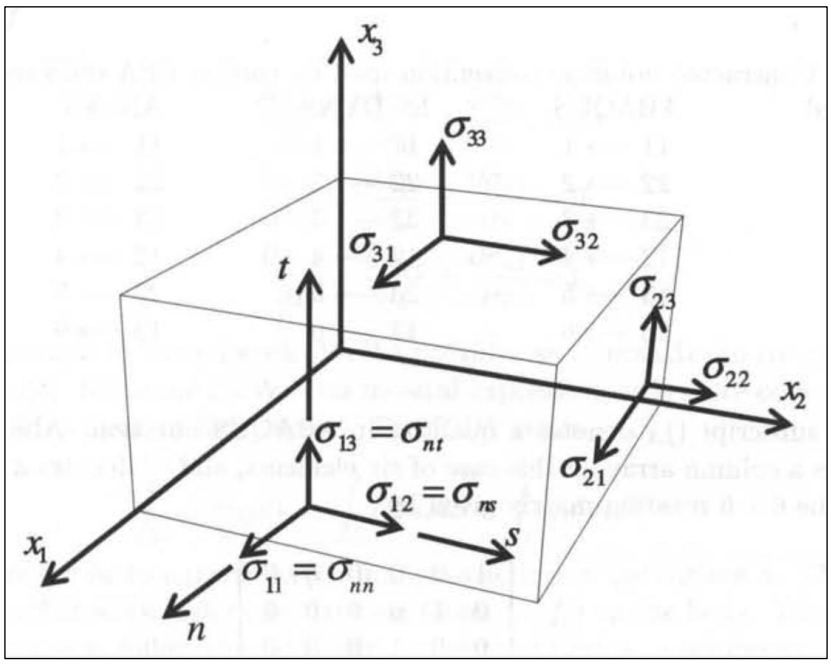

Figure 5-3: 3D Stress components (Barbero, 2013).

5.4 Interlaminar fracture (delamination)

Three crack propagation failure modes of delamination are shown in Figure 5-4 for interlaminar crack displacements. The numerical simulation of the crack propagation follows two procedures. The first is based on fracture mechanics, and the second is based on a mixture of damage mechanics and softening plasticity (Spada *et al.*, 2009).

The mechanical parameters indicate that delamination happens through the interface layer. The resistance of the interface to propagate the interlaminar crack under the opening mode (Mode-I) is different from under the shear mode (Mode-II).

The increase of force applied in Mode-I and Mode-II gives rise to tensile and shear stresses at the delamination crack front, respectively (Mathews & Swanson, 2007). A delamination crack propagates when the strain energy release rate is equal to or greater than the value of the critical energy release rate (Alfano & Crisfield, 2001).

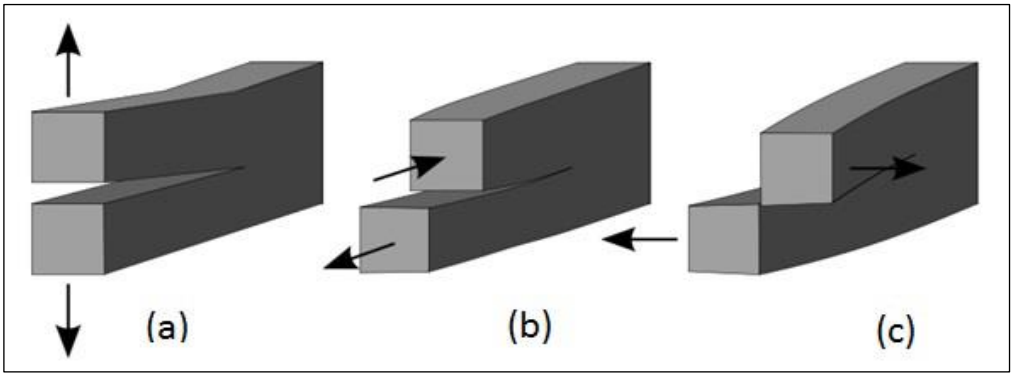

Figure 5-4: Crack growth (a) Mode-I, (b) Mode-II and (c) Mode-III (Mier, 2012).

5.5 Crack opening mode (Mode-I)

According to (Wisheart & Richardson, 1998), the strain energy release rate can be statically measured using a DCB test for Mode-I delamination. The model is designed with a pre-existing crack. By applying an opposite direction force to the end of the sample, perpendicular to the crack surface, the pre-existing crack will extend. Figure 5-5 shows the crack geometry, the reaction forces and crack displacements. The reaction forces are calculated according to Equation (5.3) and the resultant linear elastic crack displacements are used to calculate the total fracture toughness energy (G_I). A schematic diagram of the DCB is shown in Figure 5-6.

$$G_I = \frac{1}{2\,da} R_y dv \tag{5.3}$$

where:

a	Delamination crack length
b	Delamination sample width
d_v	Crack displacement in the ‘y’ direction
R_Y	Node reaction force in the ‘y’ direction

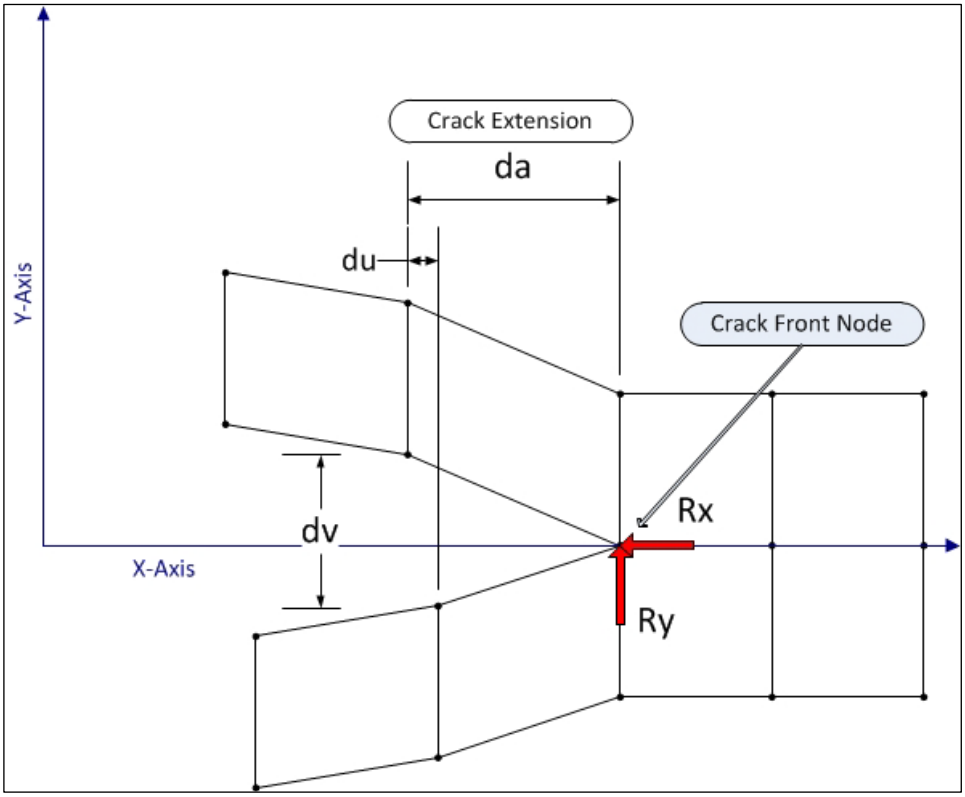

Figure 5-5: 2D crack geometry of the DCB (Krueger, 2004).

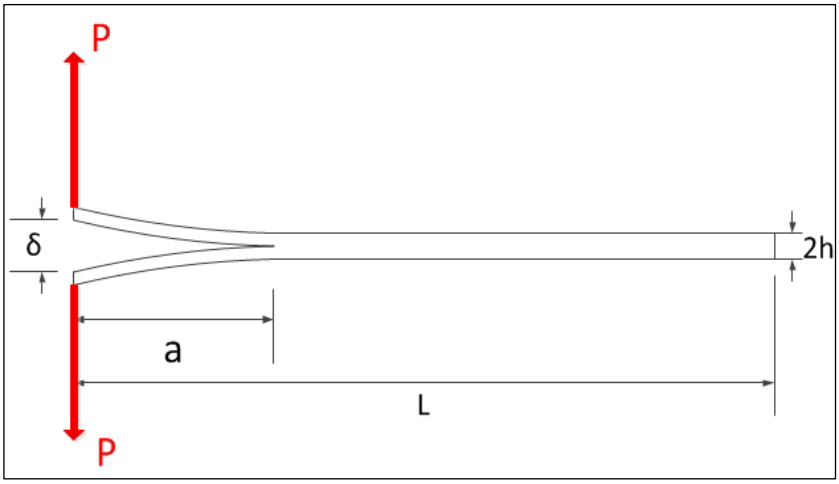

Figure 5-6: A schematic of the DCB specimen.

5.6 DCB (Mode-I)

The crack opening mode (Mode-I) test is generally performed on a unidirectional composite laminate specimen. In this method, the applied load versus crack displacement is linear, and the first deviation from linearity occurs as the crack initiation happens. According to fracture mechanics concepts, the propagation from a

pre-existing delamination can be calculated by the amount of strain energy release rate and the fracture toughness of the interface (Choupani, 2008).

The interlaminar fracture toughness (G_I) calculations are based on Equation (5.4) (Prasad *et al.*, 2011).

$$G_I = \frac{3\,P\delta}{2\,ba} \tag{5.4}$$

where:

a	Delamination crack length
b	Delamination sample width
P	Load
δ	Load point displacement

5.7 Crack sliding mode (Mode-II)

Mode-II delamination failure is a method for measuring shear stresses at the crack tip. A three-point bending load on the ENF specimen with a pre-existing linear elastic crack (as shown in Figure 5-7) can determine the strain elastic release energy rate. The pre-existing crack propagates as the bending load is applied to the specimen. The finite element model was designed to simulate a sample, similar to the set up shown in Figure 5-7. According to Equation (5.5), the total fracture toughness energy (G_{II}) is calculated from the reaction force at the crack tip, load point displacement and the crack propagation length.

$$G_{II} = \frac{1}{2\,ba} R_x du \tag{5.5}$$

where:

a	Delamination crack length
b	Delamination sample width
d_u	Crack displacement in the ‘x’ direction
R_X	Node reaction force in the ‘x’ direction

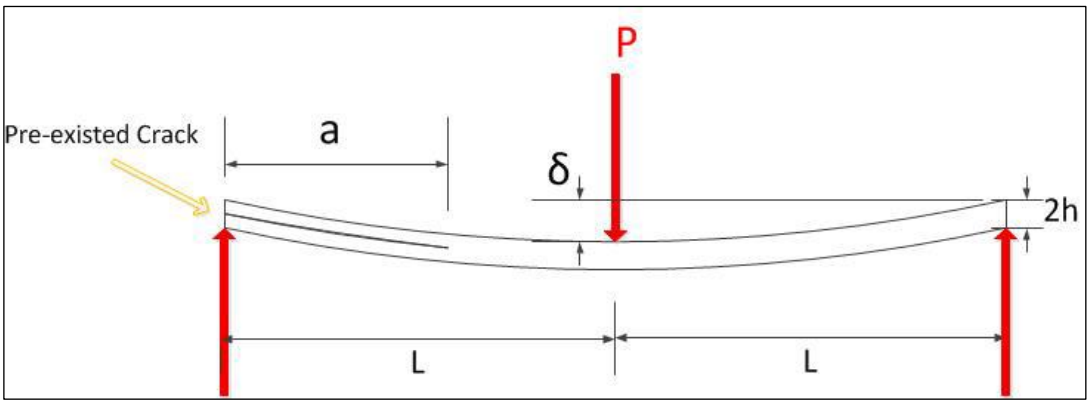

Figure 5-7: A schematic of the ENF specimen.

5.8 ENF (Mode-II)

The ENF test is a method for measuring interlaminar fracture toughness in composite materials under in-plane shear stress. The crack sliding mode (Mode-II) is a type of fracture testing method in which the crack initiation and the front face of propagation slide on each other in the direction of the crack's growth path and no crack opening mode occurs (Salehizadeh & Saka, 1992). Mode-II interlaminar fracture toughness is calculated according to Equation (5.6) and is denoted by G_{II} (Y. Zhu, 2009):

$$G_{II} = \frac{9P^2a^2}{16E_{11}b^2h^3} \tag{5.6}$$

where:

P	Load
a	Delamination crack length
b	Delamination sample width
$2h$	Sample thickness
E	Young's modulus of elasticity

Finite element modelling analysis can use the virtual crack technique and/or cohesive crack model method to compute the strain energy release rate.

5.9 Virtual crack closure technique (VCCT)

The VCCT is a fracture mechanics method that is commonly used for modelling interlaminar delamination failure. The VCCT requires an initial crack in the structure between two layers to model the crack propagation, so the VCCT computes the strain energy release rate for crack growth. Delamination failure occurs when the strain energy release rate becomes equal to or greater than the critical energy release rate (Sun *et al.*, 2009).

5.10 Cohesive zone model (CZM)

The CZM is based on strength criteria and fracture mechanics concepts. It incorporates the initiation and propagation of a crack front face. However, it cannot predict the initiation of the interlaminar crack. Mesh size and material parameters are important factors in CZM modelling. The interface between the adjacent layers of the composite structure is properly defined to determine the crack propagation. The CZM is considered to be a tool to evaluate the deterioration of cohesion between the layers, which uses the relationship between the separation and traction along the interface. Table 5-1 shows the strengths and weaknesses of the CZM and CVVT modelling methods.

Table 5-1: Comparison between the CZM and CVVT (ANSYS®, 2013).

	Cohesive Crack Model (CZM)	Virtual Crack Closure Technique (VCCT)
Strengths	Prediction of initiation and growth of crack.	Based on Fracture mechanics concepts.
	Applicable to complex structures.	Crack growth related to strain energy rate.
Weaknesses	Difficult to obtain characterization data.	Necessary to assume number, location and size of the cracks.
	Accurate assessments are strongly tied to the element size.	Difficult to incorporate with complex structures.

5.11 Interface

The laminated interface is a 3D medium and its thickness is negligible compared to the laminated specimen dimensions; therefore, modelling the interface layer is defined

as a 2D entity to evaluate the relative displacement and reaction force from one layer to the next. Due to low-strength bonding between the adjacent layers, the interface offers the best path for the crack to propagate. The interface strength only depends on matrix properties.

5.12 Finite element modelling

To study the effect of crack initiation and propagation behaviour, glass-fibre composite and carbon-fibre composite materials were modelled. The two approaches, VCCT and CZM, were implemented in the finite element analysis software (ANSYS/APDL version 15). The applied load modes evaluated were opening Mode-I using the DCB design according to ASTM D5528 standard, and shear Mode-II using the ENF design according to JIS K7086 standard. The strain energy release rates - G_I and G_{II} - due to normal and shear stresses, respectively, were evaluated.

5.13 Finite element model

The mechanical properties of the unidirectional composite glass fibre/epoxy, carbon fibre/epoxy and interface epoxy resin are presented in Table 5-3. The structure modelled a rectangular cross-section 150 mm long, 25 mm wide and 3 mm high. The pre-existing crack length was 50 mm, as listed in Table 5-2. Static analysis was performed using regular mesh eight-node Brick elements with SOLID185 for both DCB and ENF laminates and interlaminar layers.

To simulate Mode-I (the opening mode), one end of the DCB structure was fixed, and the opposite free end (with the pre-existing crack) was subjected to a total of 20 mm of displacement, as shown in Figure 5-6. For Mode-II (the sliding shear mode), a three-point loading was simulated, similar to the ENF model. Both ends of the sample were supported on one side, and on the opposite side to the sample a 10 mm displacement was exerted through the point load at the centre, as illustrated in Figure 5-7. The 3D zero thickness interfaces were modelled as an inter-layer cohesive element between the laminate to direct the interlaminar crack propagation front paths.

Table 5-2: Modelled sample dimensions.

Specimen Dimensions	Overall length = 150 mm
	Crack length = 50 mm
	Height = 3 mm
	Width = 25 mm
	Maximum load displacement = 10 mm

Table 5-3: Mechanical properties of composite specimen.

Material properties	Direction	Carbon fiber / Epoxy	Glass fiber / Epoxy
Young's Modulus	X	135.3 GPa	40 GPa
	Y	9 GPa	5 GPa
	Z	9 GPa	5 GPa
Poisson's Ratio	XY	0.24	0.27
	YZ	0.46	0.27
	XZ	0.24	0.275
Shear Modulus	XY	5.2 GPa	1.07 GPa
	YZ	3.08 GPa	0.806 GPa
	XZ	5.2 GPa	1.07 GPa
Interface	Maximum stress = 25 MPa		
	Normal separation = 0.004 mm		
	Shear Separation = 1000 mm		

5.14 Results and discussion

A DCB was used to determine Mode-I interlaminar fracture toughness, and the ENF beam was used to determine Mode-II interlaminar fracture toughness. The finite element 3D models illustrate the von-Mises stress distribution in both the ENF and DCB methods as shown in Figure 5-8 for the ENF method and Figure 5-9 for DCB method. According to Equations (5.3) and (5.4), the resultant stresses represent the reaction forces, and consequently the energy release rates G_I for the DCB and G_{II} for the ENF models were calculated (Mishani *et al.*, 2015).

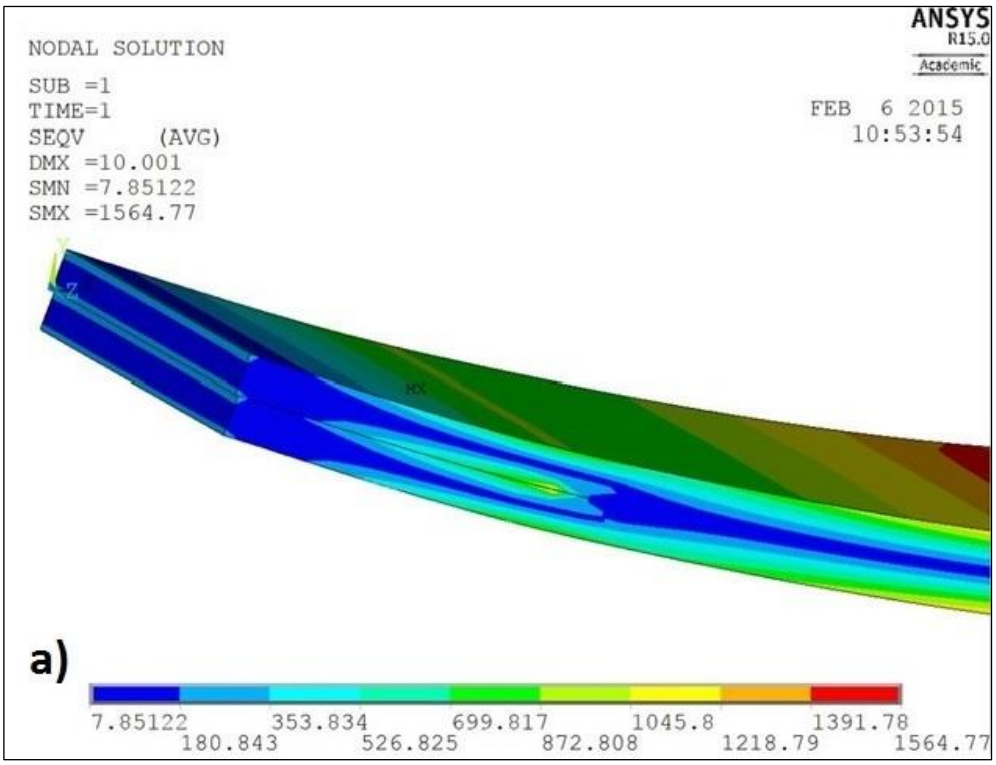

Figure 5-8: ANSYS model von-Mises stress distribution (N) for ENF.

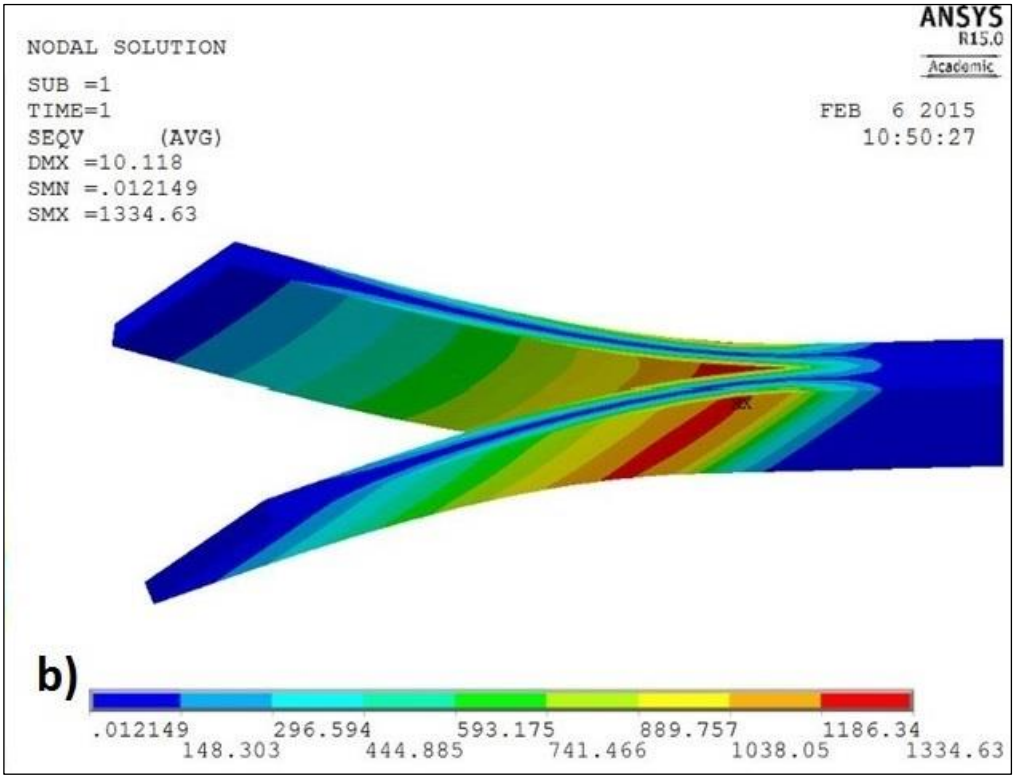

Figure 5-9: ANSYS model von-Mises stress distribution (N) for DCB.

Figure 5-10 shows a contour plot for the crack front face versus total strain energy release rate (G_T) for the DCB model in both carbon and glass fibre composite laminates. The G_I and G_T values are equal at the crack front face for both the carbon and glass fibre composite materials. The graphs illustrate that the release energy rate by the carbon fibre was almost three times more than that for the glass fibre. The results of the Mode-I testing method confirm that the DCB model represents only the pure normal stress from the release strain energy rate G_I (Brunner *et al.*, 2008).

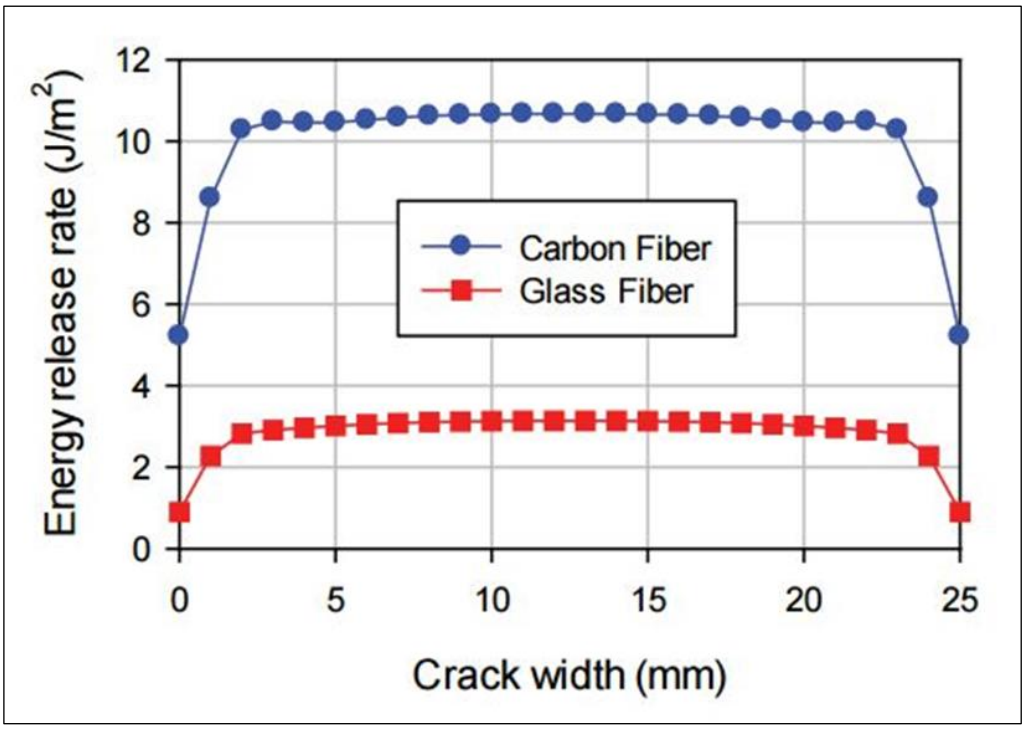

Figure 5-10: Total energy release rate (Mode-I) (Mishani *et al.*, 2015).

As presented in Figure 5-11 and Figure 5-12, the total energy release rate (G_T) and shear energy release rate (G_{II}) obtained from the ENF model correspond to a crack initiation during the application of slide shear load, Mode-II. The results show that the G_T values are slightly more than the G_{II} values (almost 2.5% and 1% at the edges for glass fibre and carbon fibre, respectively). The narrow difference between G_T and G_{II} indicates that, apart from shear stress (the evaluation of which was based on the strain energy release rate Mode-II), there are other sources contributing to the strain energy release rate (such as inter-layer frictions and normal stress) in the ENF testing mode. The result confirms (Brunner *et al.*, 2008) the suggestion that the ENF testing method cannot represent pure shear stress in delamination crack testing.

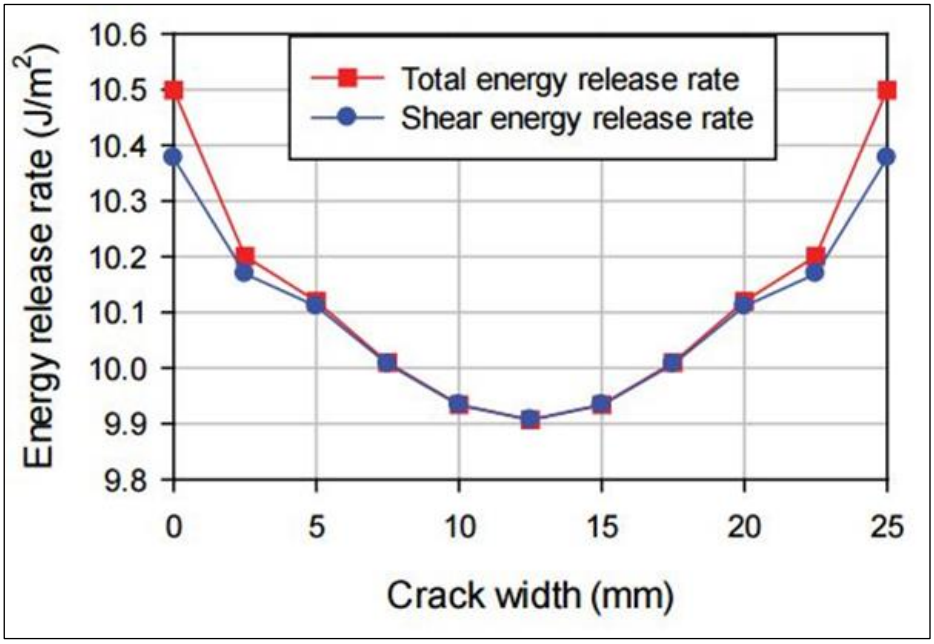

Figure 5-11: Energy release rates (Mode-II) for carbon fibre (Mishani *et al.*, 2015).

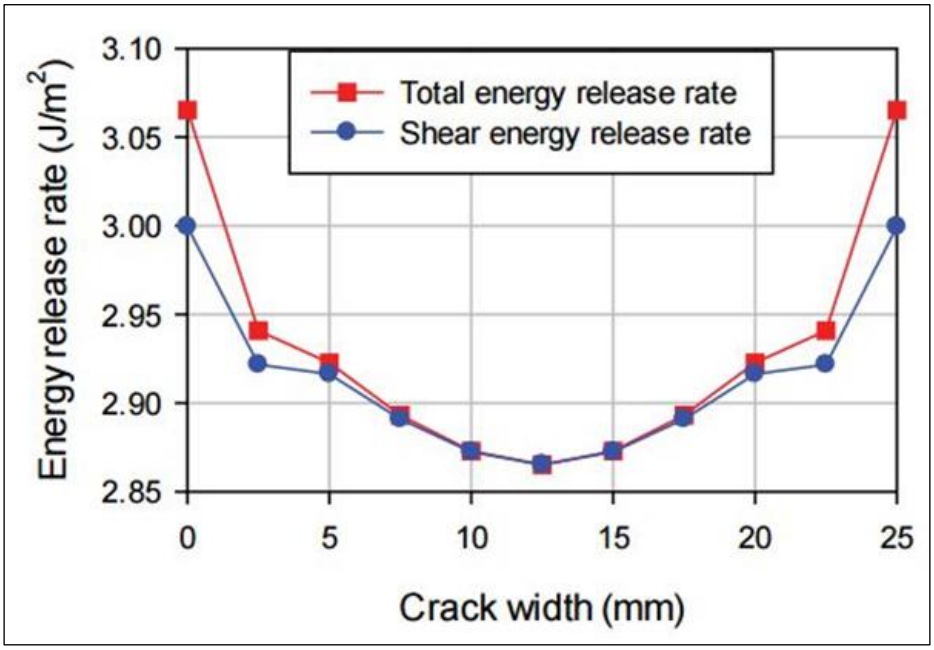

Figure 5-12: Energy release rates (Mode-II) for glass fibre (Mishani *et al.*, 2015).

5.15 Effect of load force on testing approach

The results from the analyses of the point load displacement responses of the applied force to the DCB and ENF models for the carbon- and glass-fibre composite materials are shown in Figure 5-13 and Figure 5-14. The contour plots present the relationship between carbon fibre and glass fibre in Mode-I and Mode-II modelling.

In the Mode-I, DCB model, for a 10 mm point load displacement, the applied force to the pre-existing crack edges of the model for carbon- and glass-fibre composites are 20 N and 5.6 N, respectively. A 10 mm point load displacement to the centre of Mode-II, ENF model corresponds to 1,500 N for carbon fibre and 470 N for glass fibre. This means that the applied load for the same load displacement in carbon fibre is almost three times more than that of glass fibre in the DCB and ENF models.

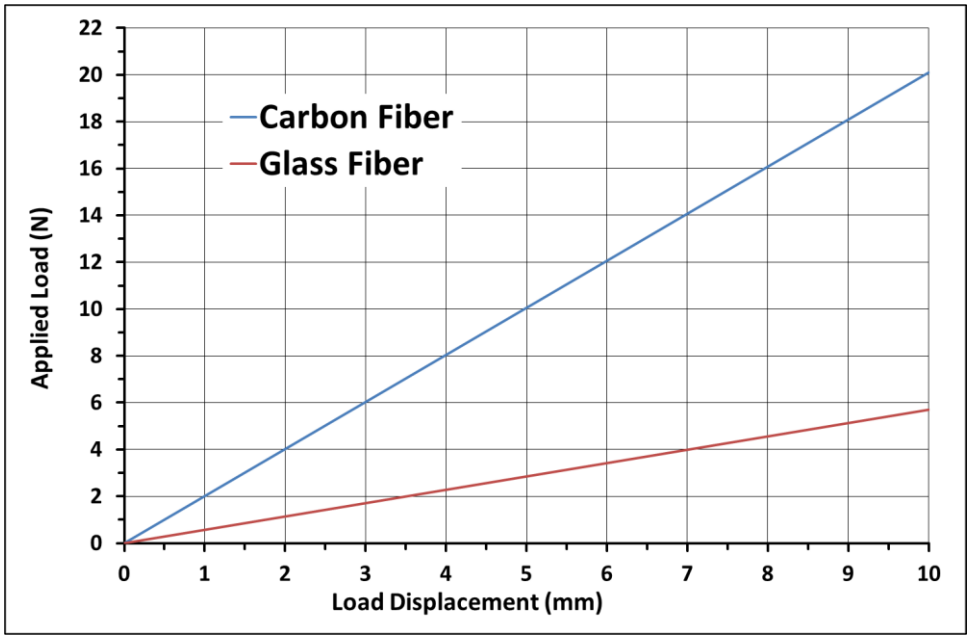

Figure 5-13: Mode-I DCB testing for (a) carbon fibre and (b) glass fibre.

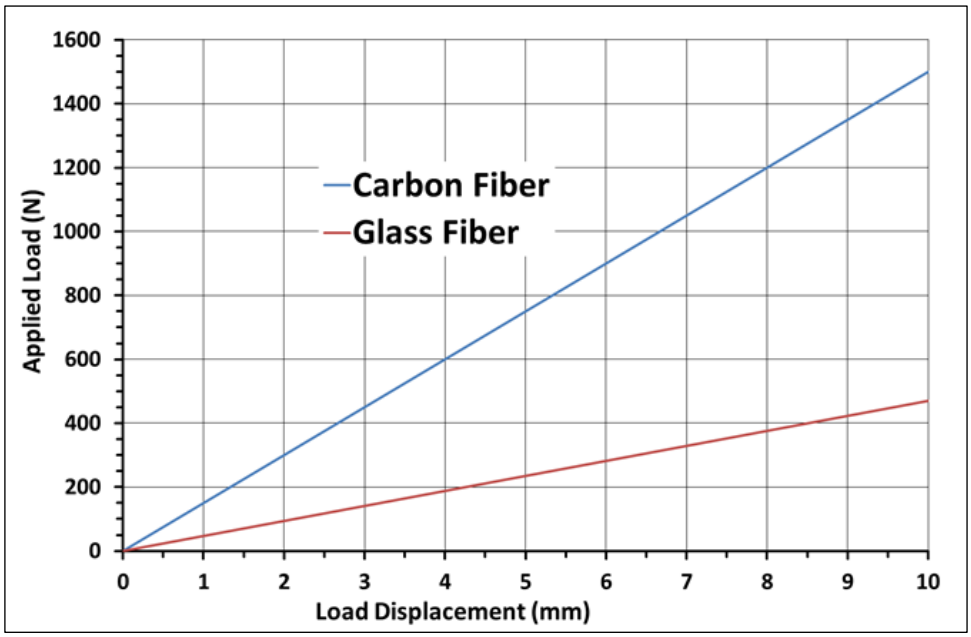

Figure 5-14: Mode-II ENF testing for (a) carbon fibre and (b) glass fibre.

5.16 Conclusions

This chapter presents the initial results of a study into the influence of failure on the properties of filament-wound coiled tubes. Numerical simulation was implemented in ANSYS V.15/APDL software to measure the delamination fracture toughness of carbon and glass fibre composite laminates and the following results have been obtained:

- The variation of strain release energy rates versus crack tip development illustrated that 2D modelling cannot express the true release strain energy rate at the crack tip front. The contour for strain energy release rate in Mode-I testing (G_I) increases - almost doubling in value - from the edge to the centre (from 5 J/m^2 to approximately 10.2 J/m^2), while strain energy release rate in Mode-II testing (G_{II}) slightly decreases from the edge to the centre (from 10.4 J/m^2 to 9.9 J/m^2). It is therefore useful to investigate and understand the mode of crack propagation in composite laminates using 3D modelling.
- The "applied load" to "load displacement" perpendicular to the crack plane for carbon fibre laminate is almost three times that of glass fibre laminate in Mode-I and Mode-II states.
- The Mode-II interlaminar fracture toughness of composite laminate is several times higher than Mode-I interlaminar fracture toughness in the same material.
- The Double Cantilever Beam (DCB) testing method presents normal resistance of the crack propagation of the interlaminar layer in the opening mode conditions. The finite element analysis result shows that the normal resistance to interlaminar delamination is much less than the shear resistance in the End-Notched Flexure (ENF) testing method.

References

Alfano, G., & Crisfield, M. (2001). Finite element interface models for the delamination analysis of laminated composites: Mechanical and computational issues. *International journal for numerical methods in engineering, 50*(7), 1701-1736.

ANSYS®, A. R. (2013). *ANSYS mechanical user's Gguide*. Canonsburg, PA: ANSYS, Inc.

Barbero, E. J. (2013). *Finite element analysis of composite materials using ANSYS®*. Boca Raton, FL: CRC Press.

Bordeu, F., & Boucard, P. (2009). *A mesoscale model for the prediction of composites materials until final failure.* Paper presented at the Proc. of ICCM17-17th International Conférence on Composite Materials.

Brunner, A., Blackman, B., & Davies, P. (2008). A status report on delamination resistance testing of polymer–matrix composites. *Engineering Fracture Mechanics, 75*(9), 2779-2794.

Burlayenko, V. N., & Sadowski, T. (2008). FE modeling of delamination growth in interlaminar fracture specimens. *Budownictwo i Architektura, 2*, 95-109.

Choupani, N. (2008). Experimental and numerical investigation of the mixed-mode delamination in Arcan laminated specimens. *Materials Science and Engineering: A, 478*(1), 229-242.

Degrieck, J., & Van Paepegem, W. (2001). Fatigue damage modeling of fibre-reinforced composite materials: review. *Applied Mechanics Reviews, 54*(4), 279-300.

Gibson, R. F. (2011). *Principles of composite material mechanics*. USA: McGraw-Hill, Inc.

Harris, B. (1986). *Engineering composite materials*. London, UK: Institute of metals London.

Hashin, Z. (1980). Failure criteria for unidirectional fiber composites. *Journal of Applied Mechanics, 47*(2), 329-334.

Jones, R. M. (1998). *Mechanics of composite materials* (Second ed.). Philadelphia, PA: Taylor & Francis.

Krueger, R. (2004). Virtual crack closure technique: History, approach, and applications. *Applied Mechanics Reviews, 57*(2), 109-143.

Li, Teng, T., Wan, Z., Li, G., & Rans, C. (2013). *Fatigue delamination growth for an adhesively-bonded composite joint under Mode-I loading.* Paper presented at the 27th ICAF Symposium, Jerusalem, Israel.

Mathews, M. J., & Swanson, S. R. (2007). Characterization of the interlaminar fracture toughness of a laminated carbon/epoxy composite. *Composites Science and Technology, 67*(7), 1489-1498.

Mier, J. G. M. v. (2012). Classical fracture mechanics approaches *Concrete Fracture* (pp. 11-34). Boca Raton, FL: CRC Press.

Mishani, S., Evans, B., Rasouli, V., Roufail, R., Soe, S., & Jaensch, P. (2015). Interlaminar modelling to predict composite coiled tube failure. *The APPEA Journal, 55*(1), 361-370.

Ochoa, O. O., & Reddy, J. N. (1992). *Finite element analysis of composite laminates* (Vol. 7). Dordrechet, The Netherland: Kluwer Academic Publishers.

Prasad, M. S., Venkatesha, C., & Jayaraju, T. (2011). Experimental methods of determining fracture toughness of fiber reinforced polymer composites under

various loading conditions. *Journal of Minerals and Materials Characterization and Engineering, 10*(13), 1263.

Reifsnider, K., Henneke, E., Stinchcomb, W., & Duke, J. (1983). Damage mechanics and NDE of composite laminates. *Mechanics of composite materials: Recent advances*, 399-420.

Salehizadeh, H., & Saka, N. (1992). Crack propagation in rolling line contacts. *Journal of tribology, 114*(4), 690-697.

Spada, A., Giambanco, G., & Rizzo, P. (2009). Damage and plasticity at the interfaces in composite materials and structures. *Computer Methods in Applied Mechanics and Engineering, 198*(49), 3884-3901.

Sun, X., Tan, V., Liu, G., & Tay, T. (2009). An enriched element-failure method (REFM) for delamination analysis of composite structures. *International journal for numerical methods in engineering, 79*(6), 639-666.

Szekrenyes, A. (2002). Overview on the experimental investigations of the fracture toughness in composite materials. *Hungarian Electronic Journal of Sciences, Mechanical Engineering Section, MET-020507-A*.

Thakur, V. K. (2014). *Green composites from natural resources*. Boca Raton, FL: CRC Press.

Turon Travesa, A. (2006). *Simulation of delamination in composites under quasi-static and fatigue loading using cohesive zone models.* (Doctor of Philosophy), Universitat de Girona, Spain.

Wisheart, M., & Richardson, M. (1998). The finite element analysis of impact induced delamination in composite materials using a novel interface element. *Composites Part A: Applied Science and Manufacturing, 29*(3), 301-313.

Wu, & Yao. (2010). A fatigue damage model of composite materials. *International journal of fatigue, 32*(1), 134-138.

Zhu, Y. (2009). *Characterization of Interlaminar Fracture Toughness of a Carbon/epoxy Composite Material.* (Master of Science), The Pennsylvania State University.

Chapter 6 Fatigue life enhancement of composite coiled tube with thermoplastic pressure barrier

6.1 Background

In comparison to conventional steel coiled tubes, composite coiled tubes can have a higher mechanical strength, stiffness and lower unit weight (Williams & Sas-Jaworsky, 2000). This makes composite coiled tubes more desirable for well site operations and especially for deep and extended reach horizontal drilling operations (Sas-Jaworsky & Williams, 1993). The resin structural dislocation is highly sensitive to the strain rates, and therefore, the fatigue life of a composite material is still an inherent constraint for bending over a low radius surface.

The practices discussed in this chapter pertain to the cyclic fatigue life of prototype filament-wound composite tube specimens constructed and tested to date. The composite tube samples were manufactured, oven-cured and both ends sealed by proprietary connectors to impose internal pressures of 3,500 psi and 1,000 psi. Cyclic bending fatigue tests were then performed on composite tube samples using a purpose-built bending machine with a 55 inches radius curved block (as discussed in chapter 4).

During the first bending event, the coiled tube specimen did not have a liner. A crack rapidly initiated and propagated, and failure occurred through the matrix structure along with a sudden depletion of internal pressure. In order to enhance the fatigue life of the composite tube during high internal pressure, two different types of epoxy resins and two different thermoplastic liners were placed inside the composite tubes.

The main contribution of this chapter is to provide the result of experimental work which would allow longer lengths of the composite tube to be spooled on a smaller

sized reel and to enhance the cyclic life potential of composite coiled tube substantially over that of conventional steel coiled tubing when subjected to plastic deformation bending cycling with high internal pressure. The practice was validated via numerical modelling to highlight the displacement and load transfer during the cyclic fatigue process.

6.2 Introduction

Composite coiled tube technology was commercialized for down hole applications in the late 1990s (Afghoul *et al.*, 1994). However, the variety of composite coiled tubing operations are many, but its drilling applications have been limited.

Composite material has a unique characteristic, in which, for the same construction material, there are different design parameters that can be tailored to exhibit optimal burst and collapse pressure rates, axial load, and strain bending strength for specific applications. Some of the benefits of using composite coiled tube are as below:

- The geometry of fibre inside the layers of composite material can be engineered to achieve a specific performance from the final product, such as higher strength, more flexibility, and greater stiffness,
- Any change in resin formula and the curing method can produce a composite material with different characteristics,
- A wide range of conductor wires can be embedded between the layers of composite material for power and data transfer,
- A liner inside and outside of the composite tube changes the corrosion rate and tube roughness properties, and can be utilized as an additional internal and external pressure barrier.

There are two main classifications for resins: thermoset resins and thermoplastic resins. The thermoplastic resin has advantages in toughness and fatigue life to the thermoset resin. From a manufacturing standpoint, a thermoset resin is liquid at room temperature, therefore easier to work with and can easily have air bubbles removed during manufacturing to allow rapid manufacture. Additionally, the mechanical behaviour of the thermoplastic resin is more non-linear than that of the thermoset resin.

A composite tube may consist of a thermoplastic liner covered by a filament-wound carbon and glass fibre, mixed with an epoxy resin. The fibre lay-up direction can be tailored to specific manufacturing conditions and be exposed to cyclic bending and

internal pressures. A ply-by-ply analytical method, ANSYS Finite element model, experimental results and CT-Scan images were applied to determine the damage mode of composite coiled tubes. Hashin's failure criterion was used to calculate First Ply Failure (FPF) characteristics in the composite layers.

6.3 Thermoset resins (Matrix)

A thermoset resin is obtained by mixing a resin and a hardener to produce a hard product. Thermoset resins (generic name for a polymer) are widely used to construct man-made composite materials. The properties and mixing process of a resin (matrix) inserted into the layers of fibre is crucial for achieving the desired mechanical properties of a composite material. The three most common thermoset resins popularly used for manufacturing fibre reinforced composite materials are:

- Polyester resin: It tends to have yellowish tint, inexpensive, no need to be cured and it has the lowest adhesive property of the other two thermoset resins.
- Vinyl ester resin: It has lower viscosity and is more transparent than polyester resin. It tends to have a greenish tint and its adhesive property, cost of production, and strength are intermediate between polyester and epoxy resin.
- Epoxy resin: It tends generally to have light yellowish tint but after curing process, it becomes transparent. Epoxy resin offers the best adhesive performance, best mechanical properties and less shrinkage to the other resins, but at a higher cost, therefore it is frequently used in many high-strength composite materials.

As epoxies cure with low shrinkage, the various surface contacts set up between the liquid resin and the adherents are not disturbed during the curing process (Mohanty *et al.*, 2005). The experimental results of curing of three different resins - polyester, vinyl ester and epoxy resins - cured at 20°C and 80°C are shown in Figure 6-1 through Figure 6-3.

The ultimate strength of a composite material is defined as being at the point in which the resin structure has failed and the fibres have broken. However, before the failure happens, when the strain rate reaches a specific level, the crack starts to initiate inside the resin body and then spreads through the matrix (de-bonding between fibres and resins) and finally a catastrophic failure (ultimate tensile strength) occurs, as shown in Figure 6-4.

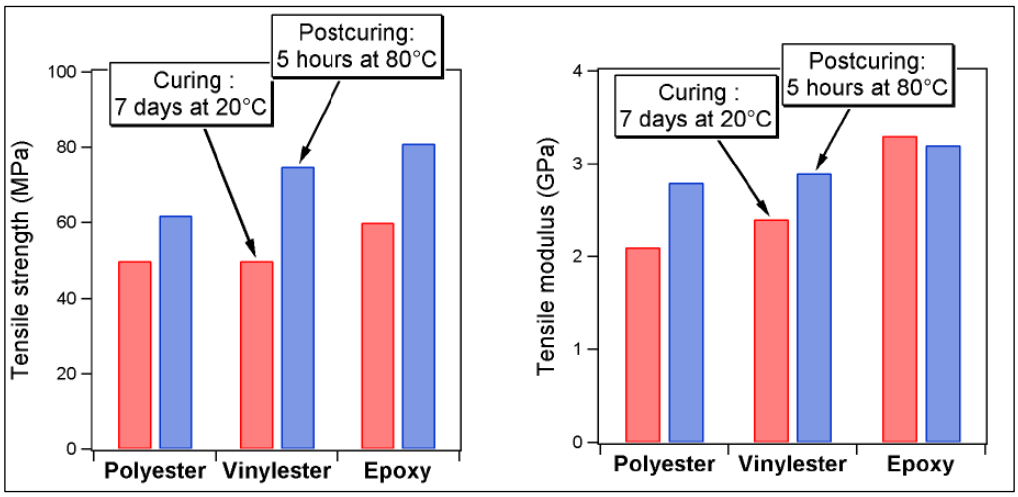

Figure 6-1: Typical tensile strength and stiffness of resins (Gurit, 2012)

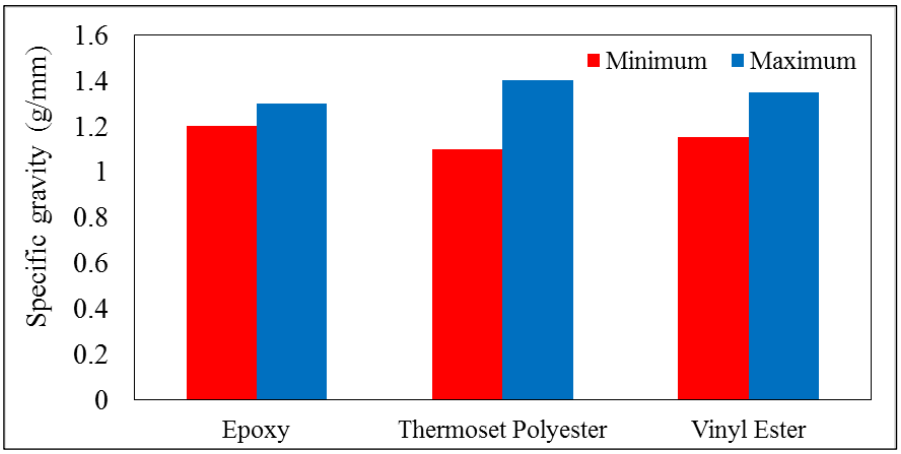

Figure 6-2: Specific gravity (g/mm) ranges of typical resin (Mallick, 2007).

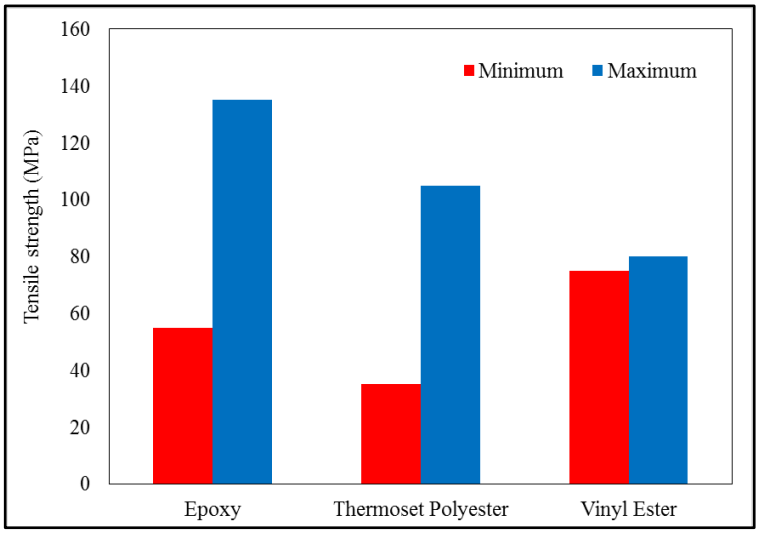

Figure 6-3: Tensile strength (MPa) ranges of typical resin (Mallick, 2007).

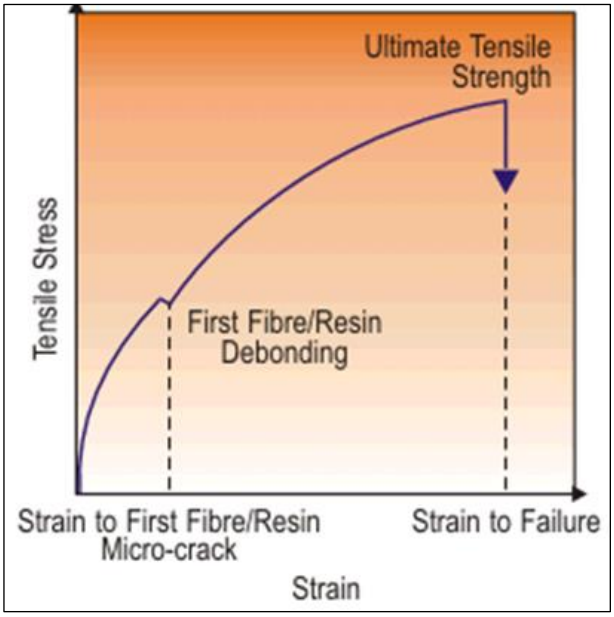

Figure 6-4: Composite material stress vs. strain plot (Mallick, 2007).

The strain rate of a composite material, before crack initiation, depends on the toughness and adhesive characteristics of the resin. Consequently, the properties of epoxy resin help composite material to achieve higher levels of maximum strain rate, as shown in Figure 6-5. The fatigue failure results from accumulated small cracks. The toughness of resin indicates the resistance of composite material to crack initiation and propagation. However, the fatigue behaviour of composite material is influenced by the toughness of the resin, and the ultimate strain to failure is the easier way to measure the fatigue index in composite materials (Gurit, 2012).

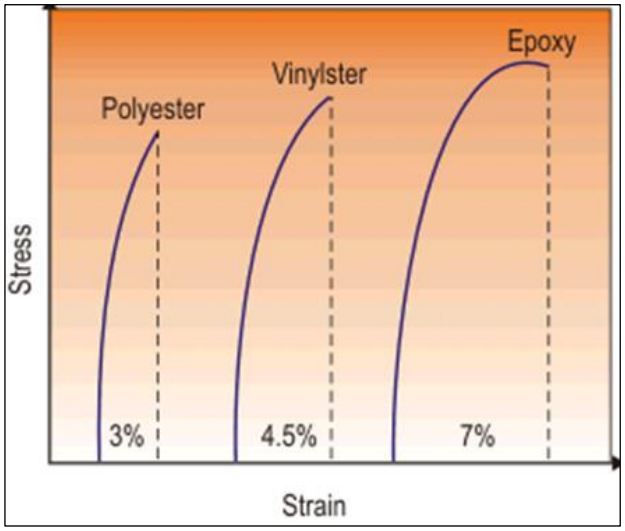

Figure 6-5: Typical comparison between strain rates in resins (Mallick, 2007).

6.4 Orthotropic material

A fibre reinforced composite material has different properties from one point to another and is called the heterogeneous characteristics of the material. Mechanical analysis of heterogeneous materials are difficult but simplified by using an average value for properties of the fibre and resin, as a homogenous material. In the simplified analysis, the properties of an individual fibre or matrix is not considered but smeared over the structure of the composite material. As an orthotropic material, the fibre and matrix properties are replaced by a single homogeneous property, in parallel and transverse to the unidirectional fibre reinforced composite material. Hence, the properties of composite material is a function of a fibre's orientation (Barbero, 2007).

Consider a single layer (called a lamina) of unidirectional fibre-reinforced composite material as shown in Figure 6-6. In the lamina, the directions of an orthogonal coordinate system are taken as:

X_1 Aligned with the direction of fibre,

X_2 Placed in the plane of lamina and perpendicular to the direction of fibre,

X_3 Placed both in and perpendicular to the plane and the direction of fibre

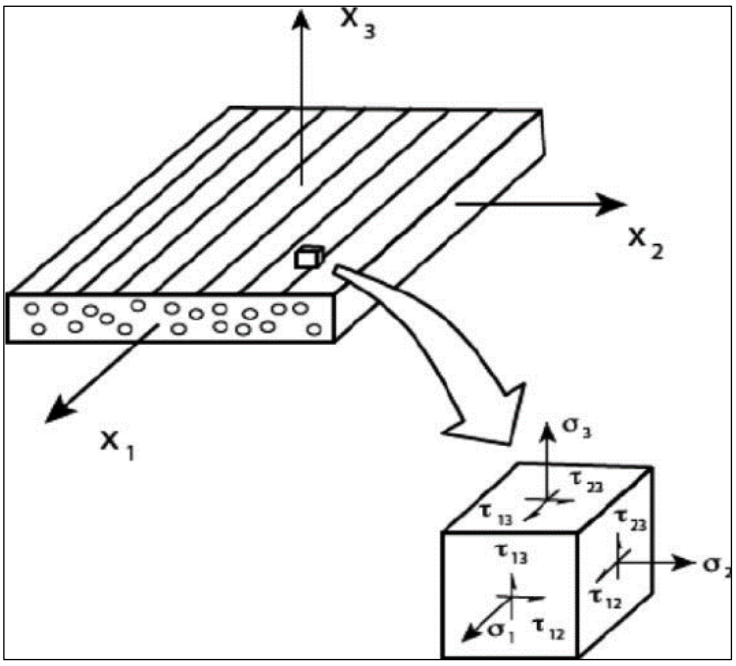

Figure 6-6: Orthotropic coordinate system in a composite laminate (Barbero, 2007).

The above composite material, in which the behaviour of two out of three coordinate directions are identical, is called a transversely isotropic material.

In orthotropic lamina, there are three normal stresses σ_1, σ_2 and σ_3, and three shear stresses τ_{12}, τ_{23} and τ_{13}. These normal and shear stresses are related to the strains ε_1, ε_2, ε_3, γ_{12}, γ_{23}, and γ_{13} (Barbero, 2007).

The Generalized Hooke's Law of any material (stress and strain relation) is given as:

$$\sigma_i = C_{ij} \times \varepsilon_j \tag{6.1}$$

where:

C_{ij} The stiffness matrix

The Equation (6.1) can also be written as:

$$\varepsilon_i = S_{ij} \times \sigma_j \tag{6.2}$$

where:

S_{ij} The compliance matrix

These coincide with the coordinate planes. Nine constants are required to describe the symmetric planes of an orthotropic composite material. The generalized Hooke's Law (Equation (6.2)) for an orthotropic material converts to Equation (6.3) which is important when we input material properties to make it into a three-dimensional orthotropic composite material model in ANSYS:

$$\begin{bmatrix} \varepsilon_1 \\ \varepsilon_2 \\ \varepsilon_3 \\ \gamma_{23} \\ \gamma_{31} \\ \gamma_{12} \end{bmatrix} = \begin{bmatrix} \frac{1}{E_1} & -\frac{\nu_{21}}{E_2} & -\frac{\nu_{31}}{E_3} & 0 & 0 & 0 \\ -\frac{\nu_{12}}{E_1} & \frac{1}{E_2} & -\frac{\nu_{32}}{E_3} & 0 & 0 & 0 \\ -\frac{\nu_{13}}{E_1} & -\frac{\nu_{23}}{E_2} & \frac{1}{E_3} & 0 & 0 & 0 \\ 0 & 0 & 0 & \frac{1}{G_{23}} & 0 & 0 \\ 0 & 0 & 0 & 0 & \frac{1}{G_{31}} & 0 \\ 0 & 0 & 0 & 0 & 0 & \frac{1}{G_{12}} \end{bmatrix} \times \begin{bmatrix} \sigma_1 \\ \sigma_2 \\ \sigma_3 \\ \tau_{23} \\ \tau_{31} \\ \tau_{12} \end{bmatrix} \tag{6.3}$$

where:

$\varepsilon_1, \varepsilon_2, \varepsilon_3$	Principal normal strain components
γ_{12}	Shear strain in-plane
γ_{12}, γ_{12}	Shear strain through thickness
$\sigma_1, \sigma_2, \sigma_3$	Principal normal stress components
τ_1, τ_2, τ_3	Principal shear stress components
E_1, E_2, E_3	Young's moduli in each material axis
G_{12}	Shear modulus in-plane
G_{13}, G_{23}	Shear moduli through thickness
ν_{12}	Poisson's ratio in-plane
ν_{13}, ν_{23}	Poisson's ratios through thickness

6.5 Failure criteria analysis

The anisotropic structural mechanism of a composite material under cycling bending load conditions forms tri-axial stresses with a complex fracture behaviour. The repetitions of a small plastic deformation (although applied once does not cause significant damage) will lead to fatigue failure, and moreover, the exposing hoop stress, under high internal pressure, changes the fatigue mode in composite coiled tube. Fatigue failure in composite material occurs with different damage configurations. Failure analysis is a tool for predicting the fatigue life of a composite material, under complex loading conditions. Therefore, for a safe structural design, it is necessary to know the fatigue behaviour of composite material under cyclic loading.

There are two main methods of modelling damage and failure in composite material, "Delamination" and "Fibre/matrix" damage. There are many failure criteria for composite material analysis, however, they need to be compatible with the finite element analysis method (Matthews *et al.*, 2000). The failure criteria are categorized into independent and interactive criteria. The maximum stress and maximum strain, as independent criteria, are simple and quite conservative methods, because these criteria evaluate the mode of failure, and they neglect the effect of stress interactions. The interactive criteria, such as Tsai-Wu, Tsai-Hill, Puck and Hashin's criteria present the stress interaction mechanisms for prediction of First Ply Failure (FPF) in a composite material. So, the interactive criteria give better predictions for failure in a composite

material. However, failure estimation at first ply level is often a conservative approach with respect to the Last Ply Failure (LPF) and fibre fracture, as shown in Figure 6-7.

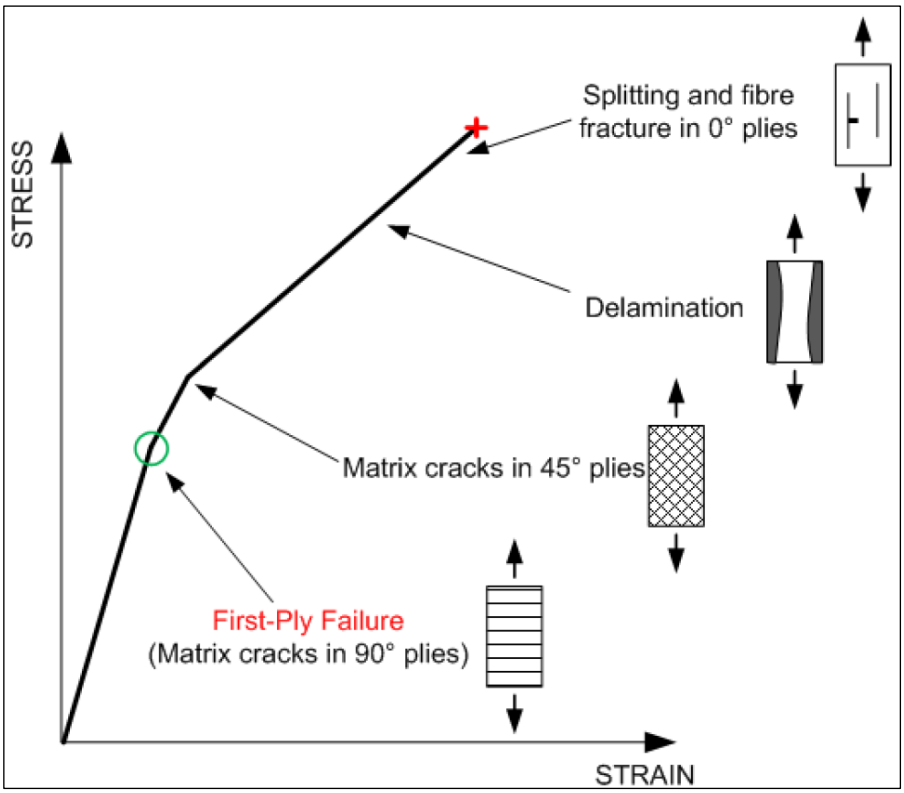

Figure 6-7: First Ply failure mode (Aymerich, 2012).

The Hashin polynomial failure criterion is selected in this failure analysis investigation, because it can distinguish between different possible failure modes in a composite material. According to a ply-by-ply approach, four stress based Hashin's criterion equations were used to predict the damage modes in composite material as follows:

Fibre tensile failure:

$$\left(\frac{\sigma_1}{X_T}\right)^2 + \left(\frac{\sigma_{12}}{S_{12}}\right)^2 + \left(\frac{\sigma_{13}}{S_{13}}\right)^2 \geq 1 \tag{6.4}$$

Fibre compressive failure:

$$\left(\frac{\sigma_1}{X_C}\right)^2 + \left(\frac{\sigma_{12}}{S_{12}}\right)^2 + \left(\frac{\sigma_{13}}{S_{13}}\right)^2 \leq 1 \tag{6.5}$$

Matrix tensile failure:

$$\left(\frac{\sigma_3}{Y_T}\right)^2 + \left(\frac{\sigma_{12}}{S_{12}}\right)^2 + \left(\frac{\sigma_{13}}{S_{13}}\right)^2 \geq 1 \tag{6.6}$$

Matrix compressive failure:

$$\left(\frac{\sigma_3}{Y_C}\right)^2 + \left(\frac{\sigma_{12}}{S_{12}}\right)^2 + \left(\frac{\sigma_{13}}{S_{13}}\right)^2 \leq 1 \qquad (6.7)$$

where:

σ_1 , σ_3	Maximum normal stresses in the lamina
σ_{12} , σ_{13}	Maximum stresses components in the lamina
S_{12} , S_{13}	Allowable shear strength components in the lamina
X_T , Y_T	Allowable tensile strength in the lamina
X_C , Y_C	Allowable compressive strength in the lamina

6.6 Numerical modelling

In order to simulate damage in a composite coiled tube under bending load conditions and imposing a constant internal pressure, a three-dimensional progressive damage finite element model was developed to predict the damage mode in layers of the laminate. The finite element parametric study including stress and strain analysis, failure analysis and the progressive damage model was performed using the workbench/ANSYS V.15 software to examine the effect of coiled tube bending radii and internal pressure upon the material property degradation, strain rate and damage accumulation. The progressive damage model in fibre and matrix layers utilizes Hashin's failure criterion and degradation of material rules to quantify and verify the material's strength properties.

The high maximum stress level results in an interlaminar crack in between the composite layers. It leads the composite structure to progressive failure that causes a significant stiffness change and redistribution of stresses. In order to predict the progressive failure, a finite element analysis model is required. The model needs to incorporate failure criteria for predicting the complex behaviour of the composite structure (Zureick & Nettles, 2002).

Based on the progressive failure model, the first step for continuum damage formulation is to define the parameters for stiffness of composite material and the next challenge is identifying the damage evolution laws for the damage parameters of composite material. The Damage Evolution Law calculates the amount of damage

during the deformation process (stiffness reduction). It takes a value from '0' to '1', where '0' indicates no damage (means no stiffness reduction), between '0' and '1' indicates some damage and '1' indicates completely damaged (maximum stiffness reduction) material (as shown in Figure 6-8).

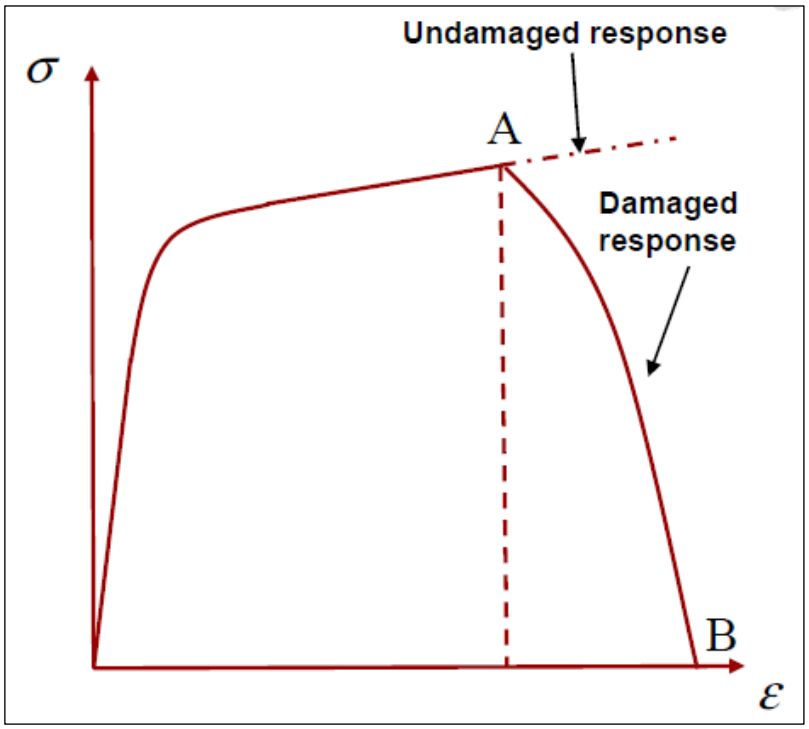

Figure 6-8: Typical progressive damage response (ANSYS®, 2013).

The finite element modelling routines involve the following steps:

1. Defining the material properties for glass/epoxy and carbon/epoxy (as shown in Table 6-1), creating the tube and bending mechanism's geometries, and set-up composite material lay-up,
2. Defining a global coordinate system for bending parameters and a local coordinate system in a direction to the components of the composite tube (as shown in Figure 6-9). In the global coordinate system, the x axis is parallel to the fibre direction, the y axis is normal to the fibres, direction in the plane of the laminate layer, and the z-axis normal to the plane of the laminate layer. The coordinate axis of the composite tube model and global coordinate axis is shown in Figure 6-10,

Table 6-1: Material properties of unidirectional carbon and glass fibre.

Orthotropic characteristics	Carbon fibre properties	Glass fibre properties
Young's Modulus X direction (MPa)	126000	45600
Young's Modulus Y direction (MPa)	11000	16200
Young's Modulus Z direction (Mpa)	11000	16200
Poisson's ratio XY	0.28	0.278
Poisson's ratio YZ	0.4	0.4
Poisson's ratio XZ	0.4	0.4
Shear Modulus XY (MPa)	6600	5830
Shear Modulus YZ (MPa)	6600	5830
Shear Modulus XZ (MPa)	6600	5830
Tensile X direction (MPa)	1950	1280
Tensile Y direction (MPa)	48	40
Tensile Z direction (MPa)	48	40
Compressive X direction (MPa)	-1480	-800
Compressive Y direction (MPa)	-200	-145
Compressive Z direction (MPa)	-200	-145
Shear XY (MPa)	79	73
Shear YZ (MPa)	79	73
Shear XZ (MPa)	79	73

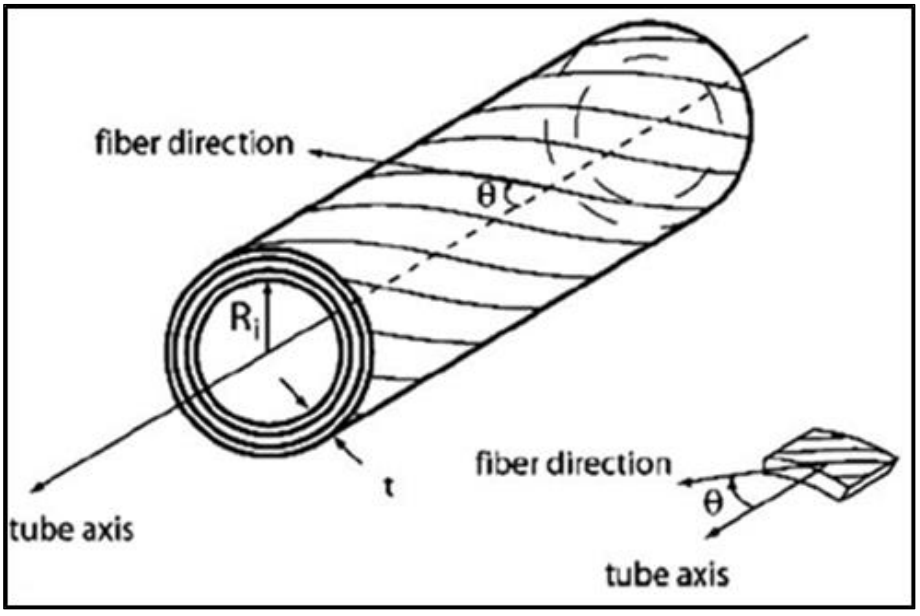

Figure 6-9: Local coordinate system for composite tube (Barbero, 2007).

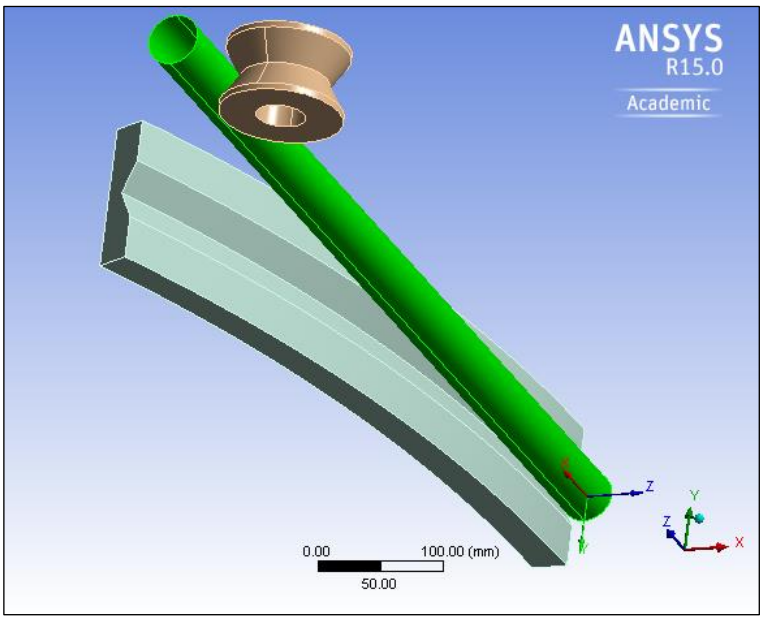

Figure 6-10: Coordinate axis of composite tube in model.

3. Choosing the Solid 191 element type. It is a 20 node element with three degrees of freedom at each node and it adapts to orthotropic properties of material,
4. Choosing the proper mesh size for analysing composite tube. In coarse mesh size, important details may not be captured and the fine mesh sizes are time consuming, so because of this, the element size of 6 mm was chosen,
5. Applying Loads, displacements and boundary conditions,
6. For large-deformation and nonlinear frictionless solid body contact between pushing/pulling rollers and bent surface with composite tube, Augmented Lagrange formulations are recommended. They augment the calculations of the contact forces,
7. Performing non-linear stress analysis and calculating the distributed stresses over each ply in a composite tube,
8. Analysing the matrix and fibre controlled types of failure analysis by applying Hashin's failure criteria,
9. Check for convergence behaviour and accuracy which are influenced by the contact stiffness parameter,
10. Check for fibre and matrix damage in compression and tension directions. These affect and govern the ultimate load that the composite tube can withstand.

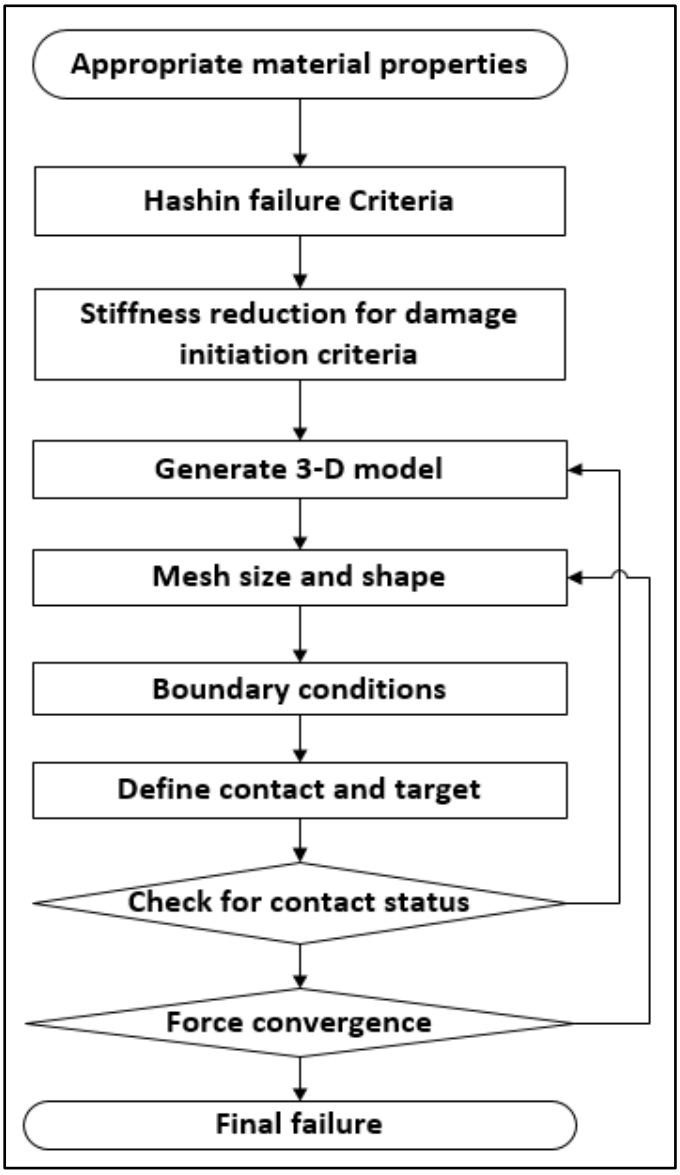

Figure 6-11: progressive failure design flowchart.

6.7 Numerical analysis results

To compare the experimental results with numerical methods, a Finite Element model was created for a composite tube sample under a cyclic bending mechanism onto a surface with a fixed radius of curvature. The composite tube with an outer diameter of 42 mm and overall thickness of 5.5 mm - including 2 mm carbon fibre in four orientation layers, 3 mm glass fibre in four orientation layers and 2.5 mm thermoplastic liner, is shown in Table 6-2, and was made using a three dimensional model and extruded to the depth of 1,200 mm.

Table 6-2: Composite tube layers properties (Lagat, 2015).

Layer (+Z)	Material	Thickness (mm)	Angle (degree)
9	Carbon Fiber	0.5	-80
8	Carbon Fiber	0.5	+80
7	Carbon Fiber	0.5	-80
6	Carbon Fiber	0.5	+80
5	Glass Fiber	0.75	0
4	Glass Fiber	0.75	0
3	Glass Fiber	0.75	0
2	Glass Fiber	0.75	0
1	Polyethyene	2.5	0

Figure 6-12 shows the arrangement of the layers of the composite tube sample with the liner. Layer 1 is on the bottom (inner layer of the tube), subsequent layers are added to the top, increasing in the '+Z' normal direction and finally, layer 9 is on the top (outer layer of the tube). The composite tube was made in eight sequences including four layers of carbon/epoxy and four layers of glass/epoxy materials. Each layer of carbon/epoxy (layers 6 to 9) and glass/epoxy (layers 2 to 5) in the composite tube consisted of stacks of fibres with '± 80' and zero orientation angle, respectively. The thickness of each ply in carbon/epoxy and glass/epoxy set to thicknesses of 0.5 mm and 0.75 mm, respectively. A high density polyethylene thermoplastic liner with 2.5 mm thickness was considered as an internal pressure barrier (layer 1).

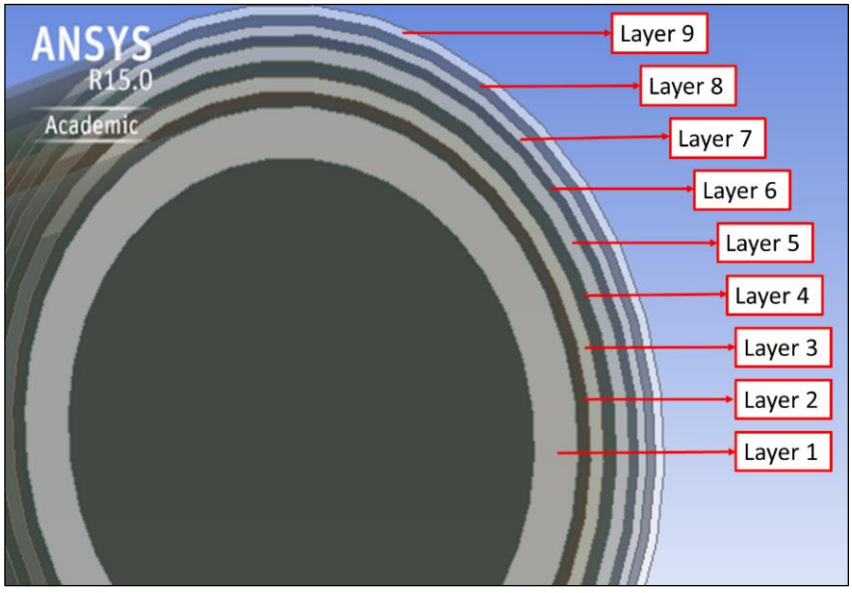

Figure 6-12: Composite tube layer arrangement.

Elastic properties of the unidirectional carbon and glass fibre, as shown in Table 6-1, were added to the model and the material type was set to lamina. In ANSYS workbench there are different ways of creating composite layers - this worksheet was chosen because of the simplicity of the method and ease of assigning a material orientation to the composite laminate. A composite tube with liner consisting of nine layers was modelled using a conventional shell as the element type. The location, material, thickness and rotation angles were added to each ply individually.

In the model, the composite tube sample is fixed at one end, by applying an 'all DOF (degree of freedom) constraint' to the end nodes, a distributed uniform force was applied to the inner surface of the tube and a concentrated transverse load applied to the other end for movement in the negative 'X' direction, as shown in Figure 6-13. This was similar to the experimental work. The exerted load simulates the bending force on top of the tube sample, to push the tube onto the curved surface with a 55 inches radius of curvature, to present a cantilever bending mechanism. Figure 6-14 shows deformation distribution of composite tube applied by a bending force.

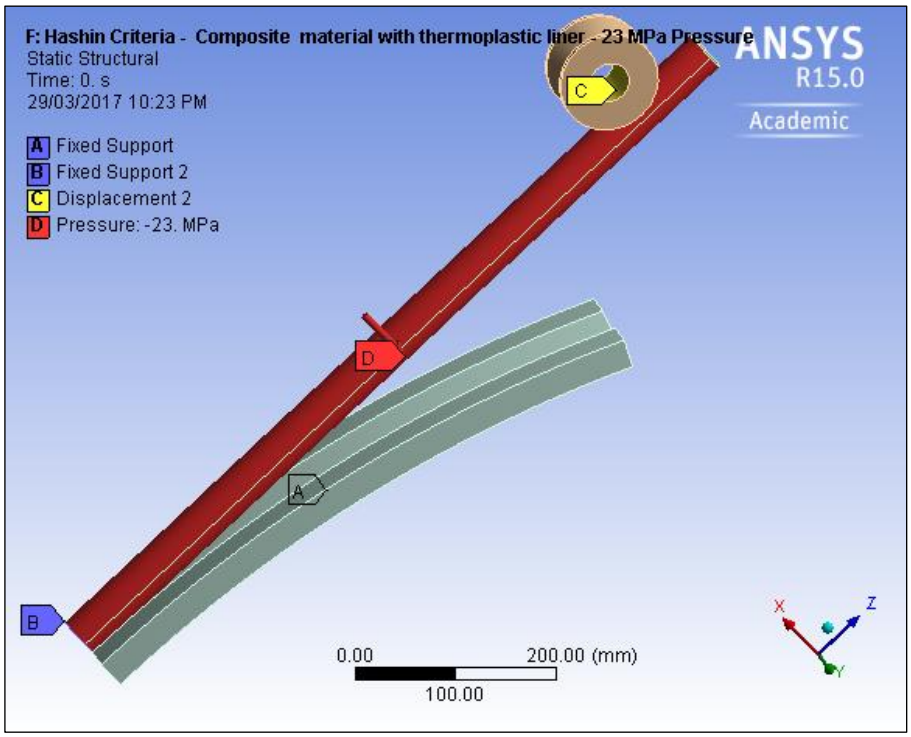

Figure 6-13: Static structure of model.

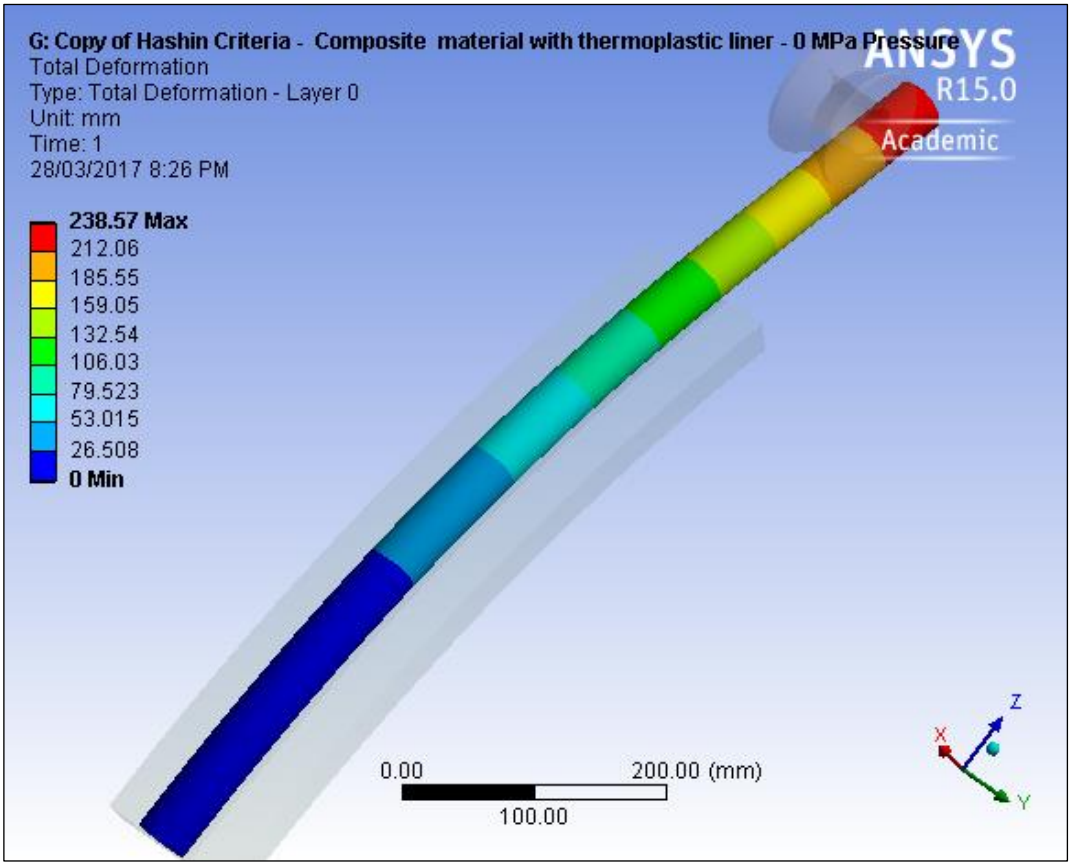

Figure 6-14: Total deformation of composite tube.

Figure 6-15 to Figure 6-17 illustrate the evolution of the maximum von-Mises stresses for every layer of the composite tube with a liner under bending, on a 55 inches curved surface with 3,500 psi of internal pressure. The carbon fibre layers (layers 6 to 9) exhibit less equivalent stress capacity than that of glass fibre (layers 2 to 5), which can effectively present the greater possibility of failure under a combination of bending and hoop stress in the glass fibre layers rather than carbon fibre. The polyethylene liner exercised the minimum equivalent stress and it was far from its ultimate stress level, so the liner could present the longest life and therefore a reliable pressure barrier layer to prevent depletion of the internal pressure.

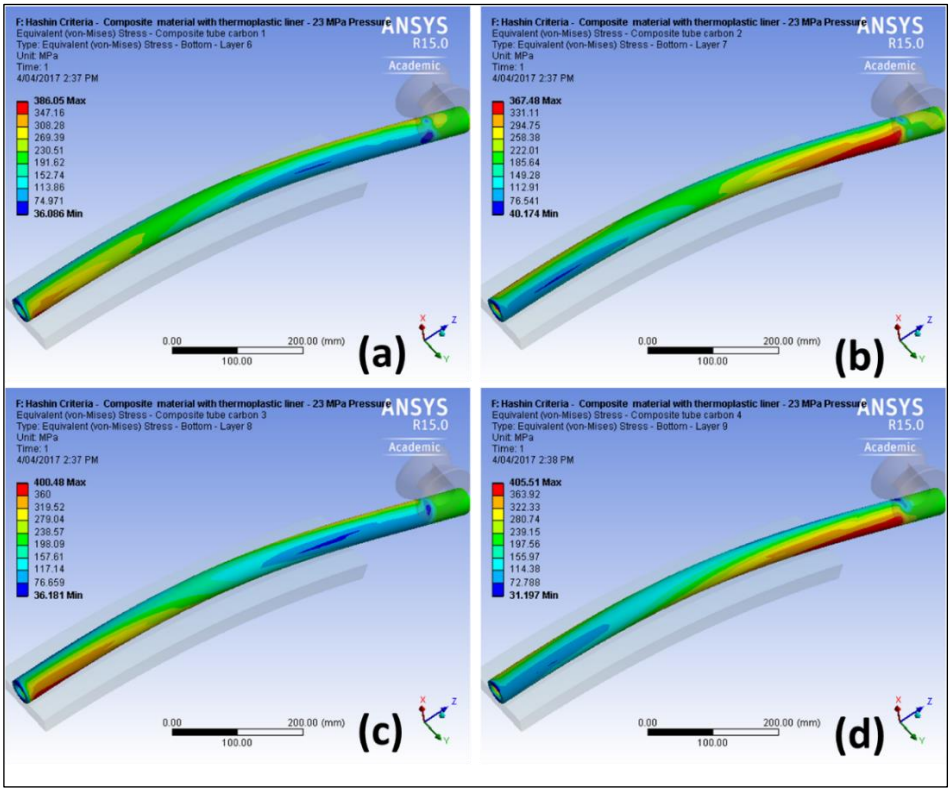

Figure 6-15: Equivalent stress in carbon fibre layers.

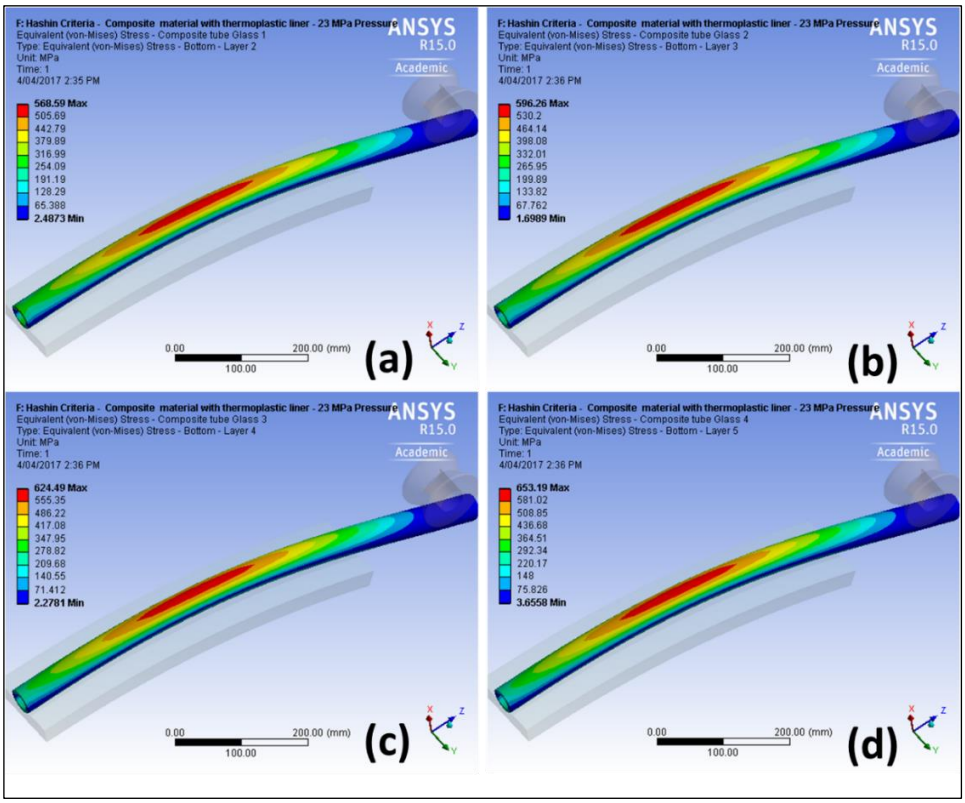

Figure 6-16: Equivalent stress in glass fibre layers.

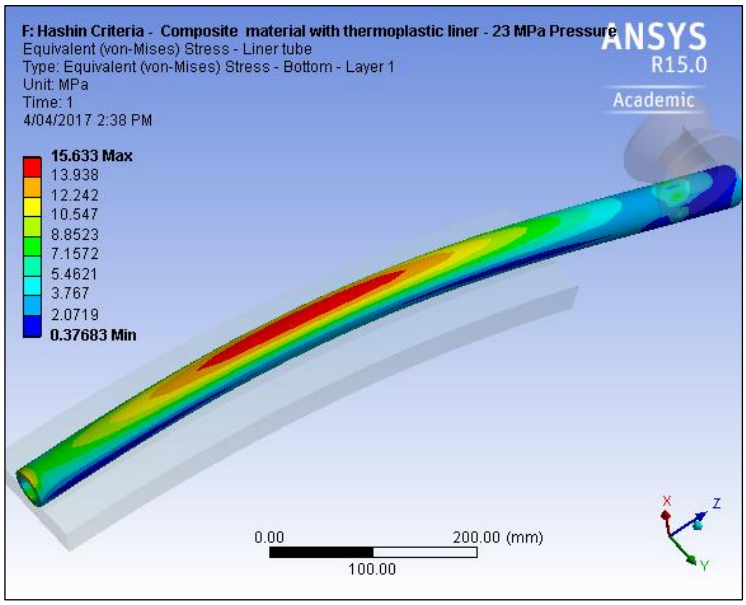

Figure 6-17: Equivalent stress in thermoplastic Liner.

Table 6-3 shows that the glass fibre layers present the highest stress level in the composite tube. The maximum stress contours (Figure 6-16) of the glass fibre layers indicate the predicted failure location on the composite tube surface, which is the outer radius of bending and it is in the same location experiments show.

Table 6-3: Maximum equivalent stress of layers.

Layer No.	Material	Maximum Equivalent Stress (MPa)
9	Carbon Fiber/Epoxy	405
8	Carbon Fiber/Epoxy	400
7	Carbon Fiber/Epoxy	367
6	Carbon Fiber/Epoxy	386
5	Glass Fiber/Epoxy	653
4	Glass Fiber/Epoxy	624
3	Glass Fiber/Epoxy	596
2	Glass Fiber/Epoxy	569
1	Polyethyene Liner	16

The matrix structure in composite materials is prone to failure at high strain rates which results from the brittle structure of the thermoplastic resin. Finite element modelling of Virtual Crack Closure Technique (VCCT) confirms that the carbon fibre

is more susceptible to a variation of strain rate than the glass fibre. The damage progression in composite tube was modelled using Hashin's failure criterion. So, this criterion will facilitate the analysis of all layers of the composite tube to investigate the results, in order to determine the stress and strain contours and obtain failure and damage criteria in the matrix and fibre separately. The progression of damage is controlled by a linear damage evolution law.

A non-linear orthotropic composite tube model was subjected to two operating conditions, one under high internal pressure (3,500 psi) and one without internal pressure (0 psi). The study of the failure and damage phenomena in layers of a composite tube is concentrated on the inner composite layer (layer 2) and outer composite layer (layer 9). Those layers present the lowest and highest stress levels among 8 composite tube layers. Figure 6-18 demonstrates the contour plot of tensile failure criterion of the outer layer of carbon/epoxy material (layer 9) under zero pressure conditions. Comparison of the maximum failure index in a fibre (a) and in matrix (b) in Figure 6-18 shows that the failure indexes are '0.33' and '8.12', respectively. It indicates that the matrix structure fails at the first bending events (even before reaching the bent surface) whist the fibre remains undamaged. According to Figure 6-20, the failure index for a high pressure model (3,500 psi internal pressure) shows '0.31' and '11.54' for fibre and matrix, respectively, which shows that the matrix structure with a higher internal pressure fails prior to the lower one. Figure 6-19 to Figure 6-21 confirm that the failure index of fibre and matrix structures at zero pressure and high pressure (3,500 psi) remains less than one. They show that the glass fibre layers will not fail due to composite tube bending on the bending surface.

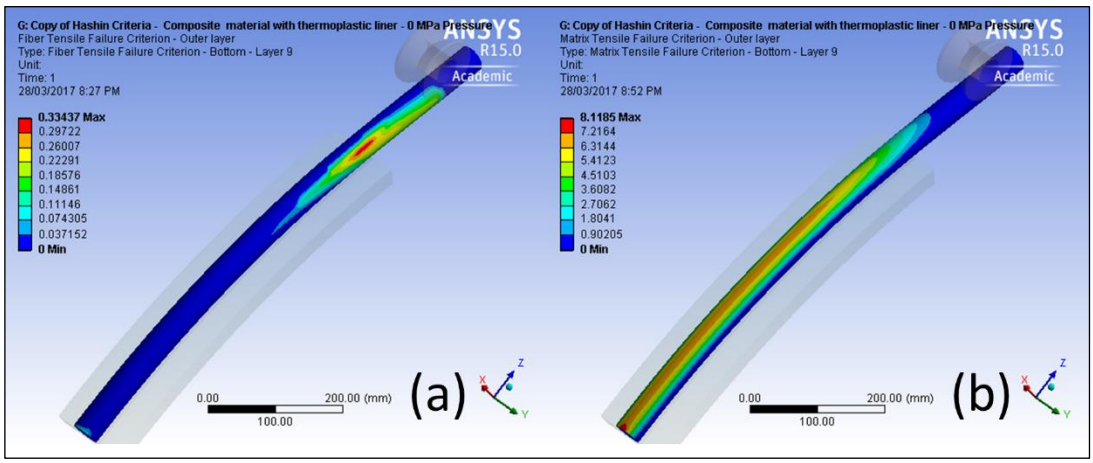

Figure 6-18: Tensile failure criterion (0 psi) of carbon/epoxy a) Fibre, b) Matrix.

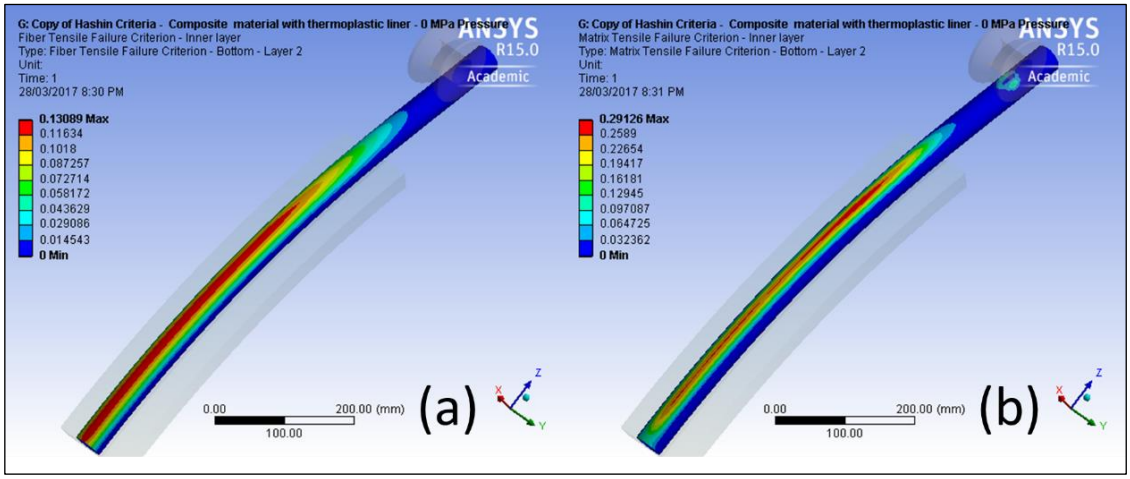

Figure 6-19: Tensile failure criterion (0 psi) of glass/epoxy a) Fibre, b) Matrix.

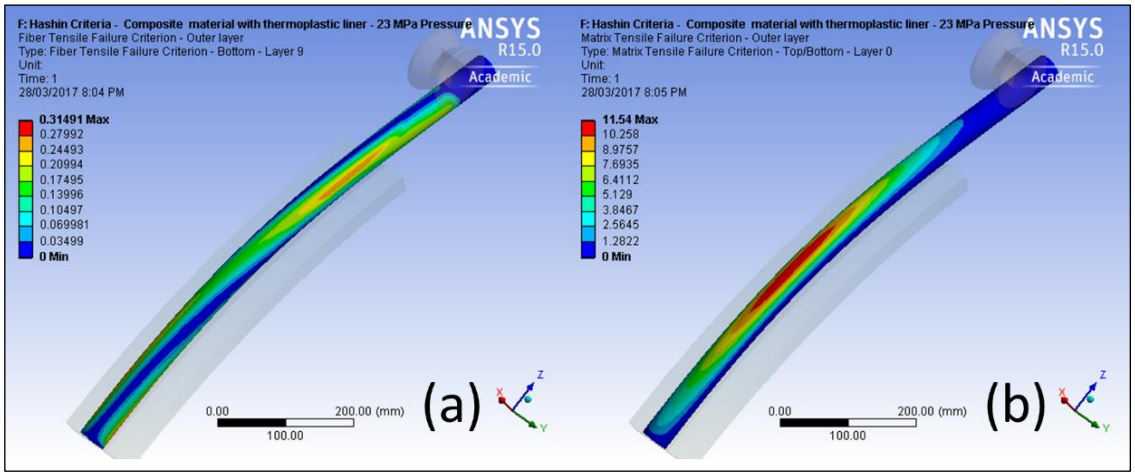

Figure 6-20: Tensile failure criterion (3,500 psi) of carbon/epoxy a) Fibre, b) Matrix.

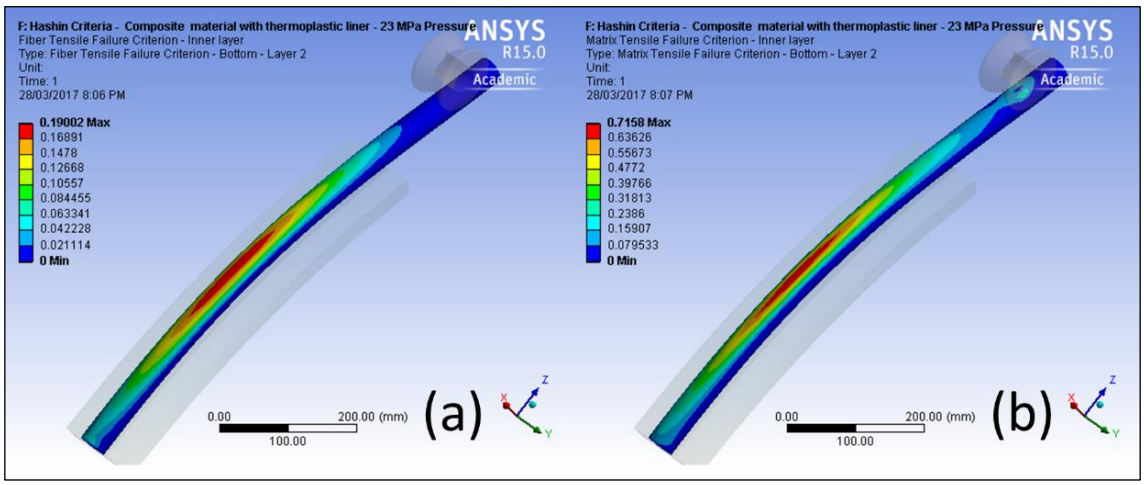

Figure 6-21: Tensile failure criterion (3,500 psi) of glass/epoxy a) Fibre, b) Matrix.

The damage status is associated with stiffness reduction in the progressive damage criteria and it governs the ultimate force that the fibre and matrix structure of a composite material can withstand. The stiffness reduction takes the value of "0" for no damage and "1" for fully damaged conditions. Figure 6-22 and Figure 6-23 present the damage status resulting from a bending load applied to the composite tube sample at no pressure (0 psi) and high pressure (3,500 psi) conditions, respectively. It clearly shows that the outer carbon fibre/epoxy layers fail during bending events while the inner glass fibre/epoxy layers do not.

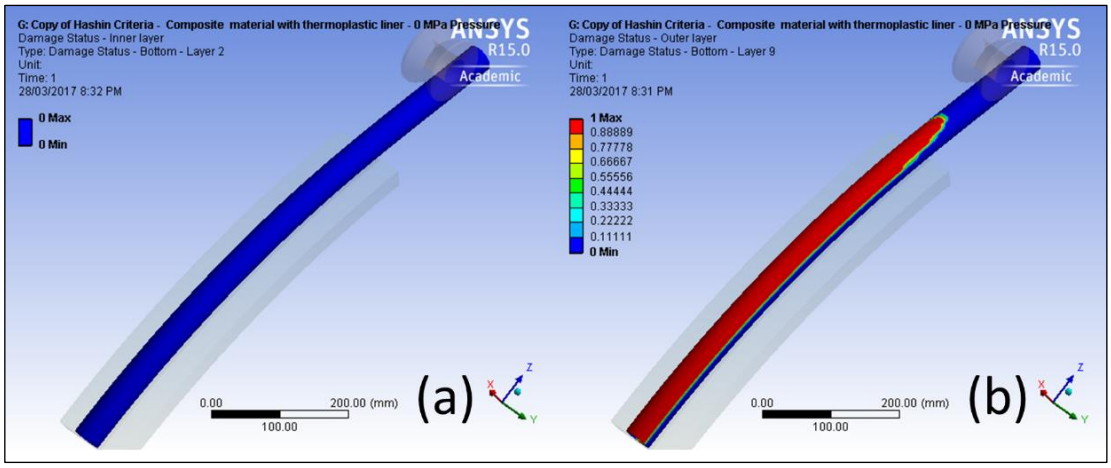

Figure 6-22: Damage status (0 psi) a) Inner glass/epoxy, b) Outer carbon/epoxy.

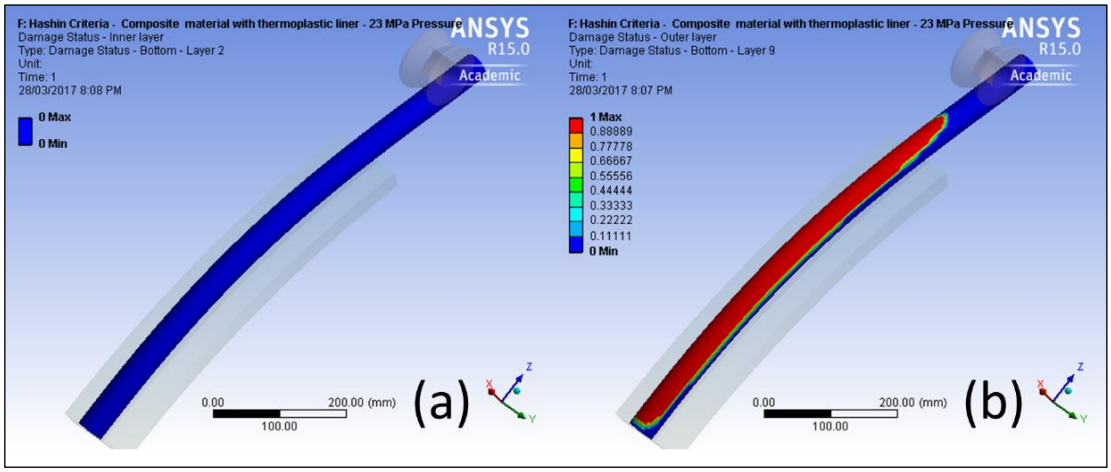

Figure 6-23: Damage status (3,500 psi) a) Inner glass/epoxy, b) outer carbon/epoxy.

In the stress analysis results, it was concluded that the maximum equivalent stress occurs in glass fibre/epoxy and not carbon fibre/epoxy. Figure 6-24 and Figure 6-25 present the damage status in fibre and matrix structures of the carbon fibre/epoxy

composite tube with 0 psi and 3,500 psi internal pressure, respectively. The contour plots display the damage in the matrix and no damage condition in the fibre structure. In other words, while under bending forces, while the matrix structure of the composite tube fails with crack initiation and propagation, the fibre structure of the tube is not facing any kind of damage. Nonetheless, the damage occurs in the matrix material and consequently pressure depletion happens, with no damage area in the fibre structure. This phenomena validates the necessity of inserting a pressure barrier liner inside the composite tube.

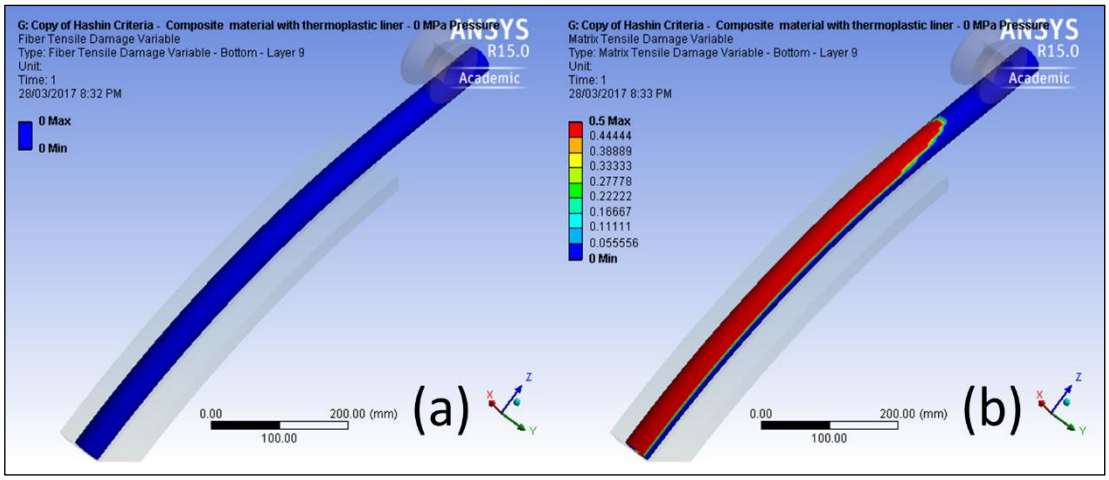

Figure 6-24: Damage status (0 psi) Carbon/epoxy a) Fibre, b) Matrix.

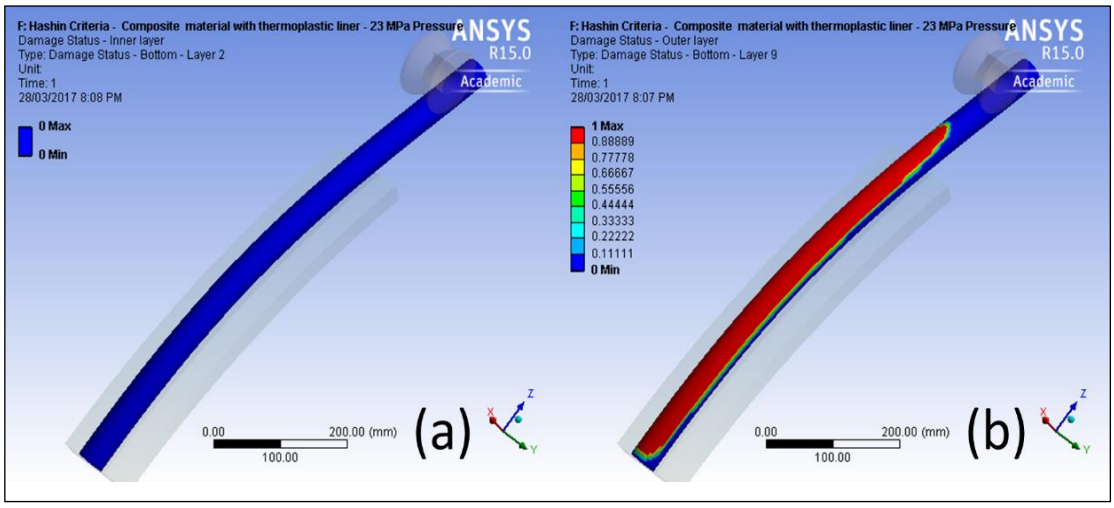

Figure 6-25: Damage status (3,500 psi) Carbon/epoxy a) Fibre, b) Matrix.

6.8 Composite tube end-connector

In the absence of any mechanical means of connection, a proprietary tubing connector was specifically designed for the composite coiled tubing pressure tests. It was used to attach the composite coiled tubing to the coiled tubing tool string and hydraulically seal the fluid inside the composite tube. The composite end-connector consisted of six elements as shown in Figure 6-26.

The connecting body holds the composite coiled tube to the pressure testing equipment by means of a high strength glue. The pressure containment comes from a double O-ring seal inserted onto a mandrel, fitted into the polished surface of the thermoplastic liner placed inside the composite coiled tube. There is a small hole through the mandrel along with a proper thread to line up pressure test facilities to the composite coiled tube. The connector is designed to have strength far exceeding the strength of the composite coiled tube and the fluid pressure. This kind of connector adapts to every size and every type of composite coiled tubing.

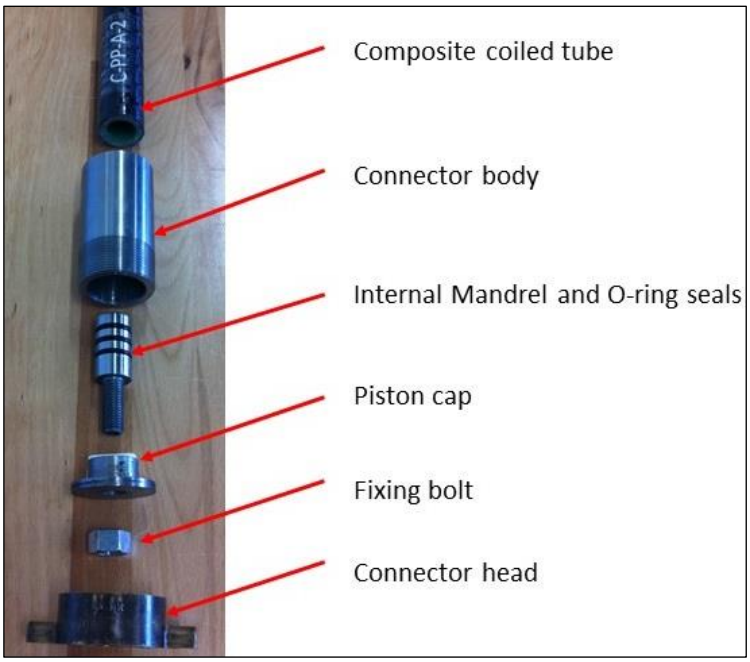

Figure 6-26: Composite coiled tubing connector.

6.9 Composite coiled tube design

Composite material consists of two separate components, the fibre and the matrix to form one single inhomogeneous bulk material. The basic design uses a prototype

composite coiled tube consisting of a hybrid laminate including a mixture of glass and carbon, filament-wound fibre structural layers in an epoxy resin with the addition of an internal liner (Figure 6-27). The internal thermoplastic liner is made of either High Density Polyethylene (HDPE) or Polypropylene (PP) compound creating an internal pressure barrier to the fluids pumped into the tube.

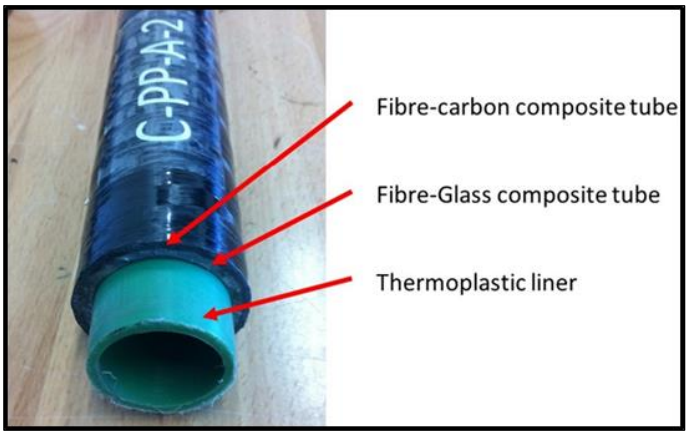

Figure 6-27: Composite tube lay-up from CST Composite.

The coiled tubes consisting of eight structural layers, having 42 mm in outer diameter and 7.5 mm wall thickness were manufactured for fatigue life analysis. According to the CST Composite manufacturing procedure, a cylindrical rod with a diameter of 32 mm was used as a mandrel, and fixed on the filament winding machine with a chuck jaw and a live tailstock centre. The main goal of the mandrel preparations is to make the surface as smooth as possible to simplify the extraction of the processed tube. First, the mandrel is polished and oil is applied to reduce the friction between the wound tube and the mandrel. Then, two layers of plastic film are wrapped around the mandrel. This is to avoid the tube sticking to the mandrel directly, making it easier to pull off. This pattern was used with a fibre thickness of 4 mm. The pattern was set to run eight times back and forth before covering the mandrel completely. When the filament winding process was finished, the tube was put in the oven for 8 hours at 70°C (1°C/min increasing temperature) as shown in Figure 6-28. A proprietary manufacturing process ensures that the thermoplastic liner is not chemically bonded to the structure of the composite tube, to enable the separation of the cyclic life of the two products. This makes the extraction of the tube easier by making it possible to pull

of the entire tube at once. The tube was pulled off the mandrel manually, and cut into 1,400 mm long test tubes.

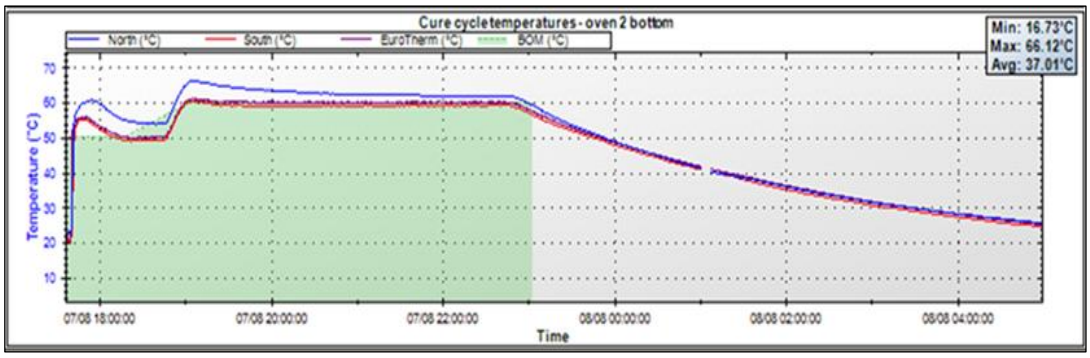

Figure 6-28: Composite tube's curing process record from CST composite.

Four types of composite tubes were examined, using a new-designed mixture of carbon/glass fibre system with two typical epoxy base resin materials along with two separate thermoplastic liners inside the composite tubes. Both materials were used in association with the same manufacturing methods, that is the filament-wound method and under the same curing process. Four samples from each method were produced, making a total of sixteen composite tube specimens as shown in Table 6-4.

Table 6-4: Composite coiled tube specimen.

Sample No.	Numbering Code	Sub-specimen specification	Main specimen specification	Liner material	Resin material
1	T-PE-A-1	1.4 meter length	3 meter length of sample (1)	HDPE	Resin Type T
2	T-PE-A-2	1.4 meter length			
3	T-PE-B-1	1.4 meter length	3 meter length of sample (2)		
4	T-PE-B-2	1.4 meter length			
5	T-PP-A-1	1.4 meter length	3 meter length of sample (1)	PP	
6	T-PP-A-2	1.4 meter length			
7	T-PP-B-1	1.4 meter length	3 meter length of sample (2)		
8	T-PP-B-2	1.4 meter length			
9	C-PE-A-1	1.4 meter length	3 meter length of sample (1)	HDPE	Resin Type C
10	C-PE-A-2	1.4 meter length			
11	C-PE-B-1	1.4 meter length	3 meter length of sample (2)		
12	C-PE-B-2	1.4 meter length			
13	C-PP-A-1	1.4 meter length	3 meter length of sample (1)	PP	
14	C-PP-A-2	1.4 meter length			
15	C-PP-B-1	1.4 meter length	3 meter length of sample (2)		
16	C-PP-B-2	1.4 meter length			

The thermoplastic pipes were High Density Polyethylene (HDPE) PE100 pipes and Polypropylene (PP) PP-RCT pipes, both with 32 mm outer diameter and 2.5 mm wall thickness. A comparison between specifications of HDPE and PP is shown in Table 6-5.

Table 6-5: Comparison between HDPE and PP (Simona-Plastics, 2016).

Specification	Unit	Testing standard	HDPE	PP
Density	g/cm3	DIN EN ISO 1183	1.0 to 1.3	0.9 to 1.2
Elongation at break	%	DIN EN ISO 527	400 to 800	70 to 500
Tensile modulus of elasticity	Mpa	DIN EN ISO 527	700 to 1,200	1,000 to 1,300
Tensile strength	MPa	DIN EN ISO 527	20 to 30	25 to 40
Notch impact strength	KJ/m2	DIN EN ISO 179	6 to 15	3 to 9
Temperature range	°C		0 to +100	-20 to +80

A composite material along with internal thermoplastic liner of the coiled tube specimen would have to withstand a bending event with no axial load. The coiled tube, with overall 42 mm outer diameter, should be capable of repeated spooling and unspooling onto a reel with the outer radius of curvature of 55 inches. The longitudinal strain rate for coiling of any tube diameter and wall thickness can be closely approximated from the following Equation (6.8):

$$\varepsilon_l = \frac{D_p}{D_R} = \frac{42}{2 * 55 * 25.4} = 1.86\ \% \qquad (6.8)$$

where:

ε_l Longitudinal strain

D_p Outside diameter of pipe

D_R Outside diameter of Reel

The internal pressure of the coiled tube specimen was maintained constant for each experiment; internal pressure was 1,000 psi and 3,500 psi. The results indicate that the internal pressure does not have a significant effect on the radial strain rate of composite tube. For a safe operation, the minimum allowable radius of curvature for spooling should be calculated, based on the maximum strain rate. The more the maximum

allowable strain rate, the larger the length of composite coiled tube to be spooled and transported.

6.10 Experimental work

The fatigue bending test, being the most reliable technique, is extensively used in the drilling industry because of its simplicity and low experimental cost. The fatigue bending machine, shown in Figure 6-29, consists of a bend forming surface with a specific radius of curvature, clamps at the fix-end, rollers of a reciprocating mechanism at the free-end, and a pressurizing system for imposing internal pressure on the test sample. The proto-type composite coiled tube specimens were fabricated from carbon fibre/epoxy, glass fibre/epoxy and thermoplastic liner using the filament winding method as explained in the previous section. This combination of glass and carbon fibres with epoxy resin, and a thermoplastic pressure barrier liner was designed to provide flexibility, axial force endurance and bending fatigue performance of composite coiled tube with hydraulic internal pressure.

Figure 6-29: Composite coiled tube test machine, courtesy of Curtin University.

As shown in Figure 6-30, composite tube samples with 42 mm outer diameter, 1.4 meters in length and 7.5 mm wall thickness were subjected to bending cycles (with maximum 3,500 psi internal pressure) using a test machine with a cantilever bending experiment apparatus. The bend radius of curvature specified for the experiment was 55 inches. The experiments were conducted using a bending test machine with a uniform internal pressure applied to the specimen during bending cycles. The composite tube samples were subjected to low (1,000 psi) and high (3,500 psi) internal pressure until they failed under iterative cyclic bending fatigue.

Figure 6-30: Composite coiled tube specimens.

Proprietary connectors (Figure 6-31) were installed on both ends of the test tube specimens in order to seal and provide pressure. Said connectors consisted of a steel bushing with a rough inside surface (for better adhesion) and threaded on the outer surface on the one end were installed by gluing on the ends of the composite tube samples. A one foot length of the fixed-end of the composite tube was clamped to the bending machine. The clamp mechanism was designed to distribute the pushing force of the clamp elements to prevent stress concentration on the composite tube body and also fix one end for simulating the cantilever bending mechanism.

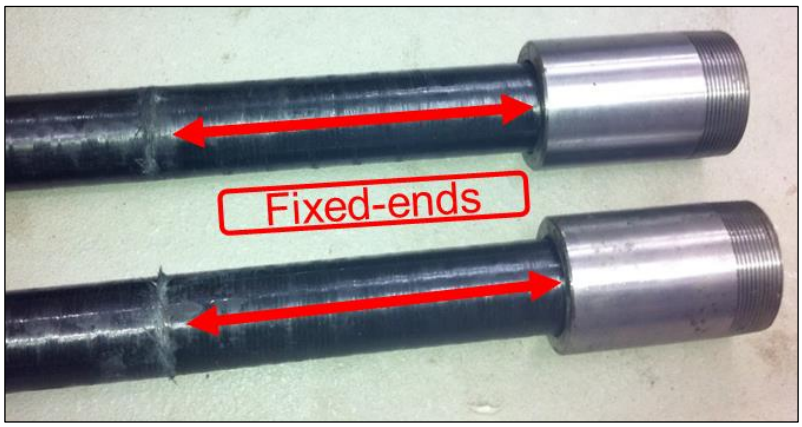

Figure 6-31: Fixed-end and connectors of composite tube samples.

Several tests were conducted to assess the cumulative effect of combined cyclic bending and internal pressure on the performance and fatigue life of composite coiled tube specimens. All composite tube specimens were tested to 20% extra pressure or 500 psi more than the test pressure setting (whichever was greater). So, in the case of any variation in internal pressure of the test tubes, the experiment will be secured from any unpredicted damage. During the experiments, the upper and lower pressure parameters on the system software were set to control variations of the pressure inside the test specimens.

Figure 6-32: Pressure test on composite tube specimen.

During the running cyclic bending tests, some failures happened on the inner surface of the bending radius and also on the edge of the bending point. Visual inspection upon completion of the tests (as shown in Figure 6-33) showed that the

outer layers of the composite tube were extremely bent in the vicinity of the connection line of the straight and bending surfaces. In the next experiments, the broken point was monitored for almost 50 bending cycles. A powder of broken resin (Figure 6-34) was observed around the breaking point, which indicated that extra strain rate at the bending point had accelerated the crack propagation in the matrix structure and caused weakening of the carbon layers, and consequently, the carbon fibres without resin became prone to rupture during bending cycles.

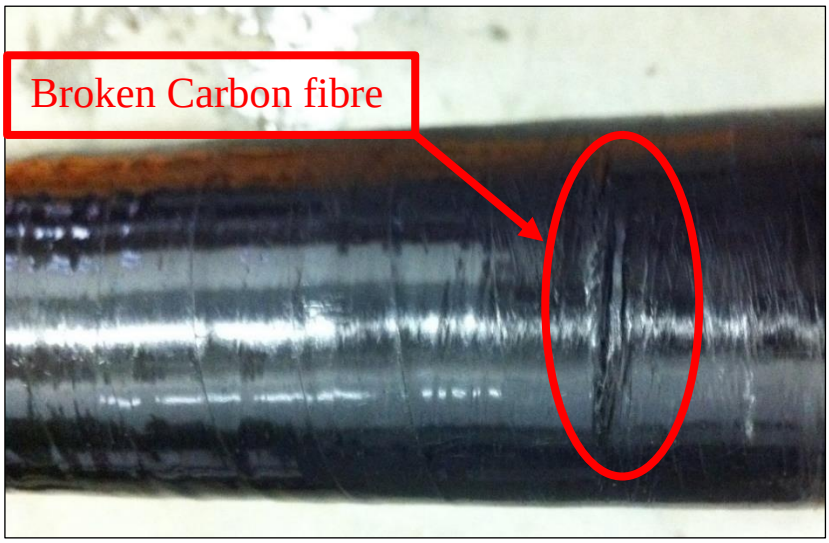

Figure 6-33: Broken part of the carbon fibre layer.

Figure 6-34: Broken resin powder in the bending point.

Investigation of the four composite tube specimens that had failed at high strain rates resulted from the sharp bending edge and presented a comprehensive understanding of properties of different existing thermoplastic liners. It was seen that the outer layer of the composite tubes (carbon fibre layer) broke in the early bending events, and it was the layers of the thermoplastic liner and glass fibres which prevented pressure depletion from inside the composite tube. Table 6-6 and Table 6-7 illustrate the cyclic life of the failed composite tubes under abnormal strain rate on the sharp edge. It can be clearly seen that the failure in the composite tube with a Polypropylene liner at 1,000 psi internal pressure occurred at an average value of 580 bending cycles, while for high density polyethylene material it occurred at an average of 271 bending cycles under similar test conditions.

Table 6-6: Composite tube samples with Polypropylene liner.

Sample No.	Fatigue Life (cycles)	Internal Pressure (psi)
T-PP-A-1	593	1,000
T-PP-B-1	568	1,000

Table 6-7: Composite tube samples with high density Polyethylene liner.

Sample No.	Fatigue Life (cycles)	Internal Pressure (psi)
C-PE-B-1	283	1,000
T-PE-A-2	259	1,000

After fixing the effect of the sharp edge on the bending test machine and running another experiment at 1,000 psi internal pressure, the composite tube specimen underwent 1,500 bending cycles without pressure depletion and failure on the outer surface of the tube. As shown in Table 6-8, on increasing the internal pressure of the existing composite tube to 3,500 psi, the bending experiment continued for an extra 568 bending cycles (total of 2,068 bending cycles) until the internal pressure was released from the composite tube specimen. The cyclic life of the composite tube was

almost 5 times more than the cyclic life of conventional steel coiled tubes. The tube failed at the surface of the outer radius of bending and at the middle of the bending curvature (Figure 6-35), which validates the results of finite element modelling. The visual inspection after completion of the experiment illustrated unbroken carbon fibre layers (only penetration of the test liquid through the composite structure). This confirms the higher strength and longer life of the carbon to glass fibre as was presented in the numerical model.

Table 6-8: Composite tube test result.

Sample No.	Fatigue Life (cycles)	Internal Pressure (psi)
C-PP-A-2	1,500	1,000
	568	3,500

Figure 6-35: Fluid leakage through the composite structure.

6.11 Failure investigation (CT-Scan analysis)

Composite materials are subject to defects either during the manufacturing processes or during the service life. Debonding, delamination, matrix cracking, fibre breakage and fibre pull-out are the type of defects that frequently occur in composite materials (Figure 6-36). The cracks and delamination are in the inner layers and cannot be viewed just using x-ray radiography. So, the CT-scan technique can record the position of the echoes from the reflecting internal layers of composite material within a specific area (Hasiotis *et al.*, 2011).

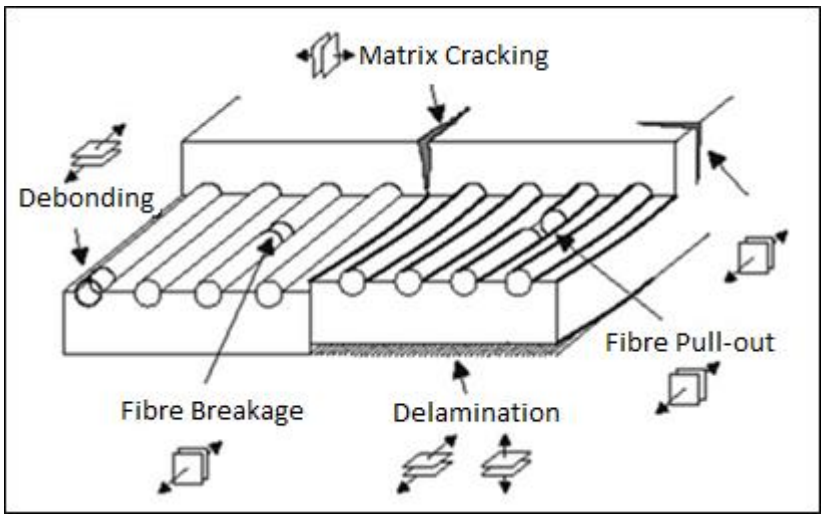

Figure 6-36: Typical defects in composite material (Vaara & Leinonen, 2012).

As shown in Table 6-9, the X-ray testing is an applicable method for detecting some types of defects in composite materials. Since the thermoplastic, carbon/epoxy and glass/epoxy composite materials are transparent to X-ray, but the Medical X-ray Computerised Tomography (Medical XCT) technique was developed to trace the defects on the composite coiled tube and thermoplastic liner resulting from bending fatigue experiments to:

- Check the general structure of the tube,
- Determinate the position and even the shape of the defects in some cases,
- Quality control the continuity of each of the three composite and thermoplastic layers that constitute the tube before and after the bending tests.

Table 6-9: Applicability of X-ray to defects.

Type of defect	Applicability of X-Ray
Void	High
Porosity	High
Delamination	Good
Crack	Good
Disbond	Good
Matrix cracking	Some
Fibre breakage	Some
Incorrect cure	Nothing

"XCT is a radiological imaging system first developed by Hounsfield in 1972. This non-destructive technique uses X-rays to create a three-dimensional data set of a sample by stacking contiguous cross-sectional two-dimensional (slices) images" (Braz *et al.*, 1999). CT-scan imagery corresponds to a 2-D or 3-D linear X-ray attenuation pixel matrix, where the attenuation is a function of the density and atomic number of the material being analysed (Delle Piane *et al.*, 2016) such as '–1000 CT' Hounsfield unit is calibrated for air, '0 CT' is for water and readings above '0 CT ' are for other materials (Bourque *et al.*, 2014).

Figure 6-37: Composite tube Scan test.

In fracture mechanics studies, the applications of XCT scanning include viewing full-diameter material sections to determine orientation relative to main structures and presence of discontinuities (crack, void, and delamination). This technique is generally suitable for visualization from meter to millimeter scale and often achieves a voxel resolution around 0.4 mm^3. Three dimensional image reconstruction helps to identify

homogeneous areas, free of abnormal structures from areas with damages or weak zones. Because the X-ray attenuation spectrum has a direct relation with density, with proper software analysis, it is possible to perform segmentation of the spectra to isolate particular materials composed of a specific density and observe them as two-dimensional or three-dimensional images.

The two and three-dimensional data of the tested material at CSIRO was acquired using a Siemens SOMATOM (as shown in Figure 6-38) definition AS with 64 slices with images acquired transversally to the composite tube axis. The XCT scan images were reconstructed using an algorithm that enhanced the maximum sharpness of the images in 512 x 512 pixels to visualize any changes in density with a resolution of about 0.001 g/cc. An energy beam of 120kV/300mAs with a helical acquisition (pitch at 0.35 mm) applied to acquire high resolution transversal images every 0.4 mm (in z-axis) and ~ 0.1 mm in x and y axes. Siemens software was used to process the X-ray images and provide 2D orthogonal views along the tube axis and 3D views of the three layers using a special colour chart filter to enhance visual depiction, where blue colours represent the outer layers of the composite tube (carbon fibre/epoxy laminate), green for mid-layers (glass fibre/epoxy laminate) and red for inner layers (thermoplastic liner).

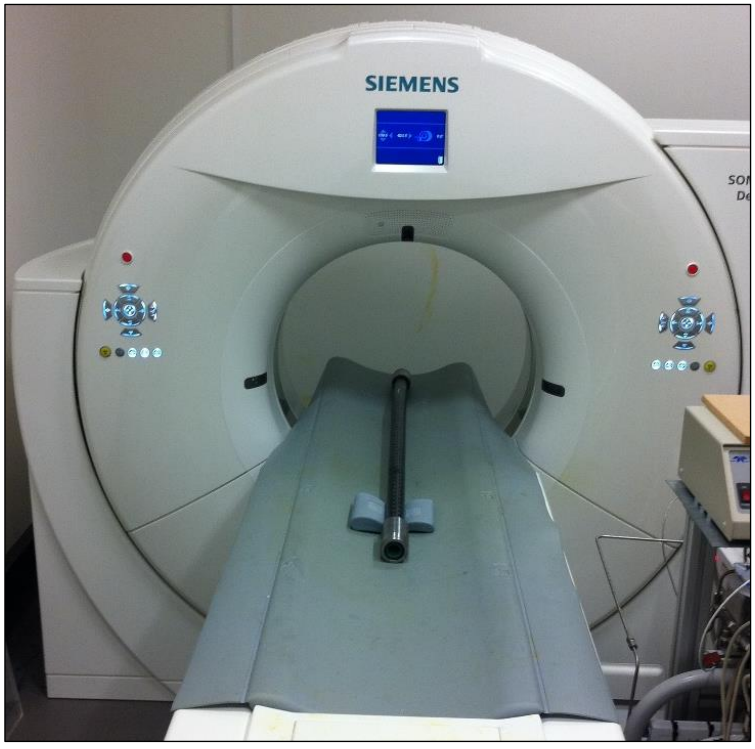

Figure 6-38: SIEMENS medical XCT Scan machine (courtesy of CSRIO).

One of the composite tube samples T-PP-A-1, as discussed in section 6.10, was tested using a curved surface with 55 inches radius of curvature and 1,000 psi internal pressure. It underwent 100 bending cycles in the fatigue test machine. It was taken out and sent for XCT scanning, shown in Figure 6-39. The longitudinal three-dimension images displayed a fibre winding defect resulting from a manufacturing malfunction and delamination in the glass fibre/epoxy layers (green colour).

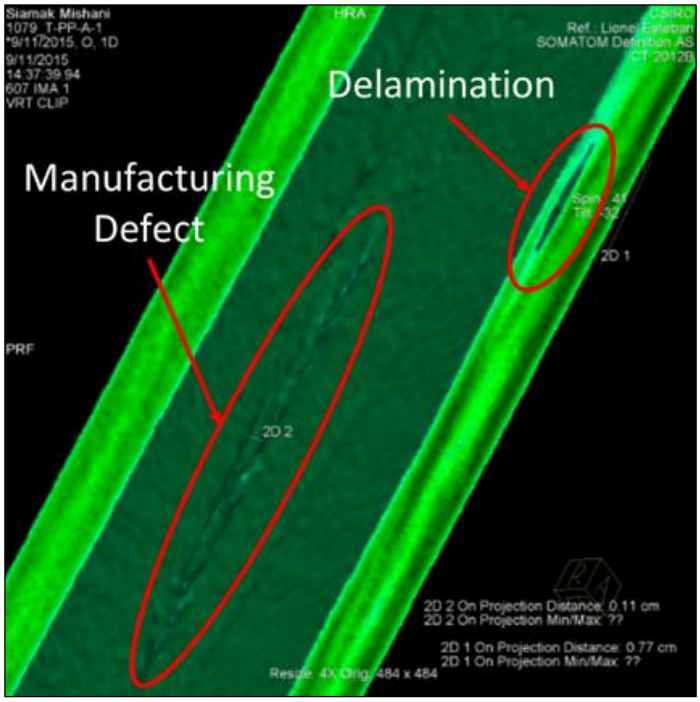

Figure 6-39: Delamination in T-PP-A-1 tube after 100 bending cycles.

The composite tube (T-PP-A-1) was returned to the fatigue test machine and the experiment continued until the tube failed at 593 bending cycles and pressure inside the tube was released. This specimen failed at the inner radius of bending and visual damage was seen to be 10 mm above the bending point. A typical picture of the damaged zone in the carbon fibre layer is shown in Figure 6-40. The radial cross-sectional area (Figure 6-41) and the longitudinal cross-section area Figure 6-42 of the XCT scan images show the fibre breakage having 1.22 mm length in the carbon (blue colour) and glass (green colour) layers. In the presence of the damaged zone, the internal pressure destroyed the soft structure of the thermoplastic liner and created a pin hole in the liner (Figure 6-42). Figure 6-43 illustrates the fracture in the glass fibre/epoxy layers of the composite tube.

Figure 6-40: T-PP-A-1 composite tube failed at 593 bending cycles.

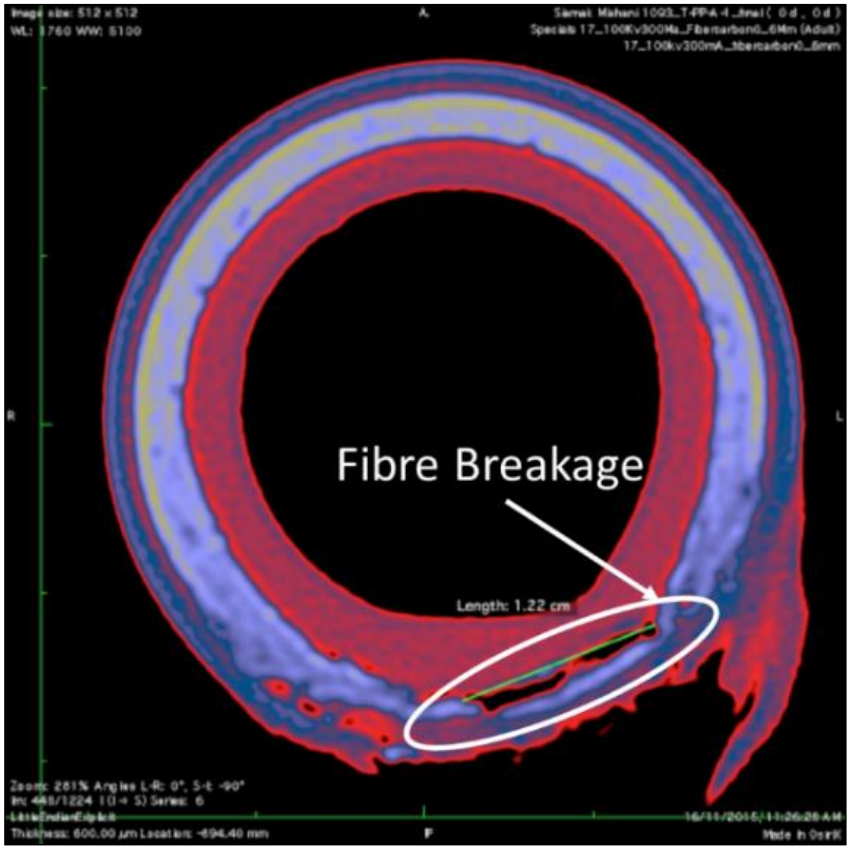

Figure 6-41: Radial cross-section area of damaged T-PP-A-1 specimen.

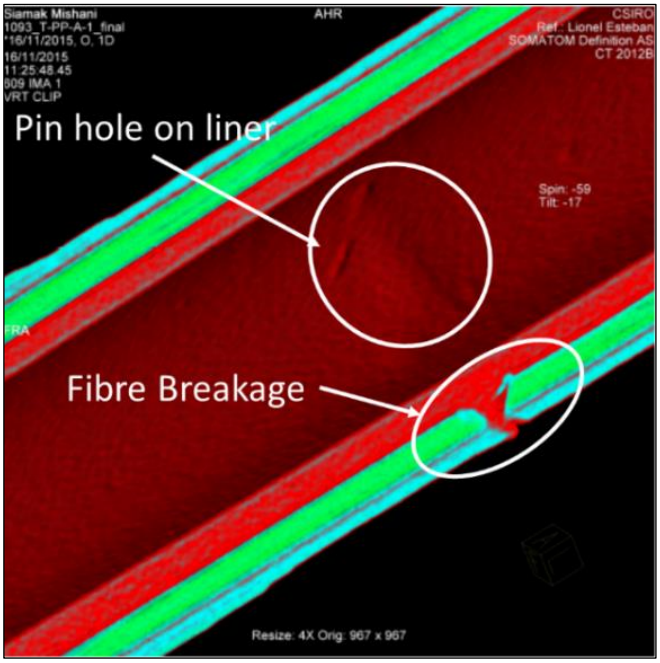

Figure 6-42: Longitudinal cross-section area of damaged T-PP-A-1 specimen.

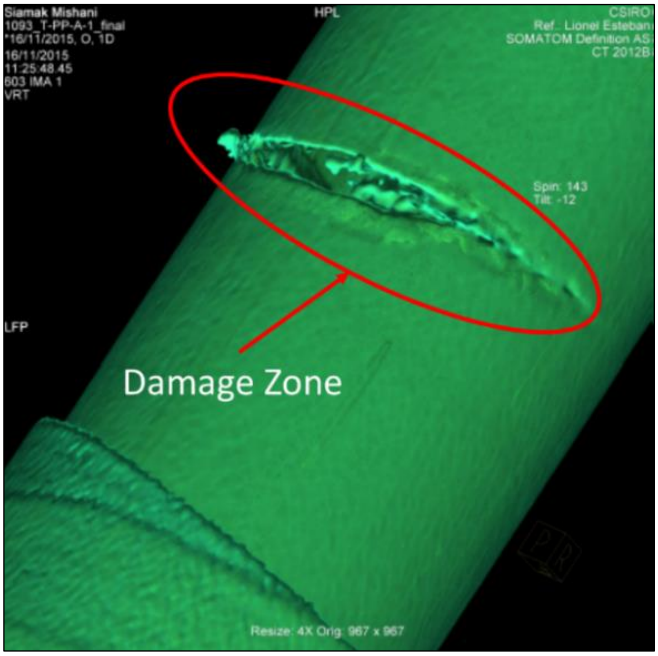

Figure 6-43: Damage in the glass fibre layers of T-PP-A-1 tube.

Figure 6-44 is the image of the composite tube specimen (C-PP-A-2). This specimen sustained bending experiments at 1,000 psi and 3,500 psi internal pressure for 2,068 bending cycles when damage occurred. Fluid leakage indicated that the composite structure failed in the outer bending radius of the tube and close to the bending point, as in the previous experiments, with a permanent bend in the damaged

zone. Visual inspection of the composite tube shows no change in appearance of the carbon fibre (outer layer), thus indicating the presence of failure in the glass fibre (inner layers) of the composite tube.

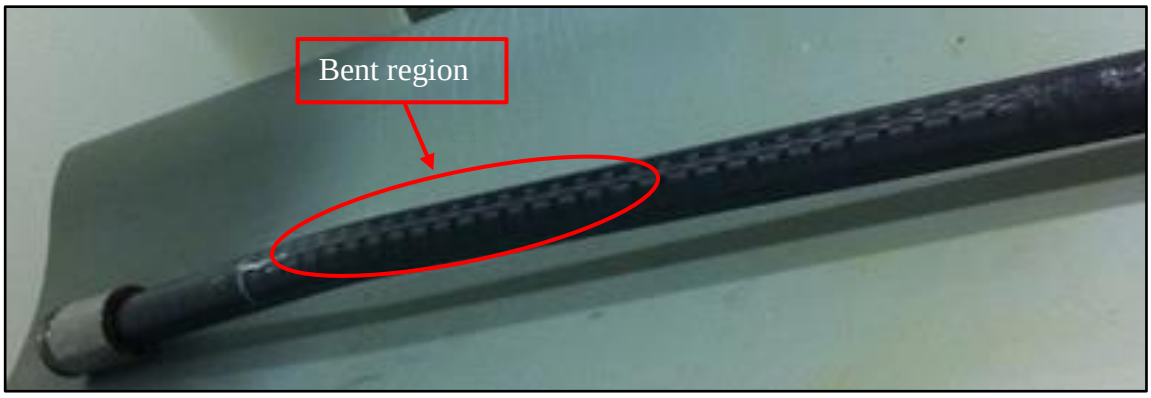

Figure 6-44: Bent region of T-PP-A-1 tube.

Figure 6-45 to Figure 6-47 show the XCT scan images of the T-PP-A-1 composite tube specimen. The images depict the damage structure of the inner layers of the composite tube. Figure 6-45 clearly illustrates broken glass fibres while the outer layers of the carbon fibre are not changed. Damage in the glass fibre structure caused the thermoplastic liner to rupture as shown in Figure 6-46. A three-dimensional XCT scan image is illustrated in Figure 6-47.

Figure 6-45: Radial cross-section area of damaged zone C-PP-A-2 tube.

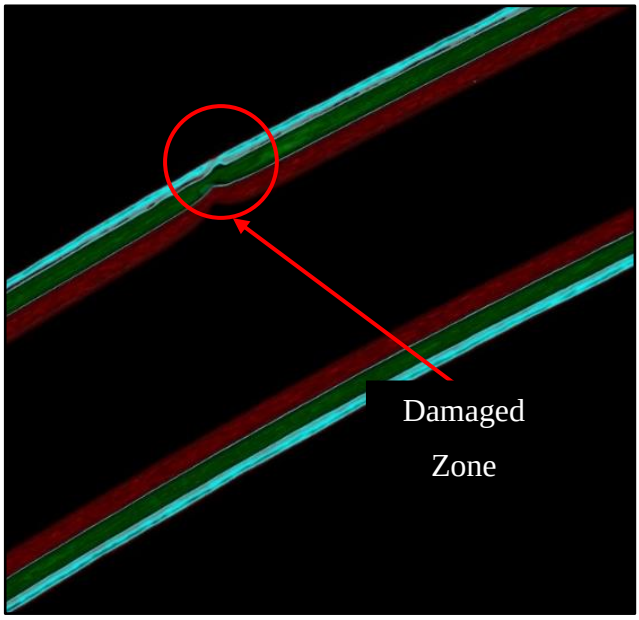

Figure 6-46: Longitudinal cross-section area of damaged zone C-PP-A-2 tube.

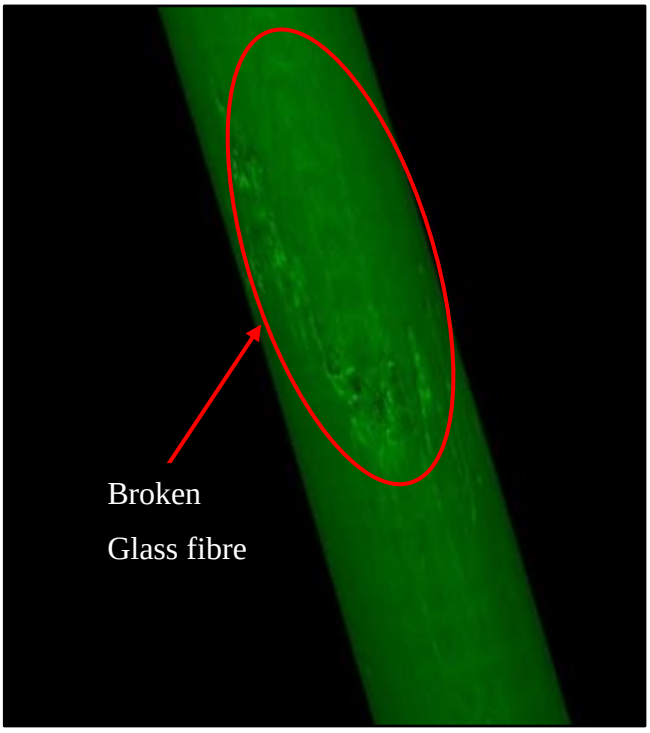

Figure 6-47: Broken glass fibre layers C-PP-A-2 tube.

6.12 Conclusions

This chapter presents the results of laboratory fatigue testing on composite coiled tube specimens, obtained from a purpose-built fatigue test machine. The finite element

modelling and analysis along with CT-Scan images were utilized to validate the results from experiments. The following results have been obtained:

- The literature review showed that properties of epoxy resin help composite materials to achieve higher levels of maximum strain rate for a specific stress level.
- Finite element analysis shows that at the tested pressures, carbon fibre/epoxy layers can fail during bending whereas a glass fibre/epoxy does not.
- The failure is within the epoxy layers and not the carbon fibres. This phenomena requires the insert of a pressure barrier liner inside of the composite tube to prevent pressure depletion.
- The stress analysis results from finite element modelling illustrate that the maximum equivalent stress occurs in the glass fibre/epoxy.
- The cyclic bending test results from the group of composite tubes which had early mechanical failure in the outer layer (carbon/epoxy fibre) were used to investigate the performance of the thermoplastic liners. The experimental bending results show that for a hybrid composite tube with a liner at 1,000 psi internal pressure, a polypropylene liner provides more than two times the fatigue life than high density polyethylene liner.
- Based on the test data results, a composite tube has demonstrated the capability of exceeding the cyclic life of HS-90 conventional steel coiled tube by a factor of five or more.
- A medical CT-Scanner can be used to detect internal defects in a tube made of carbon and glass fibre composite material and thermoplastic liner. The CT-Scanning method displays cross-sectional images as three-dimensional objects without destroying or modifying the tube, allowing different density elements of any specimen to be categorized by different colours. The CT-Scanning method is very useful for checking micro-cracks, delamination and void distributions.

References

Afghoul, A. C., Amaravadi, S., Boumali, A., Calmeto, J. C. N., Lima, J., Lovell, J., . . . Staal, T. (1994). Coiled tubing: the next generation. *Oilfield Review*, *6*(4), 9-23.

ANSYS®, A. R. (2013). *ANSYS mechanical user's Gguide*. Canonsburg, PA: ANSYS, Inc.

Aymerich, F. (2012). *Composite materials for wind turbine blades*. Retrieved from University of Cagliari, Italy:

Barbero, E. J. (2007). *Finite element analysis of composite materials*. Boca Raton, FL: CRC press.

Bourque, A. E., Carrier, J.-F., & Bouchard, H. (2014). A stoichiometric calibration method for dual energy computed tomography. *Physics in medicine and biology*, *59*(8), 2059.

Braz, D., da Motta, L. M. G., & Lopes, R. T. (1999). Computed tomography in the fatigue test analysis of an asphaltic mixture. *Applied Radiation and Isotopes*, *50*(4), 661-671.

Delle Piane, C., Giwelli, A., Clennell, M. B., Esteban, L., Kiewiet, M. C. D. N., Kiewiet, L., . . . Raimon, J. (2016). Frictional and hydraulic behaviour of carbonate fault gouge during fault reactivation—An experimental study. *Tectonophysics*, *690*, 21-34.

Gurit. (2012). Gurit Guide to Composites Retrieved from www.gurit.com. www.gurit.com

Hasiotis, T., Badogiannis, E., & Tsouvalis, N. G. (2011). Application of ultrasonic C-scan techniques for tracing defects in laminated composite materials. *Strojniški vestnik-Journal of Mechanical Engineering*, *57*(3), 192-203.

Lagat, C. K. (2015). *Evaluation and selection of an optimum material for coil tubes in CT drilling technology for hard rocks in mineral exploration.* (PhD), Curtin University, Curtin University.

Mallick, P. K. (2007). *Fiber-reinforced composites: materials, manufacturing, and design*. Boca Raton, FL: CRC press.

Matthews, F. L., Davies, G., Hitchings, D., & Soutis, C. (2000). *Finite element modelling of composite materials and structures*. Cornwall, England: CRC Press.

Mohanty, A. K., Misra, M., & Drzal, L. T. (2005). *Natural fibers, biopolymers, and biocomposites*: CRC press.

Sas-Jaworsky, A., & Williams, J. G. (1993). *Development of composite coiled tubing for oilfield services*. Paper presented at the SPE Annual Technical Conference and Exhibition, Houston, Texas.

Simona-Plastics. (2016). Technical Handbook - Global thermoplastic solutions. Kirn, Germany: SIMONA AG.

Vaara, P., & Leinonen, J. (2012). *Technology survey on NDT of carbon-fiber composites*. Kemi, Finland: Kemi-Tornio University of Applied Sciences.

Williams, & Sas-Jaworsky, A. (2000). *Composite spoolable pipe development, advancements, and limitations.* Paper presented at the Offshore Technology Conference, Houston, Texas.

Zureick, A.-H., & Nettles, A. T. (2002). *Composite Materials: Testing, Design, and Acceptance Criteria* (Vol. 1416). West Conshohocken, PA: ASTM International.

Chapter 7 Conclusions and recommendations

7.1 Conclusions

In this thesis, I investigated the fatigue failure of composite versus steel tube samples subjected to high internal pressure for use in drilling mineral exploration boreholes. The objective of the study was to develop a method for the prediction of the bending fatigue life of coiled tubes under different working conditions. I utilized both numerical and experimental methods and the conclusions can be summarized for steel as follows:

- In conventional steel coiled tube (HS-90), changes in the welding seam positioning relative to the curved surface changes the cyclic life of the steel coiled tube.
- Test results show that the minimum cyclic bending life occurs in HS-90 conventional coiled tube when the weld seam is placed against the bending block side.
- During the bending experiments with HS-90 steel coiled tube, increasing the internal pressure from 0 to 3500 psi increased the equivalent plastic strain and residual bending deformation by 10% and 4%, respectively.
- The Weibull distribution plot shows that the larger the probability of failure, the less the fatigue life of the steel coiled tube.
- The Weibull distribution analysis depicts a plot which illustrates the relation between the cyclic life and expected reliability of a specific coiled tubing string. This plot can help engineers to predict the fatigue life of the steel coiled tube for different operations with a higher level of confidence.
- The maximum equivalent stress in steel coiled tube increases as the number of the bending cycle increases. This provides a reason for failure during low-cyclic fatigue phenomena while the maximum stress is less than the ultimate stress level in the material.

- Linear FE-modelling of steel coiled tube tends to give an over-estimated prediction of the fatigue life of the materials, whereas using the non-linear FE-model gives results very close to the predicted fatigue life.
- The cumulative fatigue life of the HS-90 steel coiled tube resulted from FE modelling validated the "running meters" fatigue life prediction method.
- Visual inspection of the steel coiled tube samples following a laboratory fatigue test indicated a failure position consistent with expectations from numerical modelling. In low and high internal pressure cases the failures were distributed along the curved block, on the inside radius of the tube specimens rather than on the outside radius.
- I developed a bending fatigue numerical model using the ANSYS-FE software to accurately predict the fatigue life of a conventional steel coiled tube (HS-90) with 2 inches outer diameter and 0.190 inch thickness bent on a 55 inch radius bending block at uniform internal pressures of 3,500 psi and 1,000 psi.
- The finite element analysis method demonstrated a force of load 10,000 N was required for straightening the bent coiled tube. This showed the tendency of the steel coiled tube string to be curved, resulting in pushing against the well bore during running and pulling out of the hole.
- In conventional steel coiled tube (HS-90) significant ovality was observed for cases involving the low internal pressure (1,000 psi). The average ovality was 5.09% at low internal pressures and 3.69% at high internal pressures (3,500 psi).
- The weld seam areas of the HT-125 steel coiled tube have almost the same cyclic fatigue life and consequently the same micro-structural behaviour as the rest of the coiled tube body.
- Test results show that the HT-125 BlueCoil tube has 2.6 times and 1.9 times more average working life than conventional steel coiled tubes (HS-90) at 3,500 psi and 1,000 psi internal pressure, respectively. This illustrates a greater performance of HT-125 over HS-90 with the higher internal pressures.
- During the bending experiment of HT-125 Bluecoil at 3,500 psi internal pressure, a continuous reduction in internal pressure was recorded which

was similar to the normal behaviour of the conventional steel coiled tubes. During a bending experiment at 1,000 psi internal pressure, a continuous increase in internal pressure was recorded which showed an opposite trend with respect to the conventional steel coiled tubes. At the end of the experiments, tube size measurement indicated that the outer diameter of the HT-125 Bluecoil was slightly increasing. Therefore, the increase in internal pressure could have resulted from tube length shortening and/or tube wall thickening.

By comparison, using numerical and experimental methods, my conclusions for composite tubing are as follows:

- The literature review showed that properties of epoxy resin help composite materials to achieve higher levels of maximum strain rate for a specific stress level.
- Finite element analysis shows that at the tested pressures, a carbon fibre/epoxy layers can fail during bending whereas a glass fibre/epoxy does not.
- The variation of strain release energy rates versus crack tip development illustrated that 2D modelling cannot express the true release strain energy rate at the crack tip front. The contour for strain energy release rate in Mode-I testing (G_I) increases - almost doubling in value - from the edge to the centre (from 5 J/m^2 to approximately 10.2 J/m^2), while strain energy release rate in Mode-II testing (G_{II}) slightly decreases from the edge to the centre (from 10.4 J/m^2 to 9.9 J/m^2). It is therefore useful to investigate and understand the mode of crack propagation in composite laminates using 3D modelling.
- The Mode-II interlaminar fracture toughness of composite laminate is several times higher than Mode-I interlaminar fracture toughness in the same material.
- The “applied load” to “load displacement” perpendicular to the crack plane for carbon fibre laminate is almost three times more than that for glass fibre laminate in Mode-I and Mode-II states.
- The Double Cantilever Beam (DCB) testing method presents normal resistance of the crack propagation of the interlaminar layer in the opening

mode conditions. The finite element analysis result shows that the normal resistance to interlaminar delamination is much less than shear resistance in the End-Notched Flexure (ENF) testing method.

- The failure is within the epoxy layers not the carbon fibres. This phenomena requires the insert of a pressure barrier liner inside of the composite tube to prevent pressure depletion.
- The experimental bending results show that for a hybrid composite tube with a liner at 1,000 psi internal pressure, a polypropylene liner provides more than two times the fatigue life than high density polyethylene liner.
- A medical CT-Scanner can be used to detect internal defects in a tube made of carbon and glass fibre composite material and thermoplastic liner. The CT-Scanning method displays cross-sectional images as three-dimensional objects without destroying the tube, allowing different density elements of any specimen to be categorized by different colours. The CT-Scanning method is very useful for checking micro-cracks, delamination and void distributions.

Steel versus Composite coiled tube:

- Based on the test data results, a composite tube has demonstrated the capability of exceeding the cyclic life of HS-90 conventional steel coiled tube by a factor of five and the best (HT-125) steel coiled tube on the market by a factor of three. This is a major finding of this research.

7.2 Recommendations

To improve the understanding of the fatigue life behaviour of the steel and composite coiled tubes, different experimental work could be performed as follows:

- The study found that despite the composite fibre arrangement, the fatigue life can be affected by damage in the vicinity of the resin structure. The use of a more flexible thermoset resin or suitable thermoplastic resin can recover this brittle behaviour of the existing thermoset resin and prolong the bending fatigue life of the tube samples. So further research is required to increase tube life using better resins.
- The test result showed anomalous behaviour of the HT-125 BlueCoil sample under bending test at 1,000 psi internal pressure while the outer

diameter measurement indicated a partial ballooning occurred throughout the entire tube sample. Measuring of the other geometrical parameters of the tube sample, using a highly accurate measuring device, can be helpful to understand the HT-125 BlueCoil behaviour at low internal pressure. Further research of this phenomenon is recommended.

References

Abernethy, R. B. (2006). *The new Weibull handbook, Fifth edition*. North Plam Beach, Florida: Dr. Robert B. Abernethy.

Ackert, D., Beardsell, M., Corrigan, M., & Newman, K. (1989). The coiled tubing revolution. *Oilfield Review, 1*, 4-16.

Afghoul, A. C., Amaravadi, S., Boumali, A., Calmeto, J. C. N., Lima, J., Lovell, J., . . . Staal, T. (1994). Coiled tubing: the next generation. *Oilfield Review, 6*(4), 9-23.

Alfano, G., & Crisfield, M. (2001). Finite element interface models for the delamination analysis of laminated composites: Mechanical and computational issues. *International journal for numerical methods in engineering, 50*(7), 1701-1736.

ANSYS®, A. R. (2013). *ANSYS mechanical user's Gguide*. Canonsburg, PA: ANSYS, Inc.

Avakov, V., Foster, J., & Smith, E. (1993). *Coiled tubing life prediction*. Paper presented at the Offshore Technology Conference, houston ,Texas.

Aymerich, F. (2012). *Composite materials for wind turbine blades*. Retrieved from University of Cagliari, Italy:

Bannantine, J. (1990). *Fundamentals of metal fatigue analysis*. Englewood Cliffs, New Jersey: Prentice Hall.

Barbero, E. J. (2007). *Finite element analysis of composite materials*. Boca Raton, FL: CRC press.

(2013). *Finite element analysis of composite materials using ANSYS®*. Boca Raton, FL: CRC Press.

Bauschinger, J. (1886). On the change of the position of the elastic limit of iron and steel under cyclic variations of stress. *Mitt. Mech.-Tech. Lab., Munich, 13*(1).

Behenna, F., Myrick, D., Stanley, R., Tipton, S., & Hammond, W. (2003). *Field validation of a coiled tubing fatigue model.* Paper presented at the SPE/ICoTA Coiled Tubing Conference and Exhibition, Houston, texas.

Boles, J. A. B., Burgos, R., & Ballesteros Medina, J. A. (2008). *A field study of coiled-tubing material loss and ovality.* Paper presented at the SPE/ICoTA Coiled Tubing and Well Intervention Conference and Exhibition, The Woodlands, Texas.

Boller, K. H. (1964). Effect of pre-cycle stresses on fatigue life of plastic laminates reinforced with unwoven fibers. *Defense Technical Information center*(AD0606769).

Bordeu, F., & Boucard, P. (2009). *A mesoscale model for the prediction of composites materials until final failure.* Paper presented at the Proc. of ICCM17-17th International Conférence on Composite Materials.

Bourque, A. E., Carrier, J.-F., & Bouchard, H. (2014). A stoichiometric calibration method for dual energy computed tomography. *Physics in medicine and biology, 59*(8), 2059.

Braz, D., da Motta, L. M. G., & Lopes, R. T. (1999). Computed tomography in the fatigue test analysis of an asphaltic mixture. *Applied Radiation and Isotopes, 50*(4), 661-671.

Bridge, C. (2011). *Combining elastic and plastic fatigue damage in coiled tubing.* Paper presented at the SPE/ICoTA Coiled Tubing & Well Intervention Conference and Exhibition, The Woodlands, Texas.

Brunner, A., Blackman, B., & Davies, P. (2008). A status report on delamination resistance testing of polymer–matrix composites. *Engineering Fracture Mechanics, 75*(9), 2779-2794.

Burlayenko, V. N., & Sadowski, T. (2008). FE modeling of delamination growth in interlaminar fracture specimens. *Budownictwo i Architektura, 2*, 95-109.

Chell, G. (1984). Fatigue Crack growth laws for brittle and ductile materials including the effects of statics modes and elstic-plastic deformation. *Fatigue & Fracture of Engineering Materials & Structures, 7*(4), 237-250.

Choupani, N. (2008). Experimental and numerical investigation of the mixed-mode delamination in Arcan laminated specimens. *Materials Science and Engineering: A, 478*(1), 229-242.

Coats, A., Farabee, M., Song, H., & Berning, S. (2002). *Drilling with composites: An overview of an integrated composite coiled tubing drilling system and components.* Paper presented at the Offshore Technology Conference, Houston, Texas.

Coffin, L., & Tavernelli, J. (1959). The cyclic straining and fatigue of metals. *Trans Metall Soc AIME, 215*, 794-807.

CTES, L. (2005). Coiled tubing manual. *CTES CT Manual, 21*(7), 2005.

Degrieck, J., & Van Paepegem, W. (2001). Fatigue damage modeling of fibre-reinforced composite materials: review. *Applied Mechanics Reviews, 54*(4), 279-300.

Delle Piane, C., Giwelli, A., Clennell, M. B., Esteban, L., Kiewiet, M. C. D. N., Kiewiet, L., . . . Raimon, J. (2016). Frictional and hydraulic behaviour of carbonate fault gouge during fault reactivation—An experimental study. *Tectonophysics, 690*, 21-34.

Feechan, M., Makselon, C., & Nolet, S. (2003). *Field experience with composite coiled tubing.* Paper presented at the SPE/ICoTA Coiled Tubing Conference and Exhibition, Houston, Texas.

Fultz, J., & Pittard, F. (1990). *Openhole drilling using coiled tubing and a positive displacement mud motor.* Paper presented at the SPE Annual Technical Conference and Exhibition.

Gibson, R. F. (2011). *Principles of composite material mechanics*. USA: McGraw-Hill, Inc.

Gurit. (2012). Gurit Guide to Composites Retrieved from www.gurit.com. www.gurit.com

Hamitouche, L., Tarfaoui, M., & Vautrin, A. (2008). An interface debonding law subject to viscous regularization for avoiding instability: application to the delamination problems. *Engineering Fracture Mechanics, 75*(10), 3084-3100.

Harris, B. (1986). *Engineering composite materials*. London, UK: Institute of metals London.

Hashin, Z. (1980). Failure criteria for unidirectional fiber composites. *Journal of Applied Mechanics, 47*(2), 329-334.

Hashin, Z., & Rotem, A. (1973). A fatigue failure criterion for fiber reinforced materials. *Journal of composite materials, 7*(4), 448-464.

Hasiotis, T., Badogiannis, E., & Tsouvalis, N. G. (2011). Application of ultrasonic C-scan techniques for tracing defects in laminated composite materials. *Strojniški vestnik-Journal of Mechanical Engineering, 57*(3), 192-203.

Hillis, R. (2015). *Coiled tubing drilling and real-time sensing—Enabling 'prospecting drilling'in the 21st Century.* Paper presented at the ASEG Extended Abstracts 2015: 24th International Geophysical Conference and Exhibition.

Johnson, L. G. (1950). *The median ranks of sample values in their population with an application to certain fatigue studies.* Paper presented at the Bulletin of the American Mathematical Society.

Jones, R. M. (1998). *Mechanics of composite materials* (Second ed.). Philadelphia, PA: Taylor & Francis.

Kattan, P., & Voyiadjis, G. Z. (2005). *Mechanics of composite materials with Matlab*. Baton Rouge, LA: Springer.

Kelly, P. (2008). *Solid mechanics* Vol. 1. A. University (Ed.) *Part* (pp. 301-313).

Krueger, R. (2004). Virtual crack closure technique: History, approach, and applications. *Applied Mechanics Reviews, 57*(2), 109-143.

Lagat, C. K. (2015). *Evaluation and selection of an optimum material for coil tubes in CT drilling technology for hard rocks in mineral exploration.* (PhD), Curtin University, Curtin University.

Lai, C.-D. (2014). *Generalized Weibull Distributions*. Palmerston North, New Zealand: Springer.

Lee, Y.-L., Jwo, P., Hathaway, R. B., & Barkey, M. E. (2005). *Fatigue testing and analysis: theory and practice* (Vol. 13). Burlington, MA: ELSEVIER Butterworth-Heinemann.

Li, Teng, T., Wan, Z., Li, G., & Rans, C. (2013). *Fatigue delamination growth for an adhesively-bonded composite joint under Mode-I loading.* Paper presented at the 27th ICAF Symposium, Jerusalem, Israel.

Li, J., Crabtree, A. R., Kutchel, M., Diaz, J. D., Reyes, W., Dugarte, R., & Pena, L. (2008). *Sand/Well Vacuuming Technology With Concentric Coiled Tubing: Best Practices and Lessons Learned from Over 600 Operations.* Paper presented at the SPE Asia Pacific Oil and Gas Conference and Exhibition.

Liessem, A., Marewski, U., Groß-Weege, J., & Knauf, G. (2006). *Methods for collapse pressure prediction of UOE line pipe.* Paper presented at the 25th International Conference on Offshore Mechanics and Arctic Engineering, , Hamburg.

Mallick, P. K. (2007). *Fiber-reinforced composites: materials, manufacturing, and design*. Boca Raton, FL: CRC press.

Manson, S. (1965). Fatigue: a complex subject—some simple approximations. *Experimental mechanics, 5*(7), 193-226.

Mao, H., & Mahadevan, S. (2002). Fatigue damage modelling of composite materials. *Composite structures, 58*(4), 405-410.

Mathews, M. J., & Swanson, S. R. (2007). Characterization of the interlaminar fracture toughness of a laminated carbon/epoxy composite. *Composites Science and Technology, 67*(7), 1489-1498.

Matthews, F. L., Davies, G., Hitchings, D., & Soutis, C. (2000). *Finite element modelling of composite materials and structures*. Cornwall, England: CRC Press.

Mazerov, K. (2008). Bigger coil sizes, hybrid rigs, rotary steerable advances push coiled tubing drilling to next level. *Drilling Contractor*, 54-60.

Meggiolaro, M., & Castro, J. (2004). Statistical evaluation of strain-life fatigue crack initiation predictions. *International journal of fatigue, 26*(5), 463-476.

Mier, J. G. M. v. (2012). Classical fracture mechanics approaches *Concrete Fracture* (pp. 11-34). Boca Raton, FL: CRC Press.
Mishani, S., Evans, B., Rasouli, V., Roufail, R., Soe, S., & Jaensch, P. (2015). Interlaminar modelling to predict composite coiled tube failure. *The APPEA Journal, 55*(1), 361-370.
Mohanty, A. K., Misra, M., & Drzal, L. T. (2005). *Natural fibers, biopolymers, and biocomposites*: CRC press.
Newman. (1991). Determining the working life of a coiled tubing string. *Offshore, incorporating the Oilman, 51*, 31-32.
(2015). *Residual curvature and moments in CT due to bending.* Paper presented at the SPE/ICoTA Coiled Tubing & Well Intervention Conference & Exhibition, The woodlands, Texas.
Newman, & Brown. (1993). Development of a standard coiled-tubing fatigue test. *paper SPE, 26539*, 3-6.
Newman, Kelleher, & Smalley. (2014). *CT extended reach: Can we reach farther?* Paper presented at the SPE/ICoTA Coiled Tubing and Well Intervention Conference and Exhibition, The Woodlans, Texas.
Newman, Sathuvalli, & Wolhart. (1997). Elongation of coiled tubing during its life. *SPE paper, 38408*.
Nielsen, L. F. (2005). *Composite materials: properties as influenced by phase geometry*. Lyngby, Denmark: Springer.
Ochoa, O. O., & Reddy, J. N. (1992). *Finite element analysis of composite laminates* (Vol. 7). Dordrechet, The Netherland: Kluwer Academic Publishers.
Ong, J. (1993). An improved technique for the prediction of axial fatique life from tensile data. *International journal of fatigue, 15*(3), 213-219.
Park, J.-H., & Song, J.-H. (1995). Detailed evaluation of methods for estimation of fatigue properties. *International journal of fatigue, 17*(5), 365-373.
Prasad, M. S., Venkatesha, C., & Jayaraju, T. (2011). Experimental methods of determining fracture toughness of fiber reinforced polymer composites under various loading conditions. *Journal of Minerals and Materials Characterization and Engineering, 10*(13), 1263.
Ramberg, W., & Osgood, W. R. (1943). Description of stress-strain curves by three parameters.
Reifsnider, K., Henneke, E., Stinchcomb, W., & Duke, J. (1983). Damage mechanics and NDE of composite laminates. *Mechanics of composite materials: Recent advances*, 399-420.
ReliaSoft. (2015). *Life Data Analysis Reference*. Tucson, Arizona: ReliaSoft Corporation.
Rinne, H. (2008). *The Weibull distribution: a handbook*. Boca Raton, FL: CRC Press.
Salehizadeh, H., & Saka, N. (1992). Crack propagation in rolling line contacts. *Journal of tribology, 114*(4), 690-697.
Sas-Jaworsky, A., & Williams, J. G. (1993). *Development of composite coiled tubing for oilfield services*. Paper presented at the SPE Annual Technical Conference and Exhibition, Houston, Texas.
Shaw, P., & Kyriakides, S. (1985). Inelastic analysis of thin-walled tubes under cyclic bending. *International Journal of Solids and Structures, 21*(11), 1073-1100.
Simona-Plastics. (2016). Technical Handbook - Global thermoplastic solutions. Kirn, Germany: SIMONA AG.
Sisak, W., & Crawford, D. (1994). *The fatigue life of coiled tubing.* Paper presented at the SPE/IADC Drilling Conference, Dallas ,Texas.

Spada, A., Giambanco, G., & Rizzo, P. (2009). Damage and plasticity at the interfaces in composite materials and structures. *Computer Methods in Applied Mechanics and Engineering, 198*(49), 3884-3901.

Stanley, R. K. (1998). *An Analysis of Failures in Coiled Tubing.* Paper presented at the IADC/SPE drilling conference, Dallas, Texas.

Starbuck, J. M., & Eberle, C. (2000). Analytical solution for the design of spoolable composite tubing. *Mechanics of Materials, 3*.

Sun, X., Tan, V., Liu, G., & Tay, T. (2009). An enriched element-failure method (REFM) for delamination analysis of composite structures. *International journal for numerical methods in engineering, 79*(6), 639-666.

Szekrenyes, A. (2002). Overview on the experimental investigations of the fracture toughness in composite materials. *Hungarian Electronic Journal of Sciences, Mechanical Engineering Section, MET-020507-A*.

Thakur, V. K. (2014). *Green composites from natural resources*. Boca Raton, FL: CRC Press.

Thomeer, H., & Newman, K. (1991). *Safe Coiled-Tubing Operations.* Paper presented at the SPE Health, safety and environment in oil and gas exploration and production conference, The Hague, The Netherlands.

Tipton. (1996). *Coiled tubing deformation mechanics: Diametral growth and elongation.* Paper presented at the SPE Gulf Coast Section/ICoTA North American Coiled Tubing Roundtable, Richardson, Texas.

(2003). Achilles 4.0 CT fatigue life prediction algorithm. *CTES Technical Note, Conroe, TX*.

Tsai, S. W., & Wu, E. M. (1971). A general theory of strength for anisotropic materials. *Journal of composite materials, 5*(1), 58-80.

Turon Travesa, A. (2006). *Simulation of delamination in composites under quasi-static and fatigue loading using cohesive zone models.* (Doctor of Philosophy), Universitat de Girona, Spain.

Vaara, P., & Leinonen, J. (2012). *Technology survey on NDT of carbon-fiber composites*. Kemi, Finland: Kemi-Tornio University of Applied Sciences.

Valdez, M., Morales, C., Rolovic, R., & Reichert, B. (2015). The development of high-strength coiled tubing with improved fatigue performance and HS resistance. *SPE/ICoTA Coiled Tubing & Well Intervention Conference & Exhibition*.

Wainstein, J., & Ipiña, J. P. (2012). Ductile Instability Analysis of HSLA Coiled Tubing. *Procedia Materials Science, 1*, 297-304.

Weibull, W. (2013). *Fatigue testing and analysis of results*. The universities press, Belfast: Pergamon Press.

Williams, & Sas-Jaworsky, A. (2000). *Composite spoolable pipe development, advancements, and limitations.* Paper presented at the Offshore Technology Conference, Houston, Texas.

Wisheart, M., & Richardson, M. (1998). The finite element analysis of impact induced delamination in composite materials using a novel interface element. *Composites Part A: Applied Science and Manufacturing, 29*(3), 301-313.

Wu. (1995). Coiled tubing working life prediction. *SPE Production Operations Symposium*.

Wu, & Yao. (2010). A fatigue damage model of composite materials. *International journal of fatigue, 32*(1), 134-138.

Yoshida, F., & Uemori, T. (2002). A model of large-strain cyclic plasticity describing the Bauschinger effect and workhardening stagnation. *International Journal of Plasticity, 18*(5), 661-686.

Zhong, A., Ehtesham, A., & Howard, R. (2009). *Successful development of coiled-tubing connectors using virtual testing.* Paper presented at the SIMULIA Costumer conference.

Zhu, & Zehnder. (2016). *Experimental and applied mechanics, Volume 4: Proceedings of the 2016 annual conference on experimental and applied mechanics*. New York, NY: Springer International Publishing.

Zhu, Y. (2009). *Characterization of Interlaminar Fracture Toughness of a Carbon/epoxy Composite Material.* (Master of Science), The Pennsylvania State University.

Zifeng, L., Xuejiao, L., & Peng, W. (2012). Prebending coiled tubing and its fatigue life prediction. *Journal of Energy Resources Technology, 134*(3), 034502.

Zureick, A.-H., & Nettles, A. T. (2002). *Composite Materials: Testing, Design, and Acceptance Criteria* (Vol. 1416). West Conshohocken, PA: ASTM International.

Appendix A Vacuum Bagging Technique

Vacuum bagging is a composite laminate manufacturing method using atmospheric pressure to remove entrapped air, excess resin, compact the laminate and to hold the resin and fibre plies in place together during its curing process. The process helps in achieving a strong composite laminate. This method requires fibre, resin and flat plate mold to be contained within a sealed envelope. Depressurizing the airtight envelope make a pressure differential between the inside and outside of the envelope and put equal and even pressure force over the surface of the envelope. During a perfect vacuum technique, the maximum possible pressure can be exerted on the composite laminate to remove air from the envelope is 14.7 psi.

The vacuum bagging process offers several advantages over conventional clamping techniques:

- It removes any trapped air between laminate layers, and allows fewer voids and a stronger bond between the layers.
- It compacts the layers. The evenly distributed atmospheric pressure over the entire surface of the fibre bundles and prevents shifting of fibre orientation during curing process.
- Control excess resin in the composite laminate, thus optimizing the fibre-to-resin ratio, translating into higher strength to weight ratios and cost advantages.

Component Function of vacuum bagging materials:

Vacuum Pump: Evacuate air and excess resin from the inside of the vacuum bag.

Trap: Collects any excess resin that gets sucked into the line, before it reaches the vacuum pump.

Mold: holds the wet-out laminate in a specific shape until the resin system has cured.

Release film: This is essential for preventing the resin from sticking to the mold.

Perforated film: Holds the resin in the laminate and allows free passage of excess resin during vacuum and curing. It can be removed easily from the laminate after curing.

Bleeder fabric: It controls the excess resin flow from wet-laminate, thus the fibre of the final composite laminate can be known.

Breather fabric: The bleeder cloth assists the air and volatiles to be removed from the whole assembly.

Vacuum bag: Thermoplastic envelop provides a sealed bag to allow for removal of air and excess resin. It also distributes uniform pressure over composite laminate.

Sealant tape: The Mastic sealant provide a continuous airtight seal between the bag layers and seals the manifold entry into the bag.

Vacuum bagging procedure:

1. Select a quality vacuum pump to match the bag size, desired vacuum rate, and ultimate pressure with that of the pump for best results.
2. Connect the vacuum pump to the bag through thermoplastic rigid and flexible tubes. The basic connections configuration is as shown in Figure A-1. To maintain the vacuum, tight connections between the tubes and the vacuum pump is required. A gauge may be mounted directly to the vacuum pump.

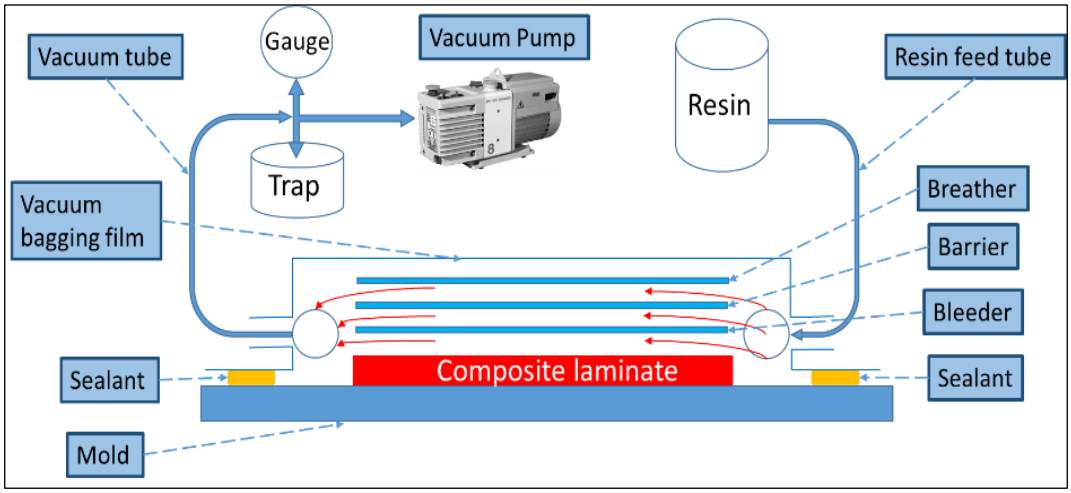

Figure A-1: Typical vacuum bagging lay-up.

3. Use a simple flat, smooth and rigid surface mold covered with a smooth plastic laminate release agent, as a base for laying the laminate layers as shown in Figure A-2.

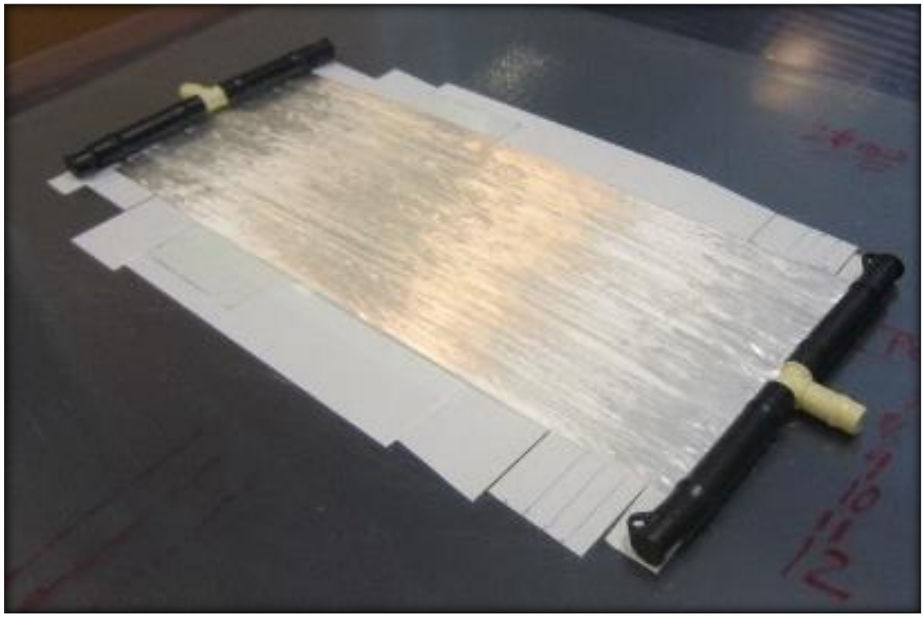

Figure A-2: Tailored fibre over mold table.

4. Use a high-strength epoxy resin with a slow-hardener. In this experiment, WEST SYSTEM 105 epoxy resin and WEST SYSTEM 206 Hardener (Figure A-3), with maximum resin and hardener to the ratio 5:1 was used. The resin system can be cured in a wide temperature range (see Figure A-4).

Figure A-3: Epoxy resin and Hardener.

HARDENER	RESIN/HARDENER USE	HARDENER TEMPERATURE RANGE (°F)*							CURE SPEEDS at room temperature*		
					Room Temp.				POT LIFE 100g cupful	OPEN TIME thin film	CURE TO SOLID thin film
		40°	50°	60°	70°	80°	90°	100°			
205	General bonding and coating								9–12 minutes	60–70 minutes	6–8 hours
206	General bonding and coating								20–25 minutes	90–110 minutes	10–15 hours
207	Clear coating								22–27 minutes	110–130 minutes	12–18 hours
209	General bonding and coating								40–50 minutes	3–4 hours	20–24 hours

*Epoxy cures faster in warmer temperatures and in thicker applications—Epoxy cures slower in cooler temperatures and in thinner applications.

Figure A-4: Hardener selection guide from WEST SYSTEM catalogue.

5. Use some layers of bleeder, barrier, breather and vacuum bag materials as shown in Figure A-5. Place a bleeder film to cover over any portion of the wet-laminate in contact with the resin, then barrier and finally breather over the bleeder film (Figure A-6).

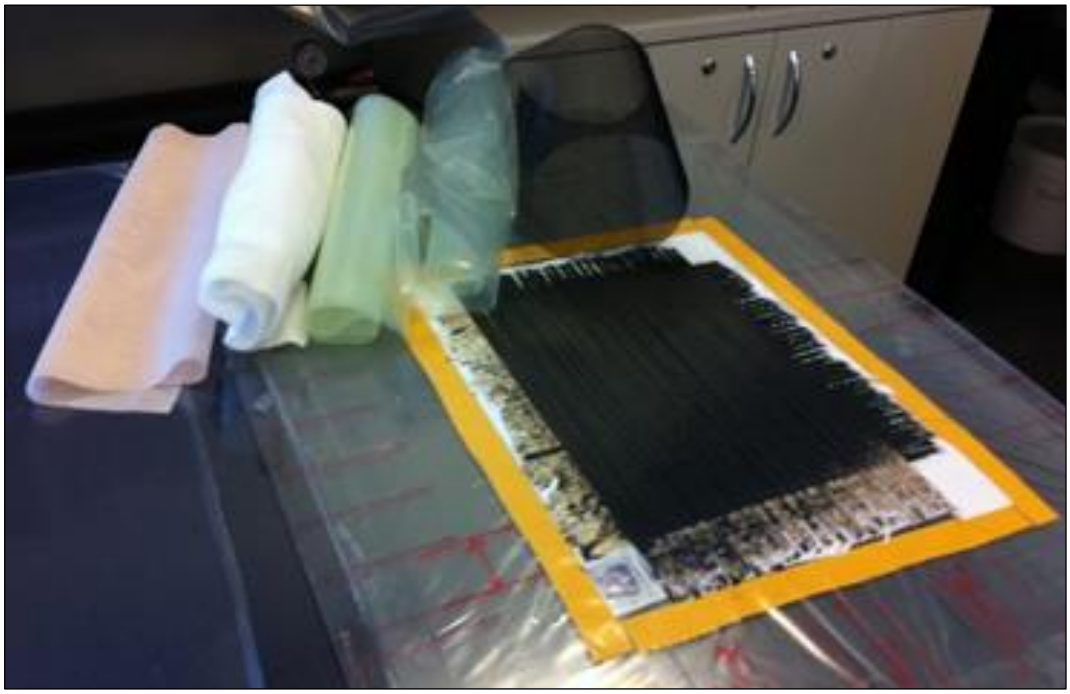

Figure A-5: Vacuum bagging components.

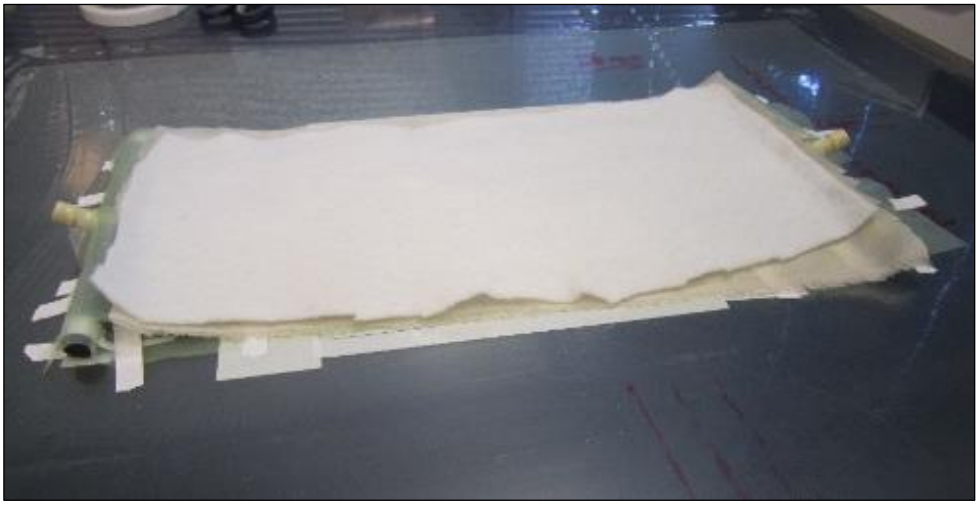

Figure A-6: Vacuum bagging breathing fabrics.

6. Set a feeding chamber on one end and collecting chamber to the other end of the laminate. This allows the flow of resin through the fibre strands from one chamber and deaerating of whole system for better composite quality. A flexible film (Nylon or Polyethylene) is placed over the wet lay-up, the edges sealed, and a vacuum bagging commenced. (Figure A-7).

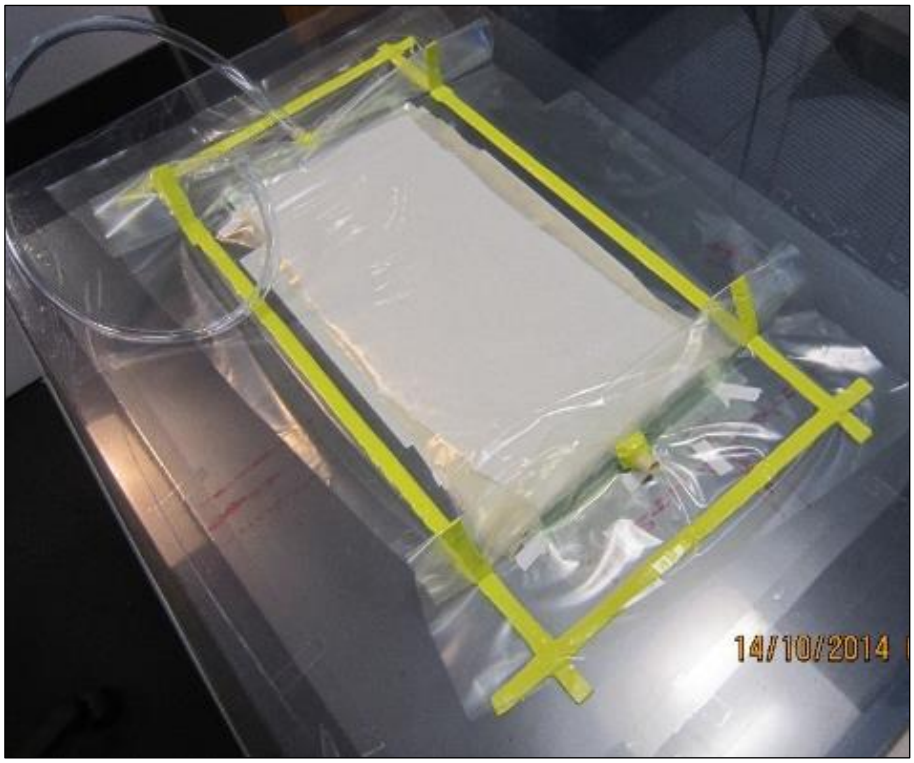

Figure A-7: sealed vacuum bag.

7. Evacuate the air from within the bag uses atmospheric vacuum pressure to eliminate voids and force excess resin from the wet-laminate. The pressure exerted on the laminate results in increased fibre concentration and provides better adhesion between layers of fibre construction (Figure A-8).

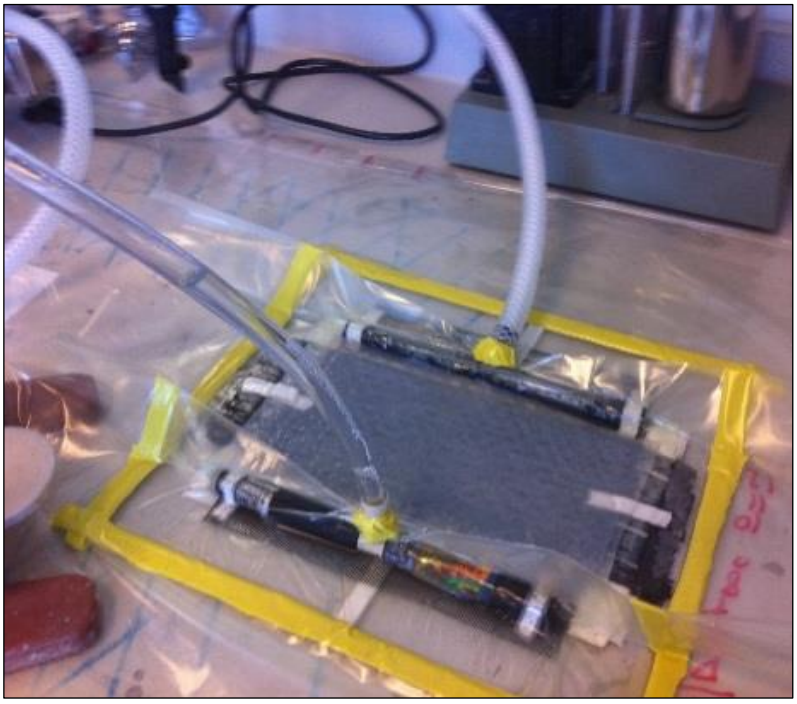

Figure A-8: Vacuum bagging set up.